

# **Emerging properties of signaling networks in cancer: a data-derived modeling approach**

Dissertation submitted to the  
Combined Faculties for the Natural Sciences and Mathematics  
of the Ruperto-Carola University of Heidelberg, Germany  
for the Degree of Doctor of Natural Sciences

presented by

M.Sc. Martí Bernardo Faura  
born in Barcelona



Oral examination date:  
30.04.2013

Referees:  
Prof. Dr. Roland Eils  
Prof. Dr. Ursula Kummer



# Acknowledgements

I would like to thank Roland Eils for the opportunity to work in this project in such an interdisciplinary group at the interface of theoretical and experimental biology; due to that, I enjoyed the experience of attending meetings, in which different research fields were discussed in depth. In addition, I am thankful for the freedom to pursue my own scientific work, while giving all the support and supervision when required.

Thanks to Nathan Brady, for supervision, advice and very fruitful discussions every time I was in need of them. I am thankful for sharing new ideas on open questions in systems biology and discussing how these could be addressed, specially on the experimental side. Furthermore, I immensely appreciated his constant support and teachings on how to communicate my scientific research.

Further, I am thankful for insightful advice. Along these lines, I would like to thank Vytaute Starkuviene and Ursula Kummer for their support as members of my thesis advisory comitee. I also would like to thank Ursula Kummer for valuable advice and discussion on key aspects of the modeling. I thank Stefan Legewie for valuable advice regarding modeling in general, and specifically for constructive criticism; his first question on my initial model "What do we learn from the fact that the model is able to reproduce the data" made me explore a wide range of modeling designs and strategies to challenge the results along the way.

Furthermore, I would like to thank Stefan Maßen and Christine Falk for the experimental dataset that was the starting point of the second part of this work.

I am grateful to Hbigs for the PhD program offered. Not only the scientific courses but also the workshops on complementary skills and the -six- friends met were highly educational; they really contributed to guide me through the path of the PhD.

I would like to thank a lot of colleagues, who made it a pleasure to work. Not only for that would I like to thank Joel, but also for scientific discussions that were very important to me, from which I learned a lot. His approach to scientific questions is a

---

source of inspiration and a standard I would be very happy to approximate. "Y"ara was not only a friend and constant support, but a keen collaborator during the first part of this work. Sven *muchacho* was also a great friend during this whole thesis, and I am extremely thankful for his endless knowledge and help on any Matlab aspect and specifically regarding optimization and implementation of objective functions. I thank Anashua for her good mood that created a great atmosphere in our office and for express corrections, and Johanna for great discussions on swingy biophysics and differential equations to investigate them, and also for help with my german. Additionally, I would like to say vielen vielen Dank to Manuela for her magic help and for being so great to work with. Further, I would like to thank Phillip, Clarissa, Barbara, Stefan, Daniela, Hannah, Corinna, Sabrina, Juergen, Nina, Sabine, Tobias A. and Tobias B., for plentiful discussion, creating an enjoyable working atmosphere and making the lab life a great experience.

*Muchisimas gracias, gueya* goes to my fellow voyager Paula. During his lucid discussion on the relationship between astrophysics and molecular biology at the EMBO meeting, Martin Rees stated "eternity is very long, specially towards the end" [citation needed]; Paula and her constant help and joy when discussing science in general made the end phase of the PhD look like a millisecond. In addition, this thesis would surely appear less visual without her latex and aesthetics teachings, and I will never again dare to modify my own figure if this means changing its aspect ratio.

I am extremely thankful to my friends in Heidelberg for their support and for making my time here very fulfilling, including the Altstadt group, the well-balanced spanish-german language exchange group, Nicole and Gisella. Special thanks goes to Elena, Tomassi and Edu, who were always ready for new adventures, always there.

I can not thank my family enough, especially my parents Teresa and Miquel and my germana *bessona* Clara. They have encouraged and helped me at all times, and I am immensely lucky to have them.

Finally, I would like to thank Aina, who contributed to this thesis more than she thinks. Her constant will to support, enthusiasm and teachings on nature and macrobiology are a continuous source of admiration and motivation to approach both science and life.

# Publications & contributions

## Related publications

The results presented in the first part of this work were published in the following paper:

- Reis Y, Bernardo-Faura M, Richter D, Wolf T, Brors B, Hamacher-Brady A, Eils R, Brady NR. (2012) Multi-Parametric Analysis and Modeling of Relationships between Mitochondrial Morphology and Apoptosis. PLoS ONE 7(1): e28694. doi:10.1371/journal.pone.0028694

A manuscript is currently in preparation consisting of the results presented in the second part of this work:

- Bernardo-Faura M, Maßen S, Falk C, Brady NR, Eils R. Data-derived modeling characterizes plasticity of MAPK signaling in melanoma. In preparation

## Contributions

This work is the outcome of a combined effort of theoretical and experimental research performed by a team of scientists. Hence, a lucid presentation of the results made it necessary to include the work of others in this text. Both in the results and methods section, I described solely those experimental procedures and datasets which aided to illustrate the specific results achieved here. For clarity, contributions by others are marked with a footnote. For reasons of style, I wrote the main text using the first person plural narrative. However, all work was carried out by me unless marked otherwise in the above-mentioned footnotes.





# Abstract

Mammalian signal transduction pathways are highly integrated within extended networks, with crosstalk emerging in space and time. This dynamic circuitry is dependent on changing activity states for proteins and organelles. Network structures govern specificity of cellular responses to external stimuli, including proliferation and cell death. Loss of regulation virtually underlies all disease. However, while the contributions of individual components to phenotype are mostly well understood, systematic elucidation for the emergence or loss of crosstalk and impact on phenotype remains a fundamental challenge in classical biology that can be investigated by systems biology. To that end, we established a mathematical modeling platform, at the interface between experimental and theoretical approaches, to integrate prior literature knowledge with high-content, heterogeneous datasets for the non-intuitive prediction of adaptive signaling events.

In the first part of this work, we investigated high-content microscopy datasets of morphological, bio-energetic and functional features of mitochondria in response to pro-apoptotic treatment in MCF-7 breast cancer cells. Data pretreatment techniques were used to unify the heterogeneous datasets. Using fuzzy logic, we established a generalized data-driven modeling formalism to model signaling events solely based on measurements, capable of high simulation accuracy via non-discrete rule sets. Employing neural networks, a generalized fuzzy logic system, i.e. its rules and membership functions, could be parameterized for each potential signaling interaction. An exhaustive search approach identified models with least error, i.e. the most related signaling events, and predicted a hierarchy of apoptotic events, in which upon activation of pro-apoptotic Bax, mitochondrial fragmentation propagates apoptosis, which is consistent with reported literature. Hence, we established a predictive approach for investigation of protein and organelle interactions utilizing cell-to-cell heterogeneity, a critical source of biologically relevant information.

In the second part of this work, we aimed to identify network evolution in the topology of MAPK signaling in the A-375 melanoma cell line. To that end, the modeling method was extended to incorporate temporal and topological structure from phosphorylation profiles of key MAPK intermediates treated with different pharmacological inhibitors and acquired over 96 hours. To increase prediction power, a parameter reduction strategy was developed to identify and fix parameters with lowest contri-

---

bution to model performance. Therefore, training datasets were bootstrapped and signatures of deviation in flexibility and accuracy were calculated. This novel strategy achieved an optimal set of free parameters. Finally, a reduced multi-treatment model encoding the behavior of the full MAPK dataset was systematically trained to a sequentially increasing subset of time points, enabling time-defined identification of discrepancies in reported vs. acquired network topology. To that end, an objective function for fuzzy logic model optimization was implemented, which accounted for time-defined model training. Analysis led to the identification of emerging discrepancies between model and data at specific time points, thus characterizing a potential network rearrangement upstream of MAPK kinase MEK1, consistent with studies reporting increased resistance to apoptosis exhibited by A-375 melanoma cell line.

Furthermore, this approach was benchmarked against a recently published fuzzy-logic-based analysis of protein signals in HT-29 human colon carcinoma cells. Our method showed high accuracy and ability to be readily trained to additional datasets for the elucidation of signaling evolution.

Taken together, we have developed a data-derived modeling formalism to elucidate non-linear signaling from high-content heterogeneous datasets. We report a hierarchy of morphological and functional features of mitochondrial regulation during apoptosis in MCF-7 breast cancer cell line. We further developed the modeling approach to incorporate temporal and topological structure, thereby enabling elucidation of network evolution and providing a means to facilitate understanding of the mechanisms that grant melanoma its molecular plasticity. Finally, we identified a potential signaling rearrangement specific in A-375 melanoma cell line and provided a quantitative measure of interest as treatment target of each signaling intermediate over time.

# Zusammenfassung

Signaltransduktionswege in Säugetieren sind integriert in komplexe Netzwerke mit Wechselwirkungen in Raum und Zeit. Diese dynamischen Kreisläufe sind abhängig von dem sich ständig ändernden Aktivierungsstatus der Proteine und Organellen. Die Struktur der Netzwerke bestimmt die spezifische Wirkung der Zellantwort auf externe Signale, einschließlich der Signale für Wachstum und Apoptose. Ein Verlust dieser Regulierungsfähigkeit ist der Grund für praktisch jede Krankheit. Während der individuelle Beitrag einzelner Komponenten zum Zellphänotyp oft gut erforscht ist, bleibt die systematische Aufklärung von Entstehen und Verschwinden der Signalwegwechselwirkungen und der Einfluss auf den Zellphänotyp eine Herausforderung für die biologische Forschung, die mit Systembiologie beantwortet werden kann. Dafür haben wir eine mathematische Modellierungs-Plattform an der Schnittstelle zwischen theoretischen und experimentellen Ansätzen erstellt, Literaturwissen mit heterogenen, sogenannten *high-content*-Datensätzen kombiniert, um nicht-intuitive Vorraussagen über adaptive Signalantworten zu treffen.

Im ersten Teil dieser Arbeit wurden *high-content*-Mikroskopiedaten von morphologischen, bio-energetischen und funktionalen Eigenschaften der Mitochondrien als Reaktion auf die Behandlung der Brustkrebszelllinie MCF-7 mit einem Apoptose-signal untersucht. Die Daten wurden vorbehandelt, um die Heterogenität der Datensätze auszugleichen. Aufbauend auf dem Verfahren der sogenannten *fuzzy logic* wurde ein datenfokussierter Modellierungsformalismus erstellt, um den Signalingablauf nur auf Messungen basierend zu simulieren. Dieser Ansatz ermöglicht eine hohe Simulationsgenauigkeit mit einem nicht-diskreten Regelsatz. Mit neuronalen Netzen konnte ein generalisiertes Fuzzy-Logic-System, d.h. Regeln und Zugehörigkeitsfunktionen, für jede mögliche Signalwechselwirkung parametrisiert werden. Mittels einer vollständigen Durchsuchung aller möglichen Beziehungskombinationen, können die Modelle mit den kleinsten Fehlern, d.h. den ähnlichsten Signalwechselwirkungen identifiziert werden und eine Rangfolge der Geschehnisse im Apoptose-Signalweg vorausgesagt werden: nach Aktivierung des pro-apoptotischen Bax, verbreitet die Mitochondrien-Fragmentierung Apoptose, eine Vorraussage die zur bestehenden Literatur konform ist. Es wurde also ein Methode etabliert zur Erforschung von Protein- und Organellen-Wechselwirkungen, mit der Vorraussagen getroffen werden können und die die Zell-zu-Zell-Variation als entscheidende Quelle für biologisch relevante Einsichten verwendet.

---

Im zweiten Teil dieser Arbeit wurde die Evolution der Topologie des MAPK-Signalnetzwerkes in der Melanom-Zelllinie A-375 untersucht. Dafür wurde die Modellierungsmethode um die zeitliche und topologische Struktur von Phosphorylierungsprofilen der Schlüssel-Signal-Glieder von MAPK erweitert, und über 96 Stunden nach Behandlung mit verschiedenen pharmakologischen Inhibitoren gemessen. Um die Vorraussage zu verbessern, wurde eine Strategie zur Reduzierung der Parameter entwickelt, so dass die Parameter mit geringstem Beitrag zur Modellveränderung identifiziert und fixiert werden konnten. Dafür wurden Training-Datensätze mit der statistischen Bootstrap-Methode erstellt und Charakteristika der Veränderung in Flexibilität und Genauigkeit des Modelles untersucht. Mit dieser neuartigen Strategie wurden optimale Parametersätze von freien Parametern erreicht. Zuletzt wurde ein Multi-Behandlungs-Modell, das das Verhalten des ganzen MAPK-Datensatzes beschreibt, systematisch gegen eine Untermenge der Zeitpunkte trainiert, so dass zeitlich definiert Unterschiede zwischen vorrausgesetzten und gemessenen Netzwerk-Topologien identifiziert werden konnten. Zu diesem Zweck wurde eine Zielfunktion für die Optimierung des Fuzzy-Logic-Modell implementiert, die das zeitlich definierte Modelltraining berücksichtigt. Analyse erlaubte Nichtübereinstimmungen von Modell und Daten zu bestimmten Zeitpunkten aufzuzeigen, und damit eine mögliche Netzwerk- Reorganisation oberhalb der MAPK-Kinase MEK1, zu charakterisieren. Dieser Befund stimmt mit Studien überein, die erhöhte Resistenz gegen Apoptose der Zelllinie A-375 beschreiben.

Desweiteren wurde dieser Ansatz gegen eine kürzlich publizierte *fuzzy-logic*-basierte Analyse von Proteinsignalen in der menschlichen Dickdarmkarzinom Zelllinie HT-29 ge-benchmarkt. Unsere Methode zeigte hohe Präzision und die Fähigkeit zur Anpassung an weitere Datensätze zum Erkenntnisgewinn über Signalling.

Insgesamt wurde ein datenbezogener Modellierungsformalismus entwickelt, um nicht-lineare, heterogene Signaling-Datensätze von *high-content*-Messungen zu erklären. Wir beschreiben eine Rangordnung von morphologischen und funktionalen Eigenschaften der Mitochondrien-Regulierung während der Apoptose in der Brustkrebszelllinie MCF-7. Desweiteren haben wir einen Modellierungsansatz entwickelt, der zeitlich und topologische Strukturen integrieren kann, so dass Erkenntnisse zu Netzwerk-Evolution bewonnen werden können und eine Messmethode zum Verstehen der Mechanismen, die das Wachstum von Melanoma und seine Verformbarkeit ermöglicht. Schlussendlich wurde mögliche spezifische Netzwerk- Reorganisation in der Melanoma-Zelllinie A-375 aufgezeigt und ein quantitative Messmethode entwickelt, von Interesse als Angriffspunkt für Behandlungen für jedes einzelne Signal-Zwischenglied über die Zeit.

# List of Abbreviations

<b>Bid</b>	BH3 Interacting-Domain death agonist
<b>DISC</b>	Death Inducing Signaling Complex
<b>EGF</b>	Epidermal Growth Factor
<b>ERK</b>	Extracellular signal-Regulated Kinase
<b>FIS</b>	Fuzzy Inference System
<b>FL</b>	Fuzzy Logic
<b>gFIS</b>	generalized Fuzzy Inference System
<b>MAPK</b>	Mitogen-Activated Protein Kinase
<b>MAPKK</b>	MAPK Kinase
<b>MAPKKK</b>	MAPKK Kinase
<b>MF</b>	Membership Function
<b>MOMP</b>	Mitochondrial Outer Membrane Permeabilization
<b>msFIS</b>	multi-scenario Fuzzy Inference System
<b>NGF</b>	Nerve Growth Factor
<b>ODE</b>	Ordinary Differential Equation
<b>PCA</b>	Principal Component Analysis
<b>PLSr</b>	Partial Least Squares regression
<b>RMSE</b>	Root-mean-square error
<b>RTK</b>	Receptor Tyrosine Kinase
<b>SISO</b>	Single Input-Single Output fuzzy logic model
<b>TKS</b>	Takagi-Sugeno fuzzy logic System



# Contents

<b>Acknowledgements</b>	<b>5</b>
<b>Publications &amp; contributions</b>	<b>7</b>
<b>Abstract</b>	<b>9</b>
<b>Zusammenfassung</b>	<b>11</b>
<b>List of Abbreviations</b>	<b>13</b>
<b>1 Introduction</b>	<b>17</b>
1.1 Signal Transduction of life and death pathways and its role in cancer . . . . .	17
1.1.1 Programmed cell death & mitochondria . . . . .	17
1.1.2 Survival & the MAPK cascade . . . . .	23
1.1.3 Cancer signaling . . . . .	30
1.2 Mathematical modeling of signal transduction networks . . . . .	32
1.2.1 Data-driven modeling . . . . .	32
1.2.2 Physicochemical modeling . . . . .	34
1.2.3 Logic modeling . . . . .	39
1.2.4 Neuro-fuzzy modeling . . . . .	42
1.3 Properties of experimental data and their impact in modeling . . . . .	44
1.3.1 Heterogeneity of measurements and cell-to-cell variability in experimental data . . . . .	44
1.3.2 Sources of topological complexity . . . . .	47
<b>2 Motivation and aims</b>	<b>51</b>
<b>3 Methods</b>	<b>55</b>
3.1 Experimental acquisition of apoptotic signatures . . . . .	55
3.1.1 Cell culture and apoptotic stimuli . . . . .	55
3.1.2 Imaging and classification of mitochondria morphology . . . . .	55

3.1.3	Reporters of apoptotic events . . . . .	56
3.2	Experimental acquisition of proliferation signatures . . . . .	58
3.2.1	Cell culture and pharmacological inhibition of MAPK . . . . .	58
3.2.2	Luminex analysis of total and phosphorylated protein level . . . . .	58
3.3	Fuzzy Logic based exhaustive search of regulatory interactions . . . . .	59
3.4	Time-defined training and evaluation of topological fuzzy logic modeling . . . . .	61
3.4.1	Parameter reduction strategy and model implementation . . . . .	61
3.4.2	Data-derived sensitivity analysis . . . . .	63
3.4.3	Benchmarking approach . . . . .	64
3.4.4	Implementation of multiple perturbation models . . . . .	65
3.4.5	Full network simulation . . . . .	66
<b>4</b>	<b>Results</b>	<b>67</b>
4.1	Modeling interactions of heterogeneous data in apoptosis . . . . .	67
4.1.1	Integration of mitochondrial and apoptotic measurements in response to diverse stimuli . . . . .	67
4.1.2	Single interaction modeling encodes nonlinear regulation . . . . .	76
4.1.3	Modeling suggests a hierarchy for mitochondrial apoptotic events . . . . .	78
4.1.4	Literature validation of hierarchy suggested by model . . . . .	78
4.2	Modeling evolution of MAPK signaling . . . . .	81
4.2.1	Study of signal transduction to identify signaling rearrangements . . . . .	81
4.2.2	Data-derived single model implementation and parameter reduction . . . . .	83
4.2.3	Prior knowledge and literature-based definition of initial topology . . . . .	92
4.2.4	Benchmarking approach . . . . .	95
4.2.5	Analysis of model evolution . . . . .	97
4.2.6	Reimplementation of starting topology to account for emerging behavior . . . . .	99
4.2.7	Identification of signaling rearrangement and literature validation . . . . .	101



<b>5 Discussion</b>	<b>107</b>
5.1 On the biological findings . . . . .	107
5.1.1 Modeling suggests a hierarchy of morphological and functional features of mitochondria . . . . .	107
5.1.2 MAPK signaling is rearranged in A-375 melanoma cell line	108
5.2 Advantages and shortcomings of the methods presented . . . . .	110
5.2.1 Benchmarking . . . . .	110
5.2.2 Network structure . . . . .	111
5.2.3 Use of literature data . . . . .	113
5.2.4 Number of free parameters . . . . .	115
5.2.5 Temporal activation . . . . .	116
5.3 Outlook . . . . .	116
<b>Appendix 1</b>	<b>119</b>
<b>Appendix 2</b>	<b>127</b>
<b>Appendix 3</b>	<b>129</b>
<b>Appendix 4</b>	<b>133</b>
<b>References</b>	<b>134</b>



# 1

## Introduction

### 1.1 Signal Transduction of life and death pathways and its role in cancer

#### 1.1.1 Programmed cell death & mitochondria

One million cells die every second in the human body [Green, 2011]. They die for a reason, by a mechanism called apoptosis, which is essential for successful embryonic development and the maintenance of normal tissue homeostasis. Apoptosis is a form of programmed cell death, i.e. a genetic and biochemical pathway of cell death that does not produce an inflammatory response and is mediated by an intracellular program. Specifically, to be termed apoptosis a program of cell death needs to culminate in cellular shrinkage with nuclear chromatin condensation and nuclear fragmentation. Disruption to the homeostasis of the programmed cell death pathways is recognized as a major factor in the pathogenesis of many diseases such as cancer, either via loss of pro-apoptotic or overexpression of anti-apoptotic proteins. Furthermore, anti-cancer drugs achieve their effect by activating apoptosis [Fadeel et al., 1999, Spencer and Sorger, 2011]. Apoptosis, however, is not the only type of programmed cell death. In response to either internal or external stimuli, the response of the cell is mediated by a cascade of coupled pro-life and pro-death pathways, such as apoptosis, also known as Type I cell death, autophagy, also known as Type II Cell death and some recently discovered mechanisms [Green, 2011]. A number of these mechanisms are not yet fully understood [Maiuri et al., 2007] (see **figure 1.1**). Two main routes activate apoptosis, which will be introduced straightaway: the extrinsic (death receptor) mediated pathway

and the intrinsic (mitochondrial) pathway.

**Extrinsic pathway of apoptosis** The classical view of the Death Receptor mediated apoptosis is that apoptosis is activated by death receptor ligands of the so-called CD95 family, also known as FAS. The intracellular death domains of the death receptors then recruit and activate adaptor molecules to form the Death Inducing Signaling Complex (DISC) . The formation of the DISC recruits amongst others a group of proteases called caspases. Caspases are enzymes that naturally occur in an inactive state, and when activated become principal mediators of programmed cell death. The caspases recruited to the DISC, such as caspase 8, are called initiator caspases and become active by undergoing a conformational change when forming the complex [Kober et al., 2011]. In turn, initiator caspases activate effector caspases (e.g. caspase 3/7), which become active by being cleaved and can thereafter proteolytically degrade up to 1000 different substrates within a cell [Green, 2011], thereby performing the cell death program and ultimately killing the cell. Cell death pathways can also be classified as being dependent or independent of caspases (see **figure 1.1**).

**Intrinsic pathway of apoptosis** Intrinsic sources of stress such as ROS or Ca<sup>2+</sup> overload can cause mitochondrial dysfunction and eventually lead to apoptosis [Desagher and Martinou, 2000]. In addition, the mitochondrial pathway can be activated by viral infection, DNA damage and growth-factor deprivation [Youle and Strasser, 2008]. To that end, a necessary step is the release of cytochrome c as a result of the outer mitochondrial membrane becoming permeable by triggering Mitochondrial Outer Membrane Permeabilization (MOMP). Cytochrome c binds to Apaf-1 to form the apoptosome and activate caspase 9, which then activates effector caspases 3/6/7, resulting in a variety of morphological changes such as cell shrinkage, nuclear fragmentation and chromatin condensation [Maiuri et al., 2007] (see **figure 1.2**).

Mitochondria play a crucial role in extrinsic apoptosis as well, since activation of effector caspases leads to cleavage of BH3-only protein Bid. The C-terminal of Bid is then called t-Bid; when activated, tBid is thought to inhibit anti-apoptotic Bcl-2 family members, including Bcl-2 and Bcl-xL, and directly activate pro-apoptotic Bax and Bak to trigger Mitochondrial Outer Membrane

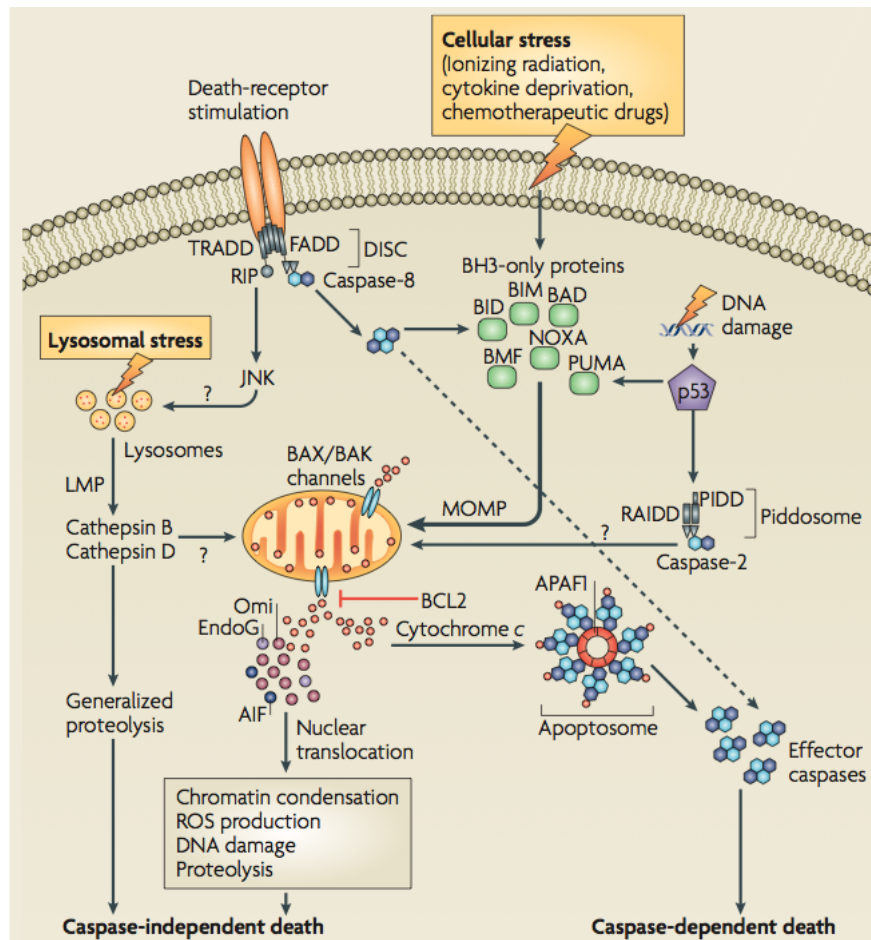


**Figure 1.1: Caspase-dependent and caspase-independent cell death pathways.**

Two main pathways lead to cell death: the extrinsic and the intrinsic or mitochondrial pathways. In the extrinsic pathways, an external signal triggers the cascade of reactions that ultimately lead to cell death, whereas in the intrinsic pathway permeabilization of the mitochondrial membrane (Mitochondrial Outer Membrane Permeabilization, MOMP) leads to efflux of proteins, resulting in the assembly of a caspase-activating complex known as apoptosome. Both pathways converge at the mitochondria. Several factors among the mitochondrial proteins that are released as a result of MOMP can promote caspase-independent cell death, which can also result from stimuli that cause Lysosomal Membrane Permeabilization (LMP), resulting in the release of cathepsin proteases into the cytosol. Such cathepsins can also trigger MOMP, thereby stimulating the mitochondrial pathway of apoptosis. ROS: Reactive Oxygen Species. Question marks point at mechanisms that are still not fully understood. Figure adapted from [Maiuri et al., 2007].

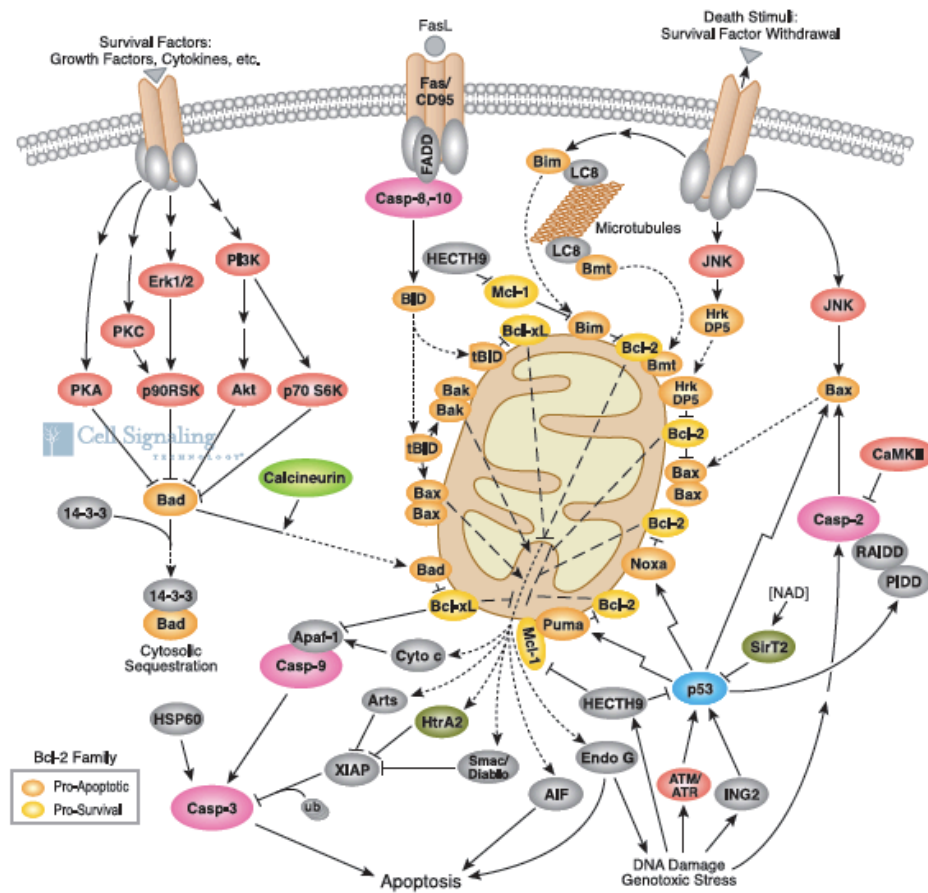


**Figure 1.2: Mitochondrial control of programmed cell death.** Mitochondria play a crucial role in programmed cell death as different routes converge on them. In the center, stimulation of CD95/Fas by its ligand leads to activation of the extrinsic pathway, in which active caspases catalytically cleave protein Bid . The active, truncated product tBid then translocates to mitochondria and activates Bax and Bak and further caspase activation. It has been shown that the relative ratio of pro-apoptotic Bax and anti-apoptotic Bcl-2 determine the susceptibility of the cell to programmed cell death driven by mitochondria [Korsmeyer, 1999]. Whether and how the pore is formed remains a controversial topic in the field of cell death research [Youle and Strasser, 2008]. The left-hand side shows prevention of apoptosis by inhibiting pro-apoptotic protein Bad in presence of survival factors. In the intrinsic pathway (right-hand side), growth factor withdrawal and other sources of stress such as viral infection leads to activation of JNK [Ley et al., 2005] and pro-apoptotic proteins such as Bim, in turn leading to inactivation of anti-apoptotic Bcl-2. Cartoon -but not the legend text- extracted from www.cellsignal.com

Permeabilization (MOMP) and thus release of pro-apoptotic factors including cytochrome c [Korsmeyer et al., 2000]. Thus, both pathways can converge at mitochondria (see the center of **figure 1.2**). This means that in addition to the very well established role in generation of adenosine triphosphate to be used by the cell as chemical energy [McBride et al., 2006], mitochondria play a central role in programmed cell death. Due to that, the author of "Means to an end: apoptosis and other cell death mechanisms", a book of highly recommended reading [Baehrecke, 2011], designates mitochondria "the suicide capsule of the cell". For an extended review of mitochondria as the central control point of apoptosis, the reader is referred to [Desagher and Martinou, 2000].

**Function and morphology of mitochondria in disease and health** Mitochondria are known to be the powerhouse of the cell, producing the majority of the cells biochemical energy via a process termed oxidative phosphorylation [McBride et al., 2006]. After being degraded from nutrients, electrons are carried by NADH and FADH<sub>2</sub> to the electron transport chain sitting in the inner mitochondrial membrane. There, electrons are passed along a series of respiratory enzyme complexes I-V located in the inner mitochondrial membrane. The energy released by this electron transfer is used to pump protons across the membrane. The resultant electrochemical gradient is expressed largely as a negative membrane potential of the order of 150-200 mV to the cytosol. That potential  $\Delta\psi_m$  enables another complex, adenosine 5'-triphosphate (ATP) synthase, to synthesize the energy carrier ATP, which is then transported to the cytosol [Saraste, 1999].

Channels, pumps and exchangers allow extracellular stimuli to induce increases in cytoplasmic  $Ca^{2+}$  concentration, that in turn induce specific cellular responses, e.g. contraction, secretion, proliferation or cell death [Rizzuto et al., 2009]. Mitochondria have also been shown to play a pivotal role in calcium signaling, as it has been shown that  $Ca^{2+}$  accumulation at the mitochondria contributes to shaping cytosolic  $Ca^{2+}$  fluctuation, which in turn modulates the above-mentioned cellular functions [Brini, 2003]. It has been shown that mitochondrial populations within the cell can change in number and morphology during development, the cell cycle or when challenged with various toxic conditions [Karbowski and Youle, 2003]. In addition, mitochondria have been shown to regulate a number of other metabolic tasks [McBride et al., 2006].

Damaged mitochondria also cause organ injury by several mechanisms, including the diminished cellular energy status (energy stress), production of reactive oxygen species (oxidative stress), disturbance of ionic balance, cytochrome c release and induction of apoptosis. In turn, such alterations have been shown to be linked to cancer, diabetes and myopathies [Kuznetsov and Margreiter, 2009].

Morphology is itself a cornerstone of mitochondrial function. Mitochondria are dynamic organelles that move. In addition, they fuse and divide, becoming a complex structure that can be seen as a network of (i) elongated and highly interconnected filaments, (ii) fragmented units, or (iii) a combination of both. The number and morphology of mitochondria within a cell are a function of regulated rates of fusion and fission events [Sesaki and Jensen, 1999]. Further, mitochondria dimensions change during the cell cycle and vary considerably in size [Kennady et al., 2004] and interconnectivity. Mitochondrial architecture and morphology are regulated by a family of GTPases, which induce mitochondrial outer membrane permeabilization [Karbowski and Youle, 2003]. As introduced above, this in turn leads to efflux of pro-apoptotic proteins to the cytosol and ultimately leads to cell death. In addition, although the exact mechanism remains unknown, members of the Bcl-2 protein family have been reported to become active during apoptosis and subsequently prevent mitochondrial fusion as shown widely in the literature (see e.g. [Karbowski et al., 2004]) and reproduced by us (see **figure 1.3**). The role of Bcl-2 proteins during cell death is further described in the following section. For an extended review on the dynamics of mitochondrial morphology, please see [Karbowski and Youle, 2003].

**BCL2 family members & mitochondrial permeability transition** The B-cell lymphoma-2 (Bcl-2) family of proteins comprises in mammals at least 12 core proteins, which display a number of activities from inhibition to promotion of apoptosis [Youle and Strasser, 2008]. The BH3 motif is common to all proteins of the family. BH3-only proteins promote apoptosis by interacting with and regulating the core Bcl-2 proteins. In turn, the Bcl-2 family strictly controls the mitochondrial pathway of apoptosis. Although still not fully understood, the pro-apoptotic Bcl-2 family members BAX and BAK exhibit a



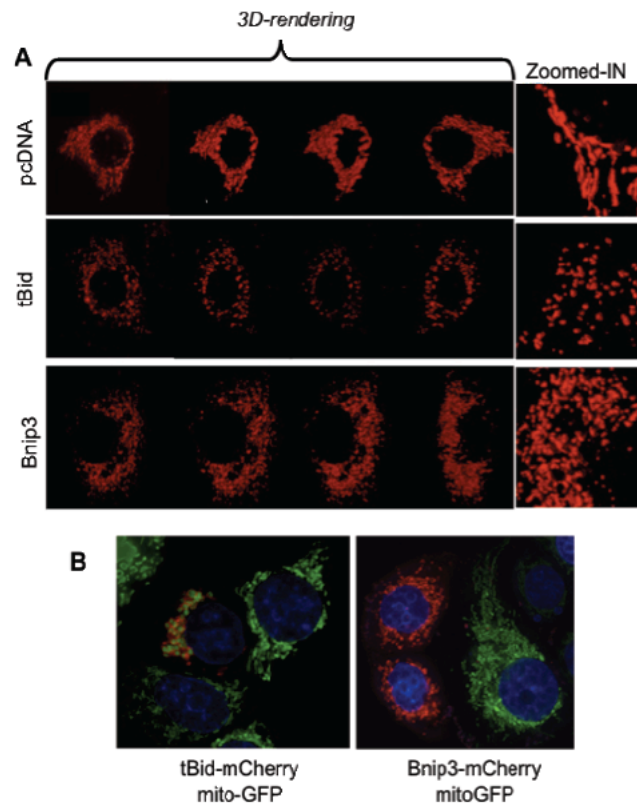


**Figure 1.3: BH3-only proteins regulate mitochondrial morphology changes.** (A) MCF-7 cells were cotransfected with mito-mCherry and BH3-only proteins (tBid or Bnip3). Images show that while control (pcDNA, mCherry alone) exhibited a network-like morphological state, cells expressing tBid or Bnip3 display a fragmented state. (B) Reproduction of (A) is shown here, where MCF-7 stably expressing mito-GFP were transiently transfected with tBid-mCherry or Bnip3-mCherry. The exact mechanism of mitochondrial morphology regulation by BH3-only proteins is unknown [Karbowski et al., 2004]. Performance of experiment and acquisition of high-resolution wide field images by Yara Reis

crucial role for inducing permeabilization of the outer mitochondrial membrane and the subsequent release of apoptotic molecules e.g. cytochrome c and DIABLO -otherwise known as SMAC-. The above-mentioned anti-apoptotic effect is then achieved by family members such as Bcl-2 and Bcl-XL by inhibiting BAX and BAK. The exact mechanisms of activation of pro-apoptotic Bax and Bak is unclear: evidence exists that BH3-only members repress anti-apoptotic members, which in turn inhibit Bax and Bak [Willis et al., 2007, Youle and Strasser, 2008], while other models suggest direct activation of Bax and Bak by BH3-only proteins [Youle, 2007, Youle and Strasser, 2008]. Subsequently, Bax and Bak are thought to polymerize and form pores in the mitochondrial

outer membrane, thereby triggering the release of the above-mentioned apoptotic molecules. Nevertheless, the biochemical nature of such pores is not yet fully understood; neither it is the induction by Bax and Bak of a change in mitochondrial morphology to a fragmented state at the same time of, or immediately after, cytochrome c release [Martinou and Youle, 2006].

### **1.1.2 Survival & the MAPK cascade**

On the flip side of the cellular life and death decisions, processes such as cell proliferation, differentiation and migration are regulated by the Mitogen-Activated Protein Kinase (MAPK) cascade. Here, a signaling cascade is activated by a broad spectrum of extracellular stimuli and regulates cell response through transduction of cell-surface signals to the nucleus via phosphorylation of protein kinases, which ultimately translocates to the nucleus to phosphorylate specifically targeted transcription factors, thereby directly regulating transcription.

The first step in the activation of the cascade is the binding of a stimulus to the extracellular region of a receptor tyrosine kinase (RTK). Growth factor binding has generally been shown to activate RTKs by inducing receptor dimerization, although some receptors such as the insulin receptor have been shown to be expressed on the cell surface as dimers [Ward et al., 2007]. Once activated, the first substrates that RTKs phosphorylate are the receptors themselves and the resulting phosphotyrosines function as sites for the assembly of downstream signaling molecules that are then recruited to the receptor [Lemmon and Schlessinger, 2010], such as adaptor protein Grb2, a guanine nucleotide exchange protein such as Sos and a small GTP binding protein. When activated at the receptor, such complex is able to phosphorylate the MAPK most upstream of the cascade.

The cascade of signals was termed "mitogen-activated" because the first member discovered, the extracellular signal-regulated kinase 1 (ERK1), is activated in response to growth factors [Cargnello and Roux, 2011]. However, MAPKs are involved in functions *a priori* paradoxical such as inflammation, apoptosis and the stress response [Zhang and Liu, 2002]. In mammalian cells, the cascade can be divided in three main routes that have been characterized. Each route

is composed of at least three sequentially acting kinases: a MAPK, a MAPK kinase (MAPKK) and a MAPKK kinases (MAPKKK). Currently at least 14 MAPKKKs, 7 MAPKKs and 12 MAPKs have been identified in mammalian cells (see **table 1.1**) [Zhang and Liu, 2002].

**Table 1.1: Components of the MAPK pathways in mammalian cells.** Table extracted from [Zhang and Liu, 2002]

MAPKKK	MAPKK	MAPK
Raf-1, A-Raf, B-Raf, Mos, TAK1, MUK, SPRK, MST, MEKK1, MEKK2, MEKK3, MEKK4, Tpl-2, ASK	MEK1(MEKK1), MEK2(MKK2), MKK3, MKK4, MKK7	ERK1, ERK2, p28a, p38b, p38g, p38d, JNK1, JNK2, JNK3, ERK3, ERK4, ERK 5

Next, we review the routes in which said kinases have been classified, the stimuli that activates them and the cellular response triggered.

**ERK pathway** ERK has been the best characterized MAPK. ERK1 and its isoform ERK2 share 83% amino acid identity and are activated by growth factors, including platelet-derived growth factor (PDGF), epidermal growth factor (EGF), nerve growth factor (NGF) and insulin. Additional alternatively spliced variants of ERK1 have been described which appear to have different localization and tissue distribution [Cargnello and Roux, 2011].

All components of the ERK module are cytosolic in quiescent cells [Chen et al., 1992]. Once activated by these ligands, ERK1/2 accumulates in the nucleus and phosphorylates a large number of substrates (see **figure 1.4**), thereby playing a crucial role in the control of cell proliferation. For instance, ERK substrate c-Fos is associated to c-Jun upon phosphorylation to form AP-1 complexes [Whitmarsh and Davis, 1996, Cargnello and Roux, 2011]. AP-1 is required for the expression of cyclin D1 [Shaulian and Karin, 2001]. In turn, cyclin D1 is a protein that interacts with cyclin-dependent kinases and enables  $G_1/S$  transition and cell cycle progression [Cargnello and Roux, 2011].

**JNK pathway** The JNK (also termed stress-activated protein kinase (SAPK)) signal transduction is implicated in several physiological processes (see **figure 1.4**) and is activated in response to various cellular stresses such as heat

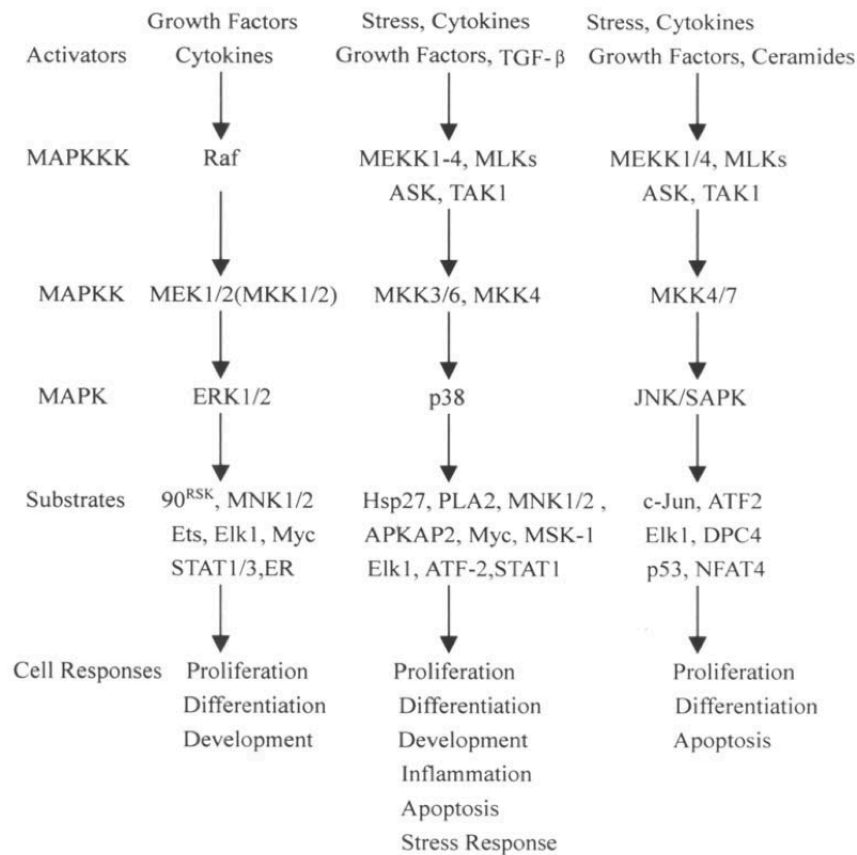


**Figure 1.4: Major MAPK signaling cascades in mammalian cells.** Numerous points of crosstalk are known that are not shown here to better illustrate the different routes. Scheme extracted from [Zhang and Liu, 2002]

shock, ionizing radiation, oxidative stress, DNA-damaging agents, cytokines, UV irradiation, growth factor deprivation and, to a lesser extent, by growth factors [Kyriakis and Avruch, 1996]. When activated, a large proportion of JNK translocates to the nucleus and activates a range of transcription factors including p53 and ATF-2. The fact that not all active JNK translocates to the nucleus suggests that there still are cytoplasmic substrates to be discovered [Cargnello and Roux, 2011]. In addition, research on tissue-specific knockout animals highlights that many tissue-specific roles of JNK have yet to be elucidated [Bogoyevitch et al., 2010].

**p38** The most important member of a third route of the MAPK pathway is p38. Similar to JNK, p38 is strongly activated by stress stimuli and is therefore also termed stress-activated protein kinase 2 (SAPK2). These stim-

uli consist at least of environmental stress, inflammatory cytokines, oxidative stress interleukin-1 and tumor necrosis factor alpha [Cuadrado and Nebreda, 2010]. At least four isoforms of p38 have been found, which can all be phosphorylated by the MAPK kinase MKK6 [Zhang and Liu, 2002]. These isoforms are present in the nuclei of quiescent cells and have been shown to translocate to the nucleus of cells subjected to the above-mentioned stresses; However, it has also been shown that one of the isoforms preferentially accumulates in the cytosol [Cuadrado and Nebreda, 2010]. The mechanism of translocation to the nucleus remains elusive [Cargnello and Roux, 2011]. When activated, p38 plays a major role in a number of mechanisms (see **figure 1.4**), one of them being production of pro-inflammatory cytokines.

**Atypical MAPKs** Recent studies have progressed into the function of other groups of MAPKs, which are classically termed "atypical MAPKs". Amongst others, the reason for such designation is that atypical kinases are organized into classical three-tiered cascades [Cargnello and Roux, 2011]. A number of other characteristics are not shared between atypical and traditional MAPKs. For further insight along these lines, the reader is referred to [Coulombe and Meloche, 2007].

**Intertwined topology and complex dynamics** The three main routes of MAPK signaling described above are not isolated. In fact, mammalian p38 and JNK kinases have most of their activators shared at the MAP3K level, e.g. MEKK1, MEKK4, ASK1, TAK1, MLK3 and TAOK1 (see **figure 1.5**). In addition, some MAP2K enzymes may activate both p38 and JNK (MKK4), while others are more specific for either JNK (as it is the case of MKK7) or p38 (e.g. MKK3). Due to these interactions that constitute points of crosstalk, there are very few stimuli that can elicit JNK activation without simultaneously activating p38 or viceversa [Cargnello and Roux, 2011]. Although mostly studied for their role in response to stress, the p38 kinases have also been shown to be important in regulation of proliferation and survival. For instance, it has been shown that p38 $\alpha$  negatively regulates cell cycle progression at the  $G_1/S$  and  $G_2/M$  transitions by downregulation of cyclins [Thornton and Rincon, 2009]. The *opposite* has also been reported: in [Xia et al., 1995] the authors show that concurrent inhibition of ERK and activation of JNK-p38 are crucial for induc-

tion of apoptosis in PC-12 rat pheochromocytoma cells upon withdrawal of nerve growth factor. Along these lines, and regarding the apoptotic pathways previously introduced in **section 1.1.1**, it has also been shown that induction of apoptosis by activation of the CD95 death receptor leads to activation of caspase 8, which in turn led to activation of ERK1/2 and p38 MAPK activation [Kober et al., 2011]. Overall, the number of proteins which interact with members of other cascades is large. This raises the following question: if one ligand can activate different cascades through cross-signaling, how is the cell able to trigger one specific response, instead of all of the responses regulated by said cascades? We explore the answer to this question and further review the mechanisms that can grant specificity of signaling in **section 1.3**.

In addition to its intertwined topology, another challenge hinders our understanding of the mechanisms regulating the MAPK cascade: its topology appears to be highly flexible and modifies according to time and context. Indeed, it has been reported that cell fate decisions are specified by the dynamic ERK interactome. In [von Kriegsheim et al., 2009] the authors showed that upon induction of differentiation, a number of proteins change their binding to ERK, indicating that ERK dynamics and differentiation are regulated by distributed control mechanisms rather than by a single master switch.

As a matter of fact, the MAPK signaling cascade has often been used as a prototype to illustrate the lack of evidence as to how emerging networks are regulated in space and time, specially taking into account the extensive catalogues of signaling network components which have been compiled to date [Kiel and Serrano, 2011, Kholodenko and Kolch, 2008, Lemmon and Schlessinger, 2010, Kholodenko et al., 2010].

For instance, it has been shown that growth factor context determines the topology of the MAPK signaling network and that the resulting dynamics govern cell fate [Santos et al., 2007], but the mechanism for such ligand-specific topological change is yet unknown. In addition, it has been shown that receptor-activated proteins with inactivation processes that are growth-factor-dependent but also -independent encode distinct physical properties into transient and sustained ERK activation [Sasagawa et al., 2005].

Furthermore, depending on the cell type, the same growth factor can give

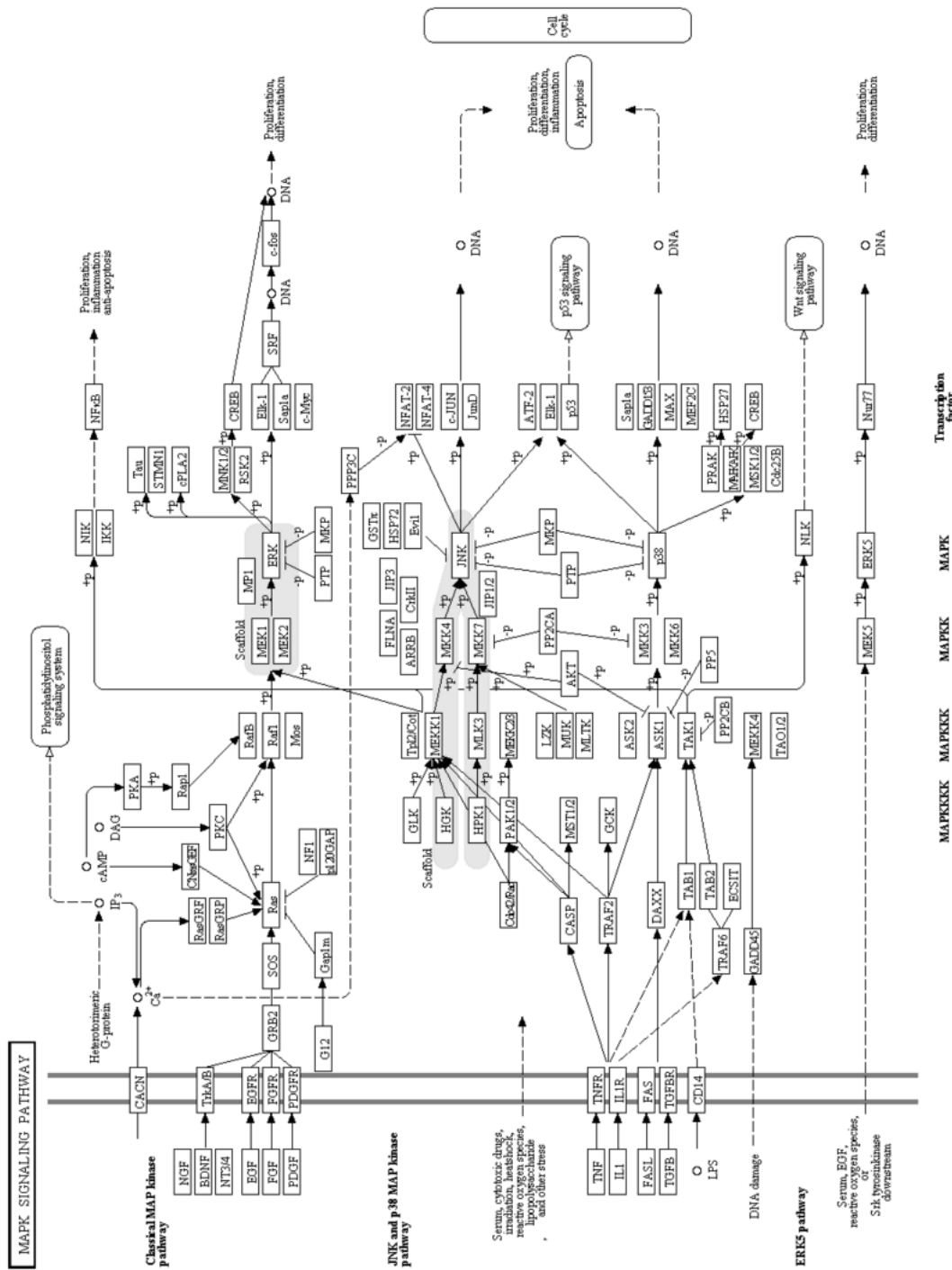


**Figure 1.5: Numerous points of crosstalk are known in the MAPK signaling cascade.** The three major routes in MAPK signaling, ERK, JNK and p38, are not isolated. Instead, they consist of numerous interactions that constitute points of crosstalk between them. For instance, see the JNK and p38 routes, which share a large number of effectors mainly at the MAPKKK level. In response to the previously described stimuli, a complex spatio-temporal balance of the proteins represented here regulates proliferation, differentiation, development, inflammation, apoptosis and the stress response. Scheme -not the legend- extracted from the kyoto encyclopedia of genes and genomes, <http://www.genome.jp/kegg/>

rise to either transient or sustained ERK activation kinetics and responses to perturbations, such as alterations of kinetic constants, could be different [Kiel and Serrano, 2009]. All of this happens despite the fact that many of the components of signal transduction pathways are present in the majority of the cells [Pontén et al., 2009]. To understand the above-mentioned mechanisms of signaling, the authors of [Kiel and Serrano, 2011] postulate the following challenges:

- Analyzing the role of spatio-temporal signaling and the role of scaffolds in RTKs activation potentially improved by the development of new imaging tools
- Investigating the role of protein concentration and competition for signaling
- Integrating alternative splicing into signaling pathways compiled in literature
- Improving our understanding of cell-type specific signaling and the differences underlying development and differentiation

In conclusion, although our understanding of these mechanisms increases rapidly, the complex and cell-type-dependent dynamics that regulate mitogenic signaling have yet to be elucidated.

### **1.1.3 Cancer signaling**

While mitogenic signaling is poorly understood in normal cells as introduced in the previous section, the mechanisms which grant cancer cells its sustained proliferative signaling are better established [Lemmon and Schlessinger, 2010]. To date, 8 hallmarks have been described as reviewed in [Hanahan and Weinberg, 2011], which enable tumor growth and metastatic dissemination: sustaining proliferative signaling, evading growth suppressors, resisting cell death, enabling replicative immortality, inducing angiogenesis, activating invasion and metastasis, reprogramming of energy metabolism and evading immune destruction. The mechanisms that grant cancer cells the ability to sustain proliferative signaling and to resist cell death are closely related to the work presented in this thesis and hence will be further reviewed.



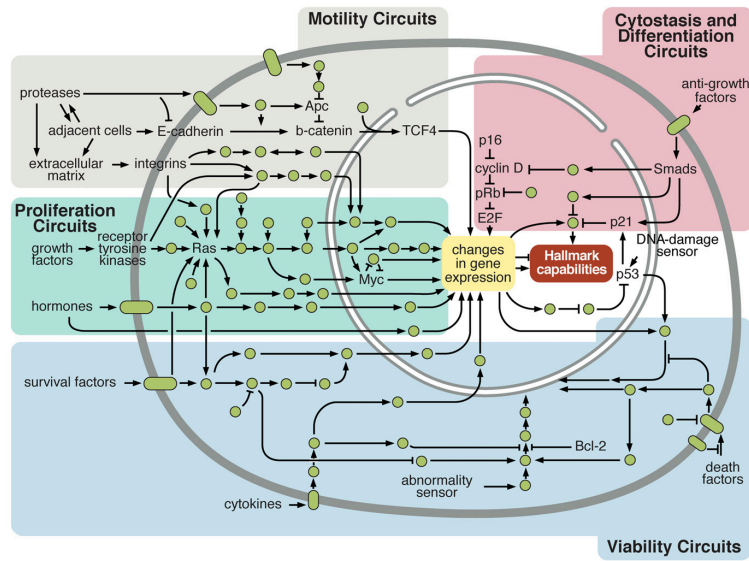


**Figure 1.6: Intracellular signaling networks regulate the operations of the cancer cell.** A complex integrated circuit consisting of four pathways regulates the operations of the cancer cell. Proliferation and viability circuits have been introduced in [section 1.1.1](#) and [1.1.2](#). Each of these pathways is connected to signals from the tumor microenvironment. The figure addresses only a subset of hallmark capabilities of cancer cells and was extracted from [Hanahan and Weinberg, 2011].

To maintain proliferative signaling, the majority of melanomas have been shown to harbor somatic mutations in the kinase signal transduction pathways RAS-RAF-MEK-MAPK and PI3K-AKT, which play a major role in regulation of proliferation (see [figure 1.6](#)), as reviewed in [Davies and Samuels, 2010]. A representative example of prevalent activating mutation is BRAF, which has been shown to be mutated in 50-70% of melanomas and in 80% of those cases the specific mutation was V600E [Davies et al., 2002]. Activating mutations affecting the structure of BRAF result in constitutive signaling through the MAPK pathway [Davies and Samuels, 2010], which has been introduced in [section 1.1.2](#). Along these lines, mutations in PI3-kinase isoforms have been detected in several tumor types, thereby hyperactivating the PI3-kinase and Akt signaling circuitry. We discuss the advantages to tumor cells of activating signaling at different intermediates in the context of their position in the network in [section 5.2.2](#). The prevalence of these mutations makes kinase signal transduction pathways an attractive target for therapy. A strategy with validated efficacy in preclinical studies relies on targeting BRAF with small molecule inhibitors such as Sorafenib, which has been shown to inhibit

the growth and survival of BRAF-mutant human melanoma cells [Karasarides et al., 2004]. Nevertheless, Sorafenib has exhibited disappointing clinical results; on the other hand, new mutant-specific BRAF inhibitor PLX4032, which targets mutated BRAF V600E selectively, has exhibited clinical efficacy [Hanahan and Weinberg, 2011]. In spite of that, resistance to treatment appeared after 8 months by mechanisms not yet understood [Fisher et al., 2010]. As our understanding of these details becomes increasingly sophisticated, it provides an important context for therapeutically countering the effects of pathogenic mutations in cancer [von Kriegsheim et al., 2009].

Another hallmark of cancer as reviewed in [Hanahan and Weinberg, 2011] is the ability to resist cell death. Here, the authors state that apoptosis is attenuated in those tumors that succeed in progressing to states of high-grade malignancy and resistance to therapy. The apoptotic machinery has been introduced in **section 1.1.1**, including the role of BCL2 family members and their role in mitochondrial permeability transition. Along these lines, P53 is able to induce apoptosis by upregulating expression of BH3-only proteins, which are members of the BCL2 family. Tumor cells circumvent apoptosis through loss of P53, thereby eliminating the critical damage sensor from the apoptosis-inducing machinery; in addition, a variety of other mechanisms such as increasing expression of anti-apoptotic regulators -e.g. Bcl-2 and Bcl-XL- have been shown [Hanahan and Weinberg, 2011].

Anti-cancer drugs have been shown to achieve their effect by activating apoptosis [Fadeel et al., 1999]. However, it is difficult to anticipate whether a tumor cell will or will not be sensitive to a pro-apoptotic stimulus or drug because the importance of specific processes varies dramatically from one cell type to the next; hence, multi-factorial, context-sensitive computational models will impact drug discovery [Spencer and Sorger, 2011].

## 1.2 Mathematical modeling of signal transduction networks

### 1.2.1 Data-driven modeling

A paradox in systems biology is that while current technologies allow gathering of high-throughput data, these large datasets by themselves often bring more confusion than understanding [Janes and Yaffe, 2006]. To circumvent this challenge, data-driven approaches build models based solely on analyzing the data itself. The majority of these approaches are also termed *reductionist*, since they are able to emphasize a reduced number of variables and their difference in the data while not requiring any prior knowledge. They are also termed *descriptive* approaches as opposed to *predictive* approaches, referring to the fact that the impossibility to include prior knowledge rules out the possibility to test hypothesis in the model, thereby limiting the prediction power (**figure 1.7**). Such formalisms are e.g. clustering and principal component analysis (PCA). An exception to that statement would be partial least square regression (PLSr), a technique based on PCA which enables hypothesis testing at a fundamental level. We next review the basic concepts of these well-established data-driven techniques and their application to modeling of signal transduction.

**PCA** PCA is a mathematical algorithm that reduces the dimensionality of the data while retaining most of the variation in the data set. In other words, it summarizes one data set. Given a dataset with  $n$  dimensions, new dimensions are calculated, i.e. the principal components. Once calculated, the principal components have the key feature that their number is smaller than the number of original variables, rendering the dataset intuitive to understand. Specifically, principal components are determined from the eigenvectors of the covariance matrix, where  $n$  eigenvectors can be calculated that represent the whole matrix. Using the corresponding eigenvalues, the eigenvectors that capture the most co-variation can be selected, in order to achieve a final space with a reduced number of dimensions. Each principal component is a combination of eigenvalue and eigenvector. By projecting the experimental data onto the principal components, these new dimensions can then be used for visualization, clustering or study of the data. For instance, PCA has been used in the

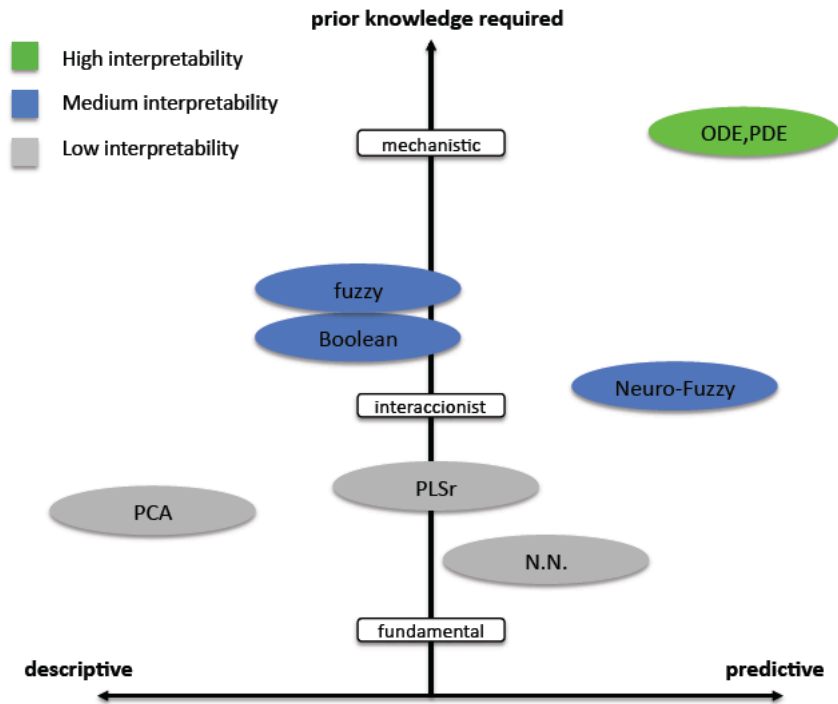


**Figure 1.7: Schematic overview of modeling techniques suitable for study of signal transduction.** A number of approaches have been used in the field of systems biology. The interpretability, i.e. potential insight gained, is high for mechanistic approaches and decreases the more fundamental and phenomenological the modeling approach is. Further details are described in the sections for individual methods.

field of systems biology to qualitatively discriminate apoptotic cell fates based on measured signaling profiles [Janes et al., 2004] and to explore genome-wide expression studies as reviewed in [Ringnér, 2008].

**PLSr** PLSr is multivariate analysis technique similar to PCA in that it summarizes the data by calculating new principal components that best capture the covariance. The above-mentioned limitation of PCA, i.e. the impossibility to incorporate and test hypothesis is addressed in PLSr. To that end, a PLSr analysis consists of two datasets and seeks to identify optimal principal components-based dimensions from a proposed relationship between the two datasets. Here, one of the datasets contains the *dependent* variables that are hypothesized to be responses to the *independent* variables on the other dataset. Therefore, the first dataset forms an independent group of variables  $X$  and the variables that are a response form a dependent group  $Y$  for the proposed relationship  $Y = f(X)$ . Finally, said relationship is quantified by reducing the

original dataset to a principal-component space and subsequently regressing the independent and dependent principal components. This is analogous to extracting the molecular-level evidence in the data that quantitatively support the hypothesis posed by the model; further, both the efficacy of PLSr for predicting data and the significance of the prediction are determined by the validity of the underlying hypothesis [Janes and Yaffe, 2006]. In [Janes, 2005], PLSr was used to calculate principal components that were able to capture apoptotic response in one principal component and survival response in a distinct principal component. Subsequently, identification of unsuspected autocrine circuits activated by cytokines revealed new molecular mechanisms of apoptosis signaling.

## 1.2.2 Physicochemical modeling

**The mechanistic approach** Conversely to data-driven approaches, physicochemical modeling describes reactions between molecules in terms of equations derived from physical and chemical theory (**figure 1.7**). The most common formalism used in physicochemical modeling to describe signaling pathways are Ordinary Differential Equations (ODEs), which can be coupled in a system of equations. ODE systems represent the rate of production and consumption of individual biomolecular species, e.g. proteins. For a protein  $X$ , the rate of change  $\frac{d[X]}{dt}$  is represented in terms of mass action kinetics. The mass action law states that rates of a reaction are proportional to the concentrations of the reacting species, and hence each biochemical transformation is represented by an elementary reaction with forward and reverse *kinetic* rate constants [Aldridge et al., 2006].

In 1913, Leonor Michaelis and Maud Menten employed the above-described principles to propose a mathematical model to approximate the kinetics of the reaction between an enzyme and its substrate as translated from their original article in [Michaelis et al., 2011]. Based on those principles, physicochemical modeling can be applied to a cascade of reactions, such as the one introduced in **section 1.1.2** for the MAPK signaling pathway. **Figure 1.8** illustrates the steps to construct a model to represent the sequence of events from ligand

binding to the receptor, activation of the dimeric receptor featuring two phosphorylation sites, subsequent activation of a kinase and phosphorylation of its substrate.

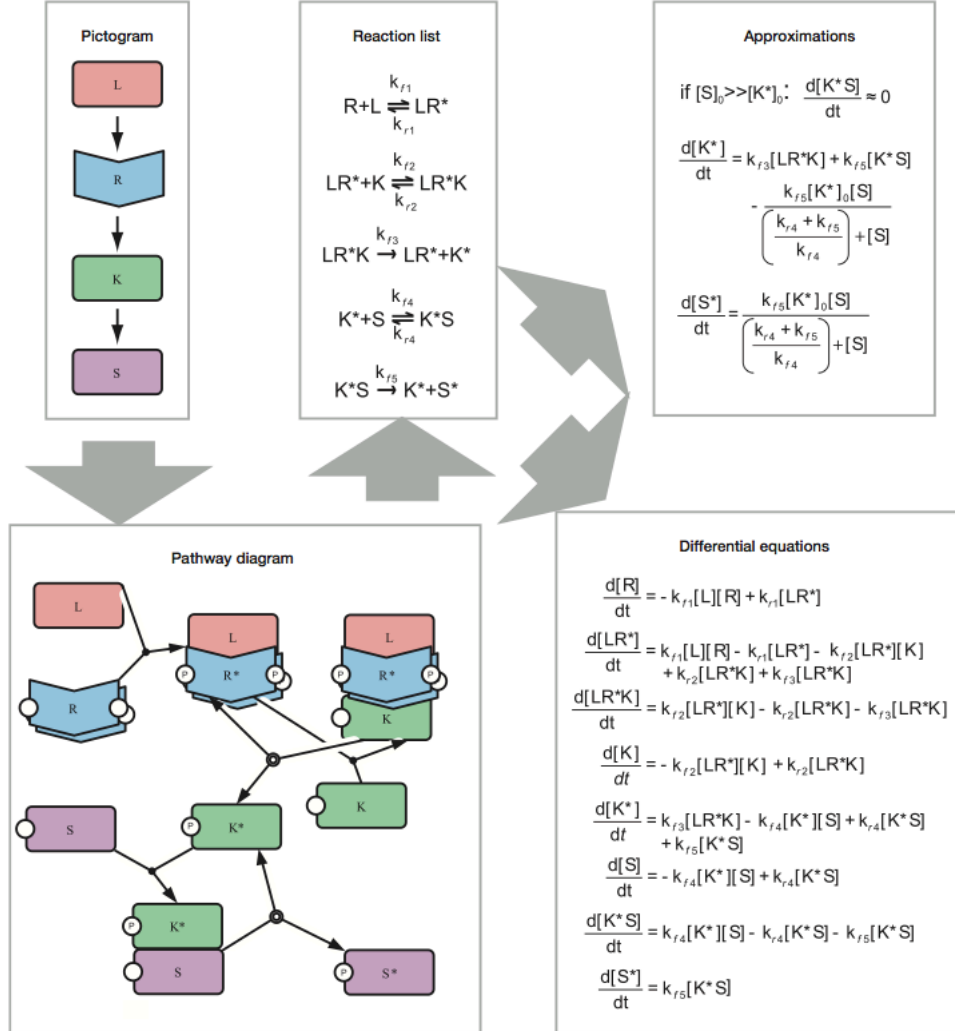


**Figure 1.8: Steps in physicochemical model implementation.** A pathway map, as shown in the pictogram, is an abstracted representation of biomolecules and their interactions. A more formal *pathway diagram* represents the complexes formed and the sequence of events from ligand (L) binding to the receptor (R), activation of the dimeric receptor featuring two phosphorylation sites (P), subsequent activation of a kinase (K) and phosphorylation of its substrate (S). These reactions can be formalized as shown in the reaction list. From the list of reactions, a system of differential equations can be defined using rate laws as e.g. mass action kinetics to calculate reaction rates. Approximations can be achieved by taking simplifying assumptions such as the Michaelis-menten approximation, which assumes a rapid equilibrium of an intermediate complex and thus reduces the number of species in the model. For further details, see the main text. Figure adapted from [Aldridge et al., 2006]

When constructing a model, representation of different localization of a biomolecule is achieved by compartmentalization, i.e. each species is assigned a cellular space. Two fundamental assumptions for application of compartmentalization to ODEs are: (i) the compartment is well-mixed and transport within is instantaneous and (ii) transport between compartments is slower and associated with a rate [Aldridge et al., 2006]. For those cases in which these assumptions are not satisfied, partial differential equations can represent biochemical systems in continuous time and space. After model construction, the values of the parameters, i.e. the rate constants and the initial conditions, need to be determined. Parameters can be measured directly, considering whether the rates in the experiment match those in physiological conditions. In the cases in which measuring all rate constants and initial conditions is not the scope of the study, parameters can be used from the literature. This is a disadvantage with respect to other methods presented in this dissertation, as it can be troublesome to assume that protein concentrations are equal to those from other studies; the reason for that is that it has been shown that even clonal populations display strong cell-to-cell variations of the level of the same protein with a standard deviation of 20–30% of the mean [Sigal et al., 2006, Fritsche-Guenther et al., 2011]. Another alternative is to estimate said parameters using experimentally acquired data for training. Estimation consists then in the computation via regression of the range of parameter values, in which the model matches the experimental data best. In the noise-free case,  $2n + 1$  observations are necessary to estimate  $n$  parameters [Aldridge et al., 2006].

Once a model is parameterized, simulation of the model enables derivation of novel insight e.g. by testing novel hypothesis implemented in the formalism and analyzing the corresponding prediction as performed for instance in [Fritsche-Guenther et al., 2011] and [Fey et al., 2012]. An interesting turn was taken in [Ma et al., 2009], where the authors provide a framework to define the range of network topologies that can achieve biochemical adaptation, where each network is represented by a system of ordinary differential equations. This study provided valuable insight on the motifs that can acquire adaptation in general.

**Current challenges in physicochemical modeling** Overall, physicochemical models are powerful tools to represent signaling pathways in a physically realistic manner, thereby aiding its understanding. However, the following challenges hinder the applicability of mechanistic models to the study of signal transduction:

- *Kinetic* models use prior knowledge to represent specific molecular reactions and hence work best in pathways that are relatively well-established, with its components and specific connections being known; therefore, when prior knowledge is sparse, data-driven statistical models are more appropriate [Aldridge et al., 2006].
- In those cases in which sufficient prior knowledge is available it is important to consider that, in models based on differential equations, each new protein can give rise to a large number of model species differing in location, binding state and degree of post-translational modification. Therefore, differential equation models are currently limited to  $\pm 20$  gene products and 50-100 model species [Spencer and Sorger, 2011].
- Signaling pathways exhibit flexible circuitries, with topologies that are modified in time and space. For instance, it has been shown that growth factor context determines the topology of the MAPK signaling network and that the resulting dynamics govern cell fate [Santos et al., 2007]. In fact, signaling networks emerge depending on the context as widely reviewed [Kholodenko and Kolch, 2008, Kholodenko et al., 2010, Santos et al., 2007, Grecco et al., 2011, Kiel and Serrano, 2011] and introduced in **section 1.1.2**. In these cases, assuming a topology that has been reported for other cell lines or circumstances can introduce a bias to the model.

We next review other modeling approaches that can constitute a solution to the problems mentioned above. Nevertheless, it is crucial to note that a trade-off exists: the more qualitative and phenomenological the modeling framework, the less mechanistic the insight [Spencer and Sorger, 2011].



### 1.2.3 Logic modeling

**Scope of different logic formalisms** To circumvent the challenges in terms of prior physicochemical knowledge required by mechanistic approaches as described in **section 1.2.2**, logic-based models can be used. Logic models are based on logic rules that can be implemented to relate two species using only the measurements of these two species and the information that they are related. To that end, logic models enable mapping of input data into output data by using logic implications, i.e. IF-THEN logic rules such as IF phosphorylation of protein  $P$  is *on* THEN activity of transcription factor  $TF$  is *on*. Such statements are based on the principles of aristotelian logic. Hence, it applies that the first part of the sentence spanning until THEN is called the premise or the antecedent of the rule, and from THEN onwards the conclusion or consequent is stated. When solely two states are defined as possible for the species at study i.e. on and off, the formalism is then two-state discrete logic, also known as Boolean logic. Two-state discrete (Boolean) logic is the simplest logical representation and offers a useful characteristic: it has no free parameters, meaning that logical models covering the same set of nodes differ only in topology as exploited in [Saez-Rodriguez et al., 2009]. Here, the authors used multi-state logic for functional analysis of extensive signal transduction networks. Increasing the number of states that the species can reach increases accuracy, but it is limited to discrete classification. As a solution, fuzzy logic (FL) offers intermediate states (see **figure 1.9**).

In the specific case of fuzzy logic, sets such as *high*, *medium*, or *low* are fuzzy sets to which the continuous experimental data belongs. This is a difference of key importance with respects to Boolean logic, as fuzzy sets have unsharp boundaries, i.e. measurements do not either belong to them or not. Instead, measurements can belong to the fuzzy sets to a certain degree, requiring a transformation known as fuzzification performed by the so-called membership functions [Zadeh, 1968]. In the next paragraph, we further describe fuzzy logic modeling as a means to study signal transduction networks. For a review on different logic formalism and their application to highly detailed case studies of signal transduction, the reader is referred to [Morris et al., 2010].

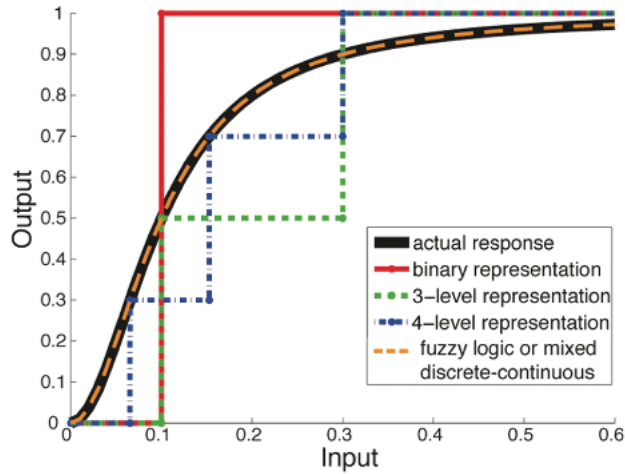


**Figure 1.9: Accuracy comparison for different logic formalisms.** The relationship between two biological species, in which the input has an effect on the output is shown here with the black line representing the experimental data. Approximations of the same relationship are represented using logic formalisms of 2,3 and 4 levels or states. Fuzzy logic and mixed discrete-continuous enable achieving the best accuracy. Figure adapted from [Morris et al., 2010].

**Fuzzy logic in modeling of signal transduction networks** To characterize the relationship between input and output membership functions, two types of fuzzy logic systems have been widely used for inference. In Mamdani or *linguistic* models [Mamdani and Assilian, 1999], the output membership functions are fuzzy sets, and hence a model can be represented as shown in **figure 1.10**.

In 1985 Takagi and Sugeno proposed an extension of the fuzzy logic formalism with  $i$  rules of the form *IF*  $u_1 = A_{i1}$  *AND* ... *AND*  $u_p = A_{ip}$  *THEN*  $y = f_i(u_1, u_2, \dots, u_p)$ , where  $u_i$  are the inputs and  $A_i$  are the fuzzy sets as described in [Takagi and Sugeno, 1985, Nelles, 2002]. Hence, in takagi-sugeno systems (TKS) the output is not a fuzzy set but a weighted combination of the input sets:

$$y = w_{i0} + w_{i1}u_1 + w_{i2}u_2 + \dots + w_{ip}u_p \quad (1.1)$$

This formalism renders the output less interpretable, since it not linguistic; conversely, the output of a mamdani system is a fuzzy set, and hence linguistic. However, this restriction of the output is a simplification that enables learning methods to estimate the weights  $w$  of the combination. Using both formalisms of fuzzy logic, a number of approaches have been implemented to encode signaling networks. These approaches can be grouped in two major

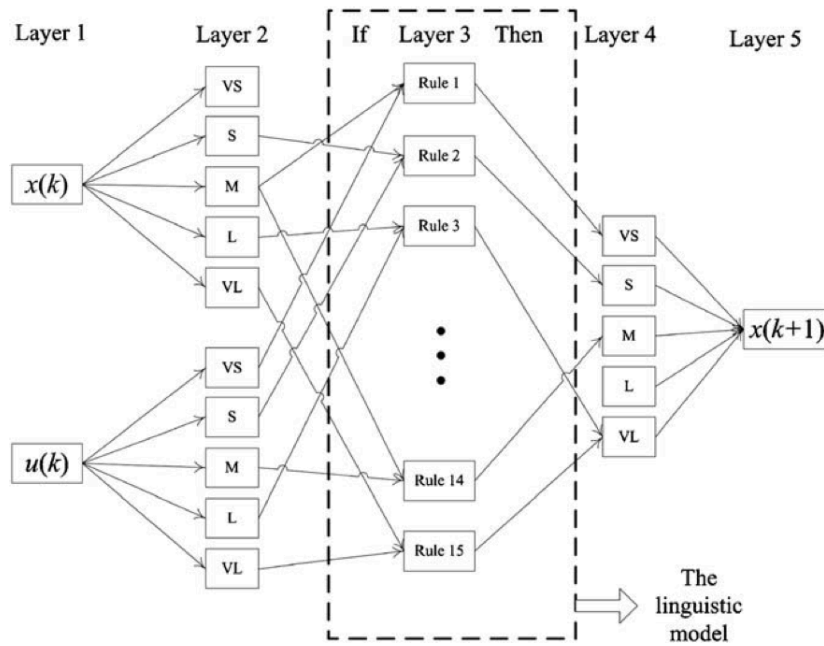


**Figure 1.10: Representation of a dynamic linguistic fuzzy logic model.** The model approximates the state of a protein  $x(k+1)$  at time  $k+1$  from its state at the previous time point  $x(k)$  and depending on the value of the input  $u(k)$  at time  $k$ . A membership function -not shown- transforms the experimental measurements of the inputs  $x(k)$  and  $u(k)$  into the fuzzy sets very small (vs), small (s), medium (m), large (l) and very large (vl). Layer 3 represents the rules, which specify which sets are related: rule 1 would be expressed as if  $x(k)$  is medium and  $u(k)$  is very small, then  $x(k+1)$  is very small. Note that this is termed linguistic model because the output membership functions (layer 4) are fuzzy sets. An alternative, non linguist, model is possible (see text). Figure -but not the text- extracted from [Huang and Hahn, 2009].

frameworks. In the first framework, models are constructed manually based on prior knowledge of topology and data. In [Aldridge et al., 2009], the authors established an approach to encode responses of colon cancer cells treated with combinations of pro-death and pro-survival cytokines successfully incorporating the role of time to model slow processes. In the same framework, FL was combined with other algorithms in order to represent hedgehog regulation of the cell cycle [Bosl, 2007]. This framework, however, has the limitation that one must manually implement the FL models, which is not only tedious but introduces the bias of own prior knowledge. To prevent this, we next review training strategies that enable fitting fuzzy logic models to experimental data.

### 1.2.4 Neuro-fuzzy modeling

**Different strategies to parameterize a fuzzy logic model according to experimental data** Another framework consists of studies, in which the parameters of the FL system are learned from the data by means of neural network training algorithms. Hence, need of extensive prior knowledge on the molecular interactions of the modeled network is circumvented by estimating the model parameters from the data.<sup>1</sup> A list of model qualities can be learned from the data, namely variables and the corresponding membership functions related in each rule [Chiu, 1994], number of rules [Wang and Palade, 2011] and type of membership functions with its corresponding parameters for both the premise and the consequent of the logic rule. Due to this broad spectrum of model qualities, the number of free parameters that need to be parameterized can range orders of magnitude.

In linguistic fuzzy logic models, a classical training approach includes learning the system rules including the number of rules and specific sets involved in each rule. In addition, the parameters of the membership function that are required to transform each data point into a fuzzy set -membership functions perform the so called fuzzification, see above- need to be estimated. To that end, approaches such as subtractive clustering can be used. Subtractive clustering is used to estimate the number of clusters in which a dataset can be grouped. To do so, each data point is considered a potential cluster center. Based on its distance to the neighboring data points, a potential is calculated, such that a data point with a high number of data points nearby has a high potential. The procedure of determining a new cluster center is repeated until the potential of all data points falls below a threshold [Chiu, 1994]. In terms of a linguist model such as the one described above, the resulting number of clusters of related data points determines the number of rules necessary to relate those data points, and the center of the cluster can be used to parameterize the membership functions. Adding to the number of free model qualities, once the number of rules and sets involved are learned, the membership functions representing all inputs and outputs need to be parameterized as well. To parameterize the dynamic model shown in **figure 1.10**, the authors of [Huang

---

<sup>1</sup>Fitting algorithms other than those in the framework of neural-networks are currently applied to fit FL systems. However, for historical reasons, such approaches are still termed neuro-fuzzy [Nelles, 2002].

and Hahn, 2009] analyze the sensitivity of the model to changes in the width of the premise membership functions, thereby determining which parameters need to be estimated from data in order to reduce the complexity of the model. Circumventing training of certain parameters was here crucial, as this approach rendered a highly accurate dynamic model model with 49 rules with inputs that were fuzzified by 5 membership functions into the sets very small (vs), small (s), medium (m), large (l) and very large (vl).

As described in the previous paragraph, a simplification of linguistic models termed Takagi-Sugeno exists, where the output is not a fuzzy set but a weighted combination of the input sets as shown in **equation 1.1**. Thereby, training of the number of rules, rule components and parameters of the consequent membership functions is avoided. Instead, only the weights  $w$  and the parameters of the premise membership functions need to be learned. For instance, a standard hybrid method was used to train a neuro-fuzzy Takagi-Sugeno model, which then enabled classification of electrocardiogram signals [Übeyli, 2009]. In this hybrid method, the least squares method is combined with the back-propagation gradient descent method. Firstly, in a forward pass the least squares method optimizes the consequent parameters with the premise parameters fixed. Subsequently, the backward pass uses the gradient descent method to adjust optimally the premise parameters corresponding to the fuzzy sets in the input domain.

**Scope of neuro-fuzzy models** When using FL-based methods in combination with training algorithms for modeling of signal transduction, the challenge lies in a definition of the system that renders the learned knowledge insightful. Specifically, data-trained systems, i.e. trained from the data rather than manually implemented, require a high number of parameters. While these parameters grant the system its flexibility, they also increase the risk of over-fitting, thereby lowering the expectation of meaningful new insight concerning the interactions regulating the network. To minimize the number of free parameters, in [Morris et al., 2011] rather than training a system with measurements at a range of time points, the authors successfully developed a constrained FL system that focus on specific states and employed it to elucidate interactions that were a priori possible but not present in actuality in the experimental data as well as interactions that were not described in the prior knowledge

network. An alternative is to explore different model setups in order to reduce the number of free parameters.

## 1.3 Properties of experimental data and their impact in modeling

In previous sections we discussed classical pathways of cell death and proliferation, together with a number of related mechanisms that are not yet understood. We continued to present methods based on mathematical modeling, which can be used to facilitate elucidation of such mechanisms. However, to apply a modeling formalism the intrinsic nature of the data needs to be taken into account. Challenges are e.g. the cell-to-cell variability acquired when measuring population data and the heterogeneity of the different events being experimentally measured such as morphological and functional features. Additionally, the complexity inherent to signaling described in **section 1.1.2** plays an important role when studying the response regulated by signaling networks. We next review concepts such as data treatment techniques, experimental methods and signaling mechanisms that are of critical importance when modeling analysis is employed to address these challenges.

### 1.3.1 Heterogeneity of measurements and cell-to-cell variability in experimental data

Understanding complex mechanisms requires a multi-factorial analysis. Neoplastic diseases constitute the prototype of problem, which requires study of several mechanisms at the same time, as it has been proposed that they are caused not by a single event, but by the intricate interplay of 8 hallmarks [Hanahan and Weinberg, 2011]. Systems biology seeks understanding of such biological processes by analyzing high-content, multivariate datasets that characterize how signaling pathways change in space and time to regulate different cell responses. To collect such datasets, the authors of [Albeck et al., 2006] describe some technologies that are currently employed in the field: Mass spectrometry, immunoblots, ELISA (and as an extension bead-based arrays), microarrays, flow cytometry and live-cell imaging (see **figure 1.11**). The authors further

enumerate the advantages and disadvantages of said methods, in which scientists ultimately need to choose between breadth and depth, low and high throughput, small versus large sample size, difficulty, fixed versus live cell and last, single-cell versus population measurements. We proceed to focus on the trade-off between single-cell and population measurements.

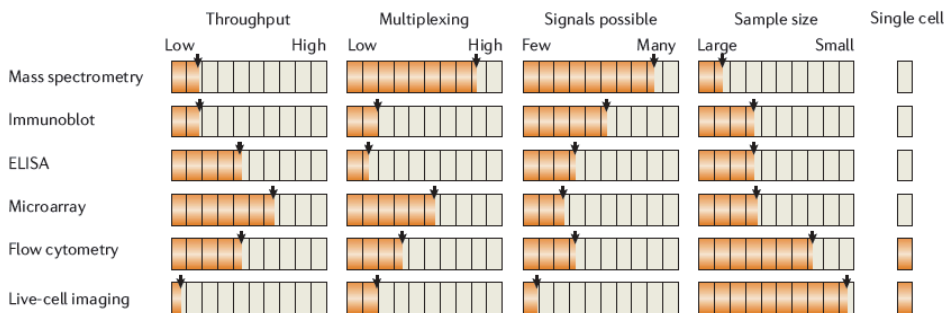


**Figure 1.11: Schematic overview of experimental techniques suitable for study of multivariate signal transduction.** Orange bars indicate the strength of each assay with regard to each criterion. Figure extracted from [Albeck et al., 2006].

When using population data, the comparison of measurements acquired using different assays, or heterogenous measurements via the same assay of variables of different nature e.g. protein concentration over time and morphology of a certain organelle, represents a challenge in terms of how to integrate the data. Traditionally, one could rely on comparison to the control measurement. However, several-fold differences can appear between variables or assays that are not proportional to the biological relevance of the changes measured. Along these lines, data pretreatment methods can correct for aspects that hinder the interpretation of the relationships existing in the experimental data. Well-established data pretreatment techniques are e.g. centering and unit variance scaling, which are calculated as shown in equations **1.2** and **1.3** respectively:

$$\tilde{x}_{ij} = x_{ij} - \bar{x}_i \quad (1.2)$$

$$\tilde{x}_{ij} = \frac{x_{ij} - \bar{x}_i}{\sigma_i} \quad (1.3)$$

where the mean  $\bar{x}_i$  is calculated as  $\bar{x}_i = \frac{1}{J} \sum_{j=1}^J x_{ij}$  and the standard deviation

$\sigma_i$  is calculated as  $\sigma_i = \sqrt{\frac{\sum_{j=1}^J (x_{ij} - \bar{x}_i)^2}{J-1}}$ . Hence, centering expresses all measurements as fluctuations around zero by removing the offset and focuses therefore in the differences and not the similarities; on the other hand, unit variance scaling uses the standard deviation as the scaling factor, which is different for every variable as described in [van den Berg et al., 2006]. In this study of high interest, the authors test different pretreatment methods in a metabolomics dataset and show how they have different impact on the interpretation of the results. Nevertheless, a disadvantage of population methods is that they neglect information underlying cell-to-cell variability.

Recently, it has been proposed that using cell-to-cell variability will define a new era in molecular biology [Pelkmans, 2012]. The reason for that is that research has focused on processes that are common between cells because of the technical difficulties in measuring the differences. Thereby, a rich source of information to understand cellular processes has been neglected. Contrary to population methods, current single-cell methods such as live-cell imaging enable study of the sources of cell-to-cell variability. Using a combination of mathematical modeling and live-cell microscopy, it has been elucidated that that naturally occurring differences in the states of proteins regulating extrinsic apoptosis are the primary causes of cell-to-cell variability in the timing and probability of death in human cell lines [Spencer et al., 2009]. This is of key importance, as it has been reported that even clonal populations display strong cell-to-cell variations of the level of the same protein with a standard deviation of 20–30% of the mean [Sigal et al., 2006, Fritsche-Guenther et al., 2011]. The topic of cell-to-cell variability is connected to the apparent complexity of signaling: indeed, it is possible that by studying signal transduction at the single-cell level it becomes clear that not all parts of a *a priori* complex pathway act together in a cell, but rather in a subpopulation of cells [Pelkmans, 2012]. It is however also possible that signaling pathways are highly complex, with topologies that are modified in time and space depending of the context as widely review [Kholodenko and Kolch, 2008, Kholodenko et al., 2010, Santos et al., 2007, Grecco et al., 2011, Kiel and Serrano, 2011] and presented in



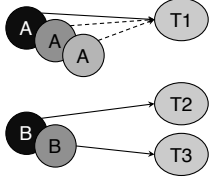
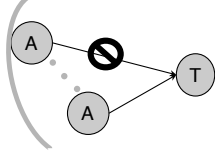
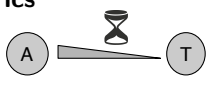
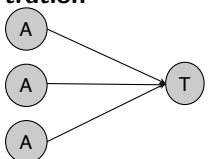
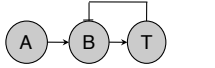
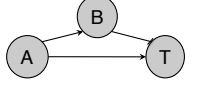
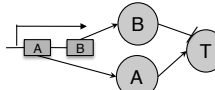
**section 1.1.2.** Along these lines, we next review signaling mechanisms that can be incorporated into modeling approaches to facilitate understanding how topological flexibility is achieved in signal transduction of mammalian cells.

### 1.3.2 Sources of topological complexity

#### Maintaining tumor proliferation

Signaling networks are compiled in literature by including reported interactions between proteins. However, reported interactions may not be present in the particular cell line being studied, or may be present only at specific time-points [Dumont et al., 2001]. Additionally, the pathway of interest may be regulated by other interactions than the ones reported. It is well-established that tumors can rearrange their signaling pathways in order to acquire resistance to the treatment, both via genetic mutations or epigenetic changes [Di Nicolantonio et al., 2005]. This resistance is achieved in melanoma through its molecular plasticity, which also has been shown to feature neovascularisation, migration, rearranging signaling through switching and enhancing certain pathways and containing multi-subpopulations of cancer cells that may contain stem cell-like properties [Ramgolam et al., 2011, Hendrix et al., 2003], reviewed in [Hanahan and Weinberg, 2011]. Specifically, resistance to treatment has been reported to be developed through switching among the serine threonine kinase BRAF isoforms to activate the MAPK pathway [Villanueva et al., 2010], a signaling network which plays a major role in proliferation and is a very attractive target for therapy due to the fact that in the majority of melanomas it has been shown to harbor somatic mutations [Davies et al., 2002, Davies and Samuels, 2010]. Alternative splicing can also be used by tumors to establish crosstalk between apoptotic and survival pathways, thereby rearranging signaling in order to develop protection against apoptosis. In [Kurada et al., 2009], the authors show that MADD, a splice variant of IG20, is overexpressed in cancer cells and tissues and can specifically activate MAPKs through Grb2 and Sos1/2 recruitment to grant protection against apoptosis upon tumor necrosis factor $\alpha$  treatment (**table 1.2**, maintaining tumor proliferation). In summary, to identify resistance mechanisms activated by the cell line at study by mathematical modeling implies evaluating changes in topology of signaling networks.

Table 1.2: Certain signaling events can render reported interactions dysfunctional in own experiments.

Mechanism	Description	References
<b>Maintaining tumor proliferation</b>		
<b>Alternative splicing</b> 	When B-Raf is inhibited, MAPK-mediated tumor proliferation can be maintained by activating splice variants. Apoptosis triggered by TNF- $\alpha$ can be escaped by expressing MADD, a splice variant of IG20, which activates MAPKs.	[Villanueva et al., 2010], [Kurada et al., 2009], reviewed in [Kiel and Serrano, 2011]
<b>Specificity of signaling</b>		
<b>Spatial dynamics</b> 	Cross-signaling is prevented when an interacting protein is recruited to e.g. the membrane or scaffold proteins	[Rocks et al., 2005], [Kholodenko et al., 2010], reviewed in [Kiel and Serrano, 2011]
<b>Temporal dynamics</b> 	A number of biological networks, e.g. p53 or ERK trigger a different response depending on stimulus being continuous or a pulse	[Batchelor et al., 2011], [Marshall, 1995], [Kholodenko et al., 2010], reviewed in [Kiel and Serrano, 2011]
<b>Protein concentration</b> 	Different protein concentrations enable same pathways to vary input-output response and trigger a cell-type specific response	[O'Shaughnessy et al., 2011], [Pontén et al., 2009], reviewed in [Kiel and Serrano, 2011]
<b>Robustness</b>		
<b>Negative feedback</b> 	The functionality of crucial pathways is maintained against changes in concentrations of protein e.g. ERK or BMP by having the output correct the upstream regulator	[Paulsen et al., 2011], [Fritsch-Guenther et al., 2011], reviewed in [Blüthgen and Legewie, 2012]
<b>Incoherent feed-forward loop</b> 	To provide robustness, a signaling intermediate activates its target by one route and deactivates the target by another	[Bleris et al., 2011], reviewed in [Blüthgen and Legewie, 2012]
<b>Operon</b> 	Effect of increase of expression of a gene can be canceled out by an opposed signal if it is expressed from the same operon	[Kollmann et al., 2005], reviewed in [Blüthgen and Legewie, 2012]

### Specificity of signaling

Adaptation to treatment by cancer cells is not the only topological change, which can lead to a discrepancy between signaling pathways established in literature and own experimental observations. Indeed, it has been established that in order to trigger specifically a cellular response, the activation initiated by a ligand is not stably propagated through the full range of reported interactions in the corresponding cascade, since so many points of crosstalk exist that a specific response would be hard to achieve. In particular, it has been shown that only four cascades of five steps can render 760 possible positive and negative interactions [Dumont et al., 2001]. Conversely, a range of mechanisms have been shown to regulate the known specificity of action of signals. For instance, tight spatial control has been shown to play a role in regulation as reviewed in [Kiel and Serrano, 2011] and [Kholodenko et al., 2010]. In fact, it has been reported that an acetylation cycle is responsible for the differential location at the plasma membrane and Golgi of different RAS isoforms, thereby triggering different amplitude and duration of MAPK signaling [Rocks et al., 2005] (**table 1.2**, specificity of signaling). Additionally, temporal properties in signaling can alter cell response, e.g. transient ERK activation in PC12 cells upon EGF stimulation induced proliferation, whereas sustained ERK activation by NGF induced differentiation [Marshall, 1995].

### Robustness mechanisms

In line with the above-mentioned mechanisms, which can alter signaling thereby enabling a specific response, it has been shown that alteration of protein abundance, which may arise due to cell-type specificity or cell-to-cell variation, can modify the strength of the response triggered by the MAPK pathway [O’Shaughnessy et al., 2011]. The fact that different levels of regulatory proteins can lead to different responses raises the question of the effect of expression noise, i.e. how does cell-to-cell variation of protein levels affect the function regulated by those proteins? To answer this question, it has been shown that a number of mechanisms can provide robustness to pathways governing cell fate and negative feedback is a prominent example (**table 1.2**, robustness). Specifically, negative feedback from Erk to Raf has been reported to confer robustness to MAPK signaling against variations in ERK

levels [Fritsche-Guenther et al., 2011] and negative feedback in the bone morphogenetic protein 4 has been shown to canalize embryogenesis [Paulsen et al., 2011]. Robustness can also be achieved by an incoherent feed-forward loop, a network motif that has been implemented using a synthetic biology approach to enable adaptive gene expression in mammalian cells [Bleris et al., 2011]; in bacteria, this signal transduction system is considered to be optimized by using bi-functional enzymes or enzymes that perform opposing biochemical functions expressed from the same operon [Kollmann et al., 2005] and reviewed in [Blüthgen and Legewie, 2012]. Although the spectrum of mechanisms compiled in **table 1.2** is not exhaustive, it justifies the need of studying, rather than assuming, which amongst the reported interactions are active in the cell line of experimental observations.

# 2

## Motivation and aims

The overall goal of this work is to establish a data-driven mathematical modeling platform for integration of prior literature knowledge with high-content, heterogeneous datasets, capable of predicting non-intuitive adaptive signaling events. To that end, the following three aims are set:

1. **Development of a generalized model implementation method to encode non-linear sub-cellular behavior using fuzzy logic and neural networks.** In collaboration with experimentalists, high-content microscopy datasets of mitochondrial morphological, pathway and bio-energetic features will be integrated to investigate relationships between morphology and onset of apoptosis. To that end, a data pretreatment pipeline will be established to unify and scale the heterogeneous measurements. Subsequently, data subsets for all mutual combinations of signaling events will be selected for model training. Neural network training algorithms will be used to fit heterogeneous datasets for each generalized fuzzy logic system representing potential signaling interaction. Thereby, parameterization of each fuzzy logic model, i.e. its rules and membership functions, will be derived from data. *Overall, a modeling platform will be developed to derive causal interactions between signaling events from high-content imaging data at the single cell level.*
2. **Development of a scalable search approach to quantify potential causality relations from heterogeneous datasets.** The root-mean-squared error will be calculated for all models representing all potentially related events as a signature of accuracy. An exhaustive search approach will be employed to identify models with least error, thereby determining

---

most related signaling events. The model implementation strategy developed for aim 1 combined with the exhaustive search undertaken during aim 2 should be scalable, i.e. enable search of direct and distributed contributions to any single measured signature of mitochondrial dynamics. *Overall, we aim to provide a tool for identification of a hierarchy of events in population and sub-cellular responses.*

- 3. Extension of the integrative fuzzy logic modeling platform from aim 1 to incorporate topological and temporal structure to investigate network evolution.** In collaboration with experimentalists, we aim to extend the above-mentioned approach to identify time-defined signaling rearrangements of the topology in the MAPK signaling pathway. To that end, we seek to utilize phosphorylation profiles of key MAPK intermediates as a signature of signal transduction over 96 hours upon treatment with different pharmacological inhibitors in A-375 melanoma cell line. To optimize prediction power, a parameter reduction strategy will be developed to allow for incorporation of time and topology as inputs to traditional fuzzy logic models. To this end free parameters with low contribution to model performance will be identified and fixed in order to achieve optimal model reduction. To maintain the data-derived approach of this work, training datasets will be bootstrapped and impact on model output will be calculated by establishing tailored signatures of deviation in flexibility and accuracy. Finally, a model encoding the behavior of the full MAPK network acquired will systematically be trained at different time points, to identify temporal discrepancies in reported vs. acquired network topology. To that end, an objective function for fuzzy logic model optimization will be implemented, which accounts for time-defined model training. *Overall, this aim achieves a data-derived modeling platform to analyze signaling topology in large datasets integrated with prior knowledge, and enables identification of biologically relevant temporal relationships within cancer cell signaling networks.*

Once aims 1 and 2 are accomplished, we seek to suggest a hierarchy of non-linear interactions in MCF-7 breast cancer cell line supported by related literature, thereby contributing to elucidate the role of mitochondrial morphology in control of apoptosis signaling. Finally, we intend to apply the method de-

veloped for aim 3 to identify time-specific topological changes in the MAPK pathway of A-375 melanoma cell line, thereby contributing to understand the mechanisms that grant melanoma its plasticity.





# 3

## Methods

### 3.1 Experimental acquisition of apoptotic signatures

#### 3.1.1 Cell culture and apoptotic stimuli

Human breast carcinoma MCF-7 cells (Cell Line Services; Heidelberg Germany) were cultured in DMEM (Invitrogen) supplemented with 10 FBS (Invitrogen), 1% penicillin/streptomycin (Invitrogen), 1% Glutamax (Invitrogen) and 1% nonessential amino acids (PAA laboratories) in a 37°C, 5% CO<sub>2</sub> incubator.

Cells were seeded overnight (56105 cells per well) and treated with the following compounds: C-6 ceramide (300 μM; Biozol), CCCP (20 μM; Calbiochem), TNFα (43 ng/mL; BASF), TRAIL (20 ng/mL; R&D Systems), thapsigargin (1 μM; Calbiochem), camptothecin (2 μM; BioVision), and oligomycin (10 μM; Sigma). Drug stocks were prepared according to manufacturer instructions. Drugs were diluted in balanced salt solution (BSS; Krebs-Henseleit Solution, pH 7.4) before application and incubated for 6 hours prior to all measurements.

#### 3.1.2 Imaging and classification of mitochondria morphology

MCF-7 cells stably expressing Mito-GFP were seeded overnight ( $5 \times 10^5$  cells per well) in an 8-well imaging  $\mu$ -slide (ibidi) and treated with apoptotic drugs. Nuclei were stained with Hoechst (100 ng/mL; Sigma) for 1 minute prior to imaging. Live cells were imaged using a 63x oil objective (NA 1.40) and Z-stacks with 0.22 μm step sizes were collected and subsequently deconvolved

using the bundled softWoRx software. Plasmid encoding Mito-GFP (fusion of the localization tag of cytochrome c oxidase IV and GFP) [Rizzuto et al., 1990] was transfected into MCF-7 cells using Effectene (Qiagen) and positive clones were selected using neomycin (G418, 1 mg/mL; Carl Roth GmbH). Stable cell lines were generated from single colonies in order to minimize genetic background. All images were acquired using a wide-field Delta Vsision RT (DVRT) deconvolution microscope.<sup>1</sup> For feature extraction of mitochondrial morphology, analysis was performed with CellProfiler software by combining available modules and submodules ([www.cellprofiler.org](http://www.cellprofiler.org)), and configured to automatically (i) perform image preprocessing, (ii) segment and identify objects within the image (iii) and measure a selection of mitochondria and cell features. A detailed description of the CellProfiler pipeline and extracted features is available in [Reis et al., 2012].<sup>2</sup> Finally, the exported features which characterized mitochondrial morphological states were analyzed using a Random Forest (RF) classification algorithm [Liaw and Wiener, 2002], which performed multidimensional data exploration and supervised machine-learning-based image classification. The RF method is an ensemble classifier that consists of a family of decision trees, and enabled calculation of mean value of each class assigned per cell (Networked/Fragmented/Swollen) to reflect mitochondrial population distributions under specific treatments.<sup>3</sup>

#### 3.1.3 Reporters of apoptotic events

Data is given as mean  $\pm$  standard error of the mean (s.e.m). Statistical significance of differences was determined using a two-tailed Student's t-test. P values  $\leq 0.05$  were considered to be statistically significant.<sup>4</sup>

**Bax activation** Plasmid encoding GFP-Bax [Wolter et al., 1997] was transfected into MCF-7 cells using Effectene (Qiagen) and positive clones were selected using neomycin (G418, 1 mg/mL; Carl Roth GmbH). Stable cell lines were generated from single colonies in order to minimize genetic background.

---

<sup>1</sup>Experiments to measure mitochondrial morphology were performed by Yara Reis.

<sup>2</sup>The CellProfiler imaging pipeline was established by Yara Reis and Daniela Richter.

<sup>3</sup>The random forest classifier was implemented by Thomas Wolf. Further details can be found in [Reis et al., 2012].

<sup>4</sup>Experimental data acquisition of signatures of Bax activation and  $\Delta\psi_m$  was performed by Yara Reis.

MCF-7 cells stably expressing GFP-Bax were incubated for 6 hours with the respective compounds and nuclei were stained with Hoechst (100 ng/mL; Sigma) before imaging (406 air objective, NA 1.20). 10 Z-stacks were acquired per condition and Z-projections (max) were performed prior to analysis. 3D rendering was performed for representative image.

**Mitochondrial membrane potential ( $\Delta\psi_m$ )** After respective drug treatments, MCF-7 wild-type (wt) cells were incubated with tetramethyl rhodamine methyl-ester (TMRM, 25 nM; Invitrogen) for 25 minutes at 37°C. Imaging was performed using a 406 air objective (NA 1.20). Sequential images of a single focal plane were acquired every second, over a period of 5 minutes. Exposure times were identical for each condition. For inhibition of the mitochondrial permeability transition pore (MPTP), MCF-7 wt cells were incubated in cyclosporine A (CsA, 5 mM; Calbiochem) for 30 minutes at 37°C or pre-treated with Bongkreikic acid (BA, 50 mM; Santa Cruz Biotechnology) for 1 hour at 37°C. The release kinetics of the TMRM dye is here reported by the standard deviation of the signal intensity from individual cells. Under normal conditions, mitochondrial TMRM is highly localized (high standard deviation) and upon  $\Delta\psi_m$  loss, redistribution of the dye throughout the cell occurs and both total signal intensity and standard deviation decreases per cell [Toescu and Verkhratsky, 2000]. From the standard deviation i.e. signal dissipation curves plotted for each condition, three parameters were extracted:

- *t<sub>1/2</sub>decay*: time for the signal dissipation curve to reach half of its initial value.
- *Yspread*: total standard deviation signal decrease over time.
- **MAX**: initial maximum value of standard deviation. The median of the first and last 10 points of each data set were used to calculate the maximum and minimum intensity. The *t<sub>1/2</sub>decay* is defined as the time point at which the signal dissipation curve reaches half of its initial starting value.

For more details on the measurement of mitochondrial membrane potential, the reader is referred to [Reis et al., 2012].

## **3.2 Experimental acquisition of proliferation signatures**

### **3.2.1 Cell culture and pharmacological inhibition of MAPK**

MEK1/2 specific inhibitor U0126 was solved in DMSO (stock solution, 10mM), and used at a final concentration of 10 $\mu$ M. One pill of Sorafenib was solved in 31,4ml DMSO (stock solution, 10mM) and used at a final concentration of 5 $\mu$ M. MEK1/2 specific inhibitor AZD6244 was solved in DMSO (stock solution, 10mM) and used at a final concentration of 3 $\mu$ M. Measurements were acquired at 0 min, 30 min, 6h, 12h, 24h, 36h, 48h, 72h and 96h. 0.1x10<sup>6</sup> cells per sample were seeded in 6-well plates, one 6-well plate for each time point. Medium was discarded and cells washed with 2ml PBS per well, prior to addition of medium containing drug. Cell supernatants were harvested for subsequent luminex analysis and stored at -80°C until the measurement.

### **3.2.2 Luminex analysis of total and phosphorylated protein level**

We used the cell lysis kit from Bio-Rad for the preparation of tumor cell lysates. After treatment and lysis, the Pierce BCA Protein Assay Kit (Thermo Scientific) was used. 10 $\mu$ l of each sample was pipetted into a 96-microplate well. 200 $\mu$ l of the working reagent were added to each well, and mixed with the sample on a plate shaker for about 30 seconds. The plate was covered and incubated at 37°C for 30 minutes. After the incubation period, the absorption was measured at 562nm with an Elisa reader. The use of a standard dilution series and the calculation of standard curves, allowed for the exact determination of protein concentrations in each sample. Protein concentrations were set to the lowest necessary concentration amongst all lysates within one group, diluted with assay buffer. To allow for the comparison of drug perturbations as well as comparison between cell lines, we detected the lowest protein concentration within this set of samples, and adjusted all other sample concentrations accordingly. 50 $\mu$ l of lysates were incubated on a plate shaker at RT in the dark with bead mixtures over night. The following day biotinylated detection antibodies were added after three washing steps, and plates were incubated at RT

for 30 minutes. For quantification SAPE was added, and after three further washing steps plates were measured and analyzed in 125 $\mu$ l assay buffer with the Luminex machine and the Bio-Rad Manager 5.0 and 6.0. For phosphoprotein detection, at least 50 beads for each analyte region were collected. Reported median fluorescence intensity values for each analyte were used as a measure for the total or phosphorylated protein content in the samples.<sup>5</sup>

### 3.3 Fuzzy Logic based exhaustive search of regulatory interactions

In the first part of the work presented here (see **section 4.1**), we established a modeling pipeline based on fuzzy logic (FL) to perform an exhaustive search for highly-related combinations of heterogeneous events measured during apoptosis. To that end, the FL toolbox was used (MATLAB R2009a). In fuzzy logic, membership functions allow transformation of the experimental data thereby enabling the use of logic rules. To parameterize input and output membership functions, two types of fuzzy logic systems have been widely used for inference, namely Takagi-Sugeno models [Takagi and Sugeno, 1985] and Mamdani models [Mamdani and Assilian, 1999]. While the output membership functions are constant or linear in a Takagi-Sugeno model, the output membership functions in a Mamdani model are fuzzy sets. To ease the process of parameter estimation, the Takagi-Sugeno framework was used in this work to implement every Single input-single output (SISO) FL model. An exhaustive search results in a classification of those models which suggest most likely interactions. Because this is a relative metric, the main aim was to use the same setup for all models and no method was established to reduce the number of free parameters. Instead, as a first attempt to reduce the number of free parameters, input membership functions (MF) were fixed to Gaussian functions, and thereby the number of input parameters was excluded from the model training. The number of rules constitutes a free parameter as well, which we eliminated by using a fix number of rules. This number was the total of pos-

---

<sup>5</sup>Experimental measurements of total and phosphorylated protein levels were performed by Stefan Maßen. Cell culture and luminex analysis are described in detail in the doctoral dissertation of Stefan Maßen, [www.ub.uni-heidelberg.de/archiv/11169](http://www.ub.uni-heidelberg.de/archiv/11169).

sible combinations of input MFs. As output, linear MFs were chosen, and thus their stepwise combination allowed for the approximation of nonlinearity upon simulation. We further developed the parameter reduction strategy to enable the method investigation of a different question posed in **section 4.2** and further described in **section 3.4.1** Parameter fitting extracted from the data the degree to which this was happening in the specific measurement. Again, because the focus of this first approach was the exhaustive search of heterogenous datasets, model training was achieved via standard MATLAB algorithms. Training of the model was performed using a hybrid algorithm combining back propagation and iterative least-squares procedure [Reis et al., 2012]. Conversely, an extension of the method to use an objective function tailored to our specific aim was established as shown in **section 3.4.1**. Simulations of the SISO FL models were run using Simulink and root-mean-square errors (RMSE) were calculated. For the final step of the exhaustive search we selected the models with least error.

The detailed workflow for model implementation and exhaustive search of relationship between morphological and functional mitochondrial events during apoptosis was performed in MATLAB R2009a according to the following:

1. **Data Processing.** Raw data from the various experimental procedures was scaled to each maximal observed value in order to make datasets comparable.
2. **Assembly of a Sugeno FLS.** The fuzzy logic Toolbox was used to generate a fuzzy logic system (FLS) automatically with the existing function `genfis1`, thereby creating a grid of rules to relate one input MF to exclusively one output membership Function (MF). 2 gaussian functions were used to fuzzify one input. In `genfis1`, the number of rules is  $m$  to the power of  $n$ , where  $m$  is the number of input MFs and  $n$  is the number of inputs; hence in our single-input case the number of rules was 2 per model. Upon exploration of the MF parameter space we observed slightly better performance using other non-linear functions. However, the above-mentioned setting was used due to its smaller number of parameters. Linear MFs were chosen as output with standard settings previous to training. `Genfis1` requires the experimental data as a matrix. In the case of multiple events and a single functional feature, all columns in the

---

matrix except the last one are considered causative events and the last column is accepted as functional feature.

3. **Training of the FLS.** Once generated, the FLS was trained using adaptive neuro-fuzzy inference systems (ANFIS). As a learning algorithm, a hybrid of backpropagation coupled to least-squares was employed.
4. **Simulation of the FLS.** Simulink, the simulation platform coupled to Matlab, was used to create a simulink model to simulate the trained FLS. This model was then run for each experimental datapoint to estimate the value of the desired phenotype. The resulting estimated values were saved in an excel sheet together with the experimental dataset, which were used to calculate the root mean squared error (RMSE).
5. **Exhaustive search.** The process stated in steps 1, 2 and 3 was then iterated to create the FLS for a total of 30 models representing all potential interactions: Each morphology class influencing a MPT parameter (9 models), the mirror models (9 models), Bax activation influencing each one of the three morphological classes (3 models) and the mirror models (3 models) as well as Bax influencing each MPT parameter (3 models) and the mirror models (3 models).
6. **Model selection.** For follow-up analysis of the least-error models, please see results.

## 3.4 Time-defined training and evaluation of topological fuzzy logic modeling

### 3.4.1 Parameter reduction strategy and model implementation

In the second part of the work presented here (see **section 4.2**), the modeling approach presented previously was further developed to enable study of evolution of the MAPK signaling network. In doing so, the computational challenge was at including the role of time, evaluate a prior knowledge network in an

absolute manner and determine its evolution through time. To that end, a series of methods were developed that are presented below.

#### **Fixing number of rules and value of premise membership function parameters.**

As previously described (**section 3.3**), to ease the process of parameter estimation, the Takagi-Sugeno framework was used in this work [Takagi and Sugeno, 1985]. The number of rules was fixed by considering only the combinations of low sets with themselves and analogously for high sets. The degree to which each input contributes to the output was later extracted during the fitting process. Because output parameters cannot be shared in TKS fuzzy inference systems, the parameters of all input membership functions were fixed to a generalized gauss function (**equation 4.1**). In the case of *low* sets, the function was centered at  $a=0$  and in the case of high datasets to 1. For both cases, we took 0.4247 for  $\sigma$ , as this is the default MATLAB standard. The effect of fixing said parameters was assessed by resampling the training dataset in fixed versus free setups (see **section 4.2.2**).

#### **Model implementation**

In the second part of this work (**section 4.2**), MATLAB version R2011b was used for model implementation, fitting and simulation. **Equation 4.2** and its extension shown in **section 4.2.2**, i.e. a gFIS for single and another for double regulated intermediates, were implemented as a MATLAB function. Another function was implemented to fit them using an unconstrained nonlinear optimization process. Due to the flexibility of the fuzzy inference system, the solver converged to solutions which were very accurate at the data points but out of range between them. In turn, poor interpolation power led to large error propagation when the signal of upstream models was propagated to simulate downstream models. To correct for this by selecting those fits with the best interpolating power, 20 equidistant points were synthesized to evaluate the model between the data points and a Euclidean penalty was calculated by taking all distances for those simulations over 1 and below 0, which we respectively termed *PositiveOffset* and *NegativeOffset*. This penalty was then used to punish the root-mean-square error calculated in the objective function



$\phi(P)$  as shown in **equation 3.1** for a given vector  $P$  containing the parameters calculated by the optimization algorithm:

$$\phi(P) = \sqrt{\sum_{i=1}^n \frac{y_i - \hat{y}_i}{n}} = \sqrt{\sum_{j=1}^m \frac{PositiveOffset_j - NegativeOffset_j}{m}} \quad (3.1)$$

where  $n$  is the number of data points,  $m$  is the number of synthetic i.e. interpolated points  $j$ ,  $\hat{y}$  is the simulation calculated by the model at a given data point  $i$  and  $y$  is the experimental measurement at the same data point. The use of the number of data points for the root mean squared calculation of the model error served as simple means to account for the number of training data points when comparing models during network evolution. To prevent the fitting process being trapped in local optima, all values for initial parameters were randomized following a uniform distribution. Finally, a MATLAB structure formatted as a Sugeno fuzzy inference system (e.g. p53.fis) was created with rules and input membership functions parameterized as mentioned above and the different parameters resulting of the fitting process as output membership function parameters for each rule. All other FIS qualities were implemented as default in MATLAB's Fuzzy Logic Toolbox.

### 3.4.2 Data-derived sensitivity analysis

The reference model for the fixed-linear setup (**figure 4.12A**, left) was implemented as previously shown. The adaptive-constant setup (**figure 4.12A**, center) was implemented by creating a structure consisting of a zero-order Takagi-Sugeno FIS, i.e. the input membership functions were Gaussian and parameterized as mentioned above and the output membership functions were set as constant. Fitting was performed via a combination of the least-squares method and the backpropagation gradient descent method for training FIS in the Fuzzy Logic Toolbox. Analogously, the adaptive-linear setup (**figure 4.12A**, right) was implemented by creating a structure consisting of first-order Takagi-Sugeno system and using same fitting process. The bootstrapped predictions were calculated by submitting the three above-mentioned "create system and fit it" functions to bootstrapping for 100x resampling with repetition, a method introduced in [Efron, 1979]. All models are shown in **figure 4.12B**, and standard

deviation was calculated for the prediction at each data point. As a signature of model flexibility in terms of impact of training dataset in the simulation at each data point, the mean of the standard deviation across models is displayed. As a signature of accuracy, the error  $\varepsilon$  was calculated as root-mean-squared error for all models and deviation  $\sigma(\varepsilon)$  was calculated across errors. The result was displayed as histogram (**figure 4.12C**).

#### 3.4.3 Benchmarking approach

In our experimental setup, inhibitors were used at single concentrations and were therefore either present or absent. Conversely, the dataset presented in [Gaudet et al., 2005] was acquired in 10 combinations of different concentrations of TNF/EGF/Insulin. To enable comparison in same conditions, 4 datasets were selected: measurements acquired in control conditions and maximum conditions of each single treatment, i.e. (i) 100 ng/mL TNF, no EGF and no Insulin, (ii) no TNF, 100 ng/mL EGF and no Insulin and (iii) no TNF, no EGF and 500 ng/mL Insulin. For the selected datasets, we calculated the RMSE corresponding to the simulations presented in [Aldridge et al., 2009] (see **figure 4.15**). In the benchmark method, a SIMULINK model was implemented to represent and simulate the logic gates (see supplementary data in [Aldridge et al., 2009]). Here, the inputs implemented to account for different concentrations of treatment in the SIMULINK model were removed, since only maximum concentration datasets were selected. Additionally, some changes needed to be implemented in the topology of the SIMULINK model. IRS(Y), IRS(S), Akt, ERK, MK2, JNK, FKHR and IKK were implemented analogously to the benchmark model. The modeling of feedback loops is not addressed in the method presented here, hence the feedback ERK-MEK was removed. Consequently, no delay and max gates were required, and hence casp8 and proc3 had to be removed. See below for more details on model simulation. Following this topology, a gFIS for each node in the network was trained to the corresponding data by using the model implementation and training process described above. Subsequently, the SIMULINK model was simulated and RMSE was calculated. **Figure 4.14** shows the experimental data and the simulation for each node in the network performed with both methods. For a detailed description on how models were implemented to account for multiple

treatments using naive condition switches, please see section Implementation of multiple perturbation models.

### 3.4.4 Implementation of multiple perturbation models

The free parameters for a gFIS corresponding to each species in the signaling network were fitted to the experimental data separately for each condition. To compile all parameters in a multi-treatment trained FIS at no increased parameter cost, two Boolean functions were introduced to represent absence  $\alpha(d)$  and presence  $\rho(d)$  of each drug  $d$ , which we together termed naive condition switch as shown in **equation 3.2** and **equation 3.3**:

$$\alpha(d) = \begin{cases} 1 & \text{for } 0 < x < 0.5 \\ 0 & \text{for } 0.5 < x \leq 1 \end{cases} \quad (3.2)$$

$$\rho(d) = \begin{cases} 0 & \text{for } 0 < x < 0.5 \\ 1 & \text{for } 0.5 < x \leq 1 \end{cases} \quad (3.3)$$

Automation of the model building process was achieved by modifying the above-mentioned MATLAB function to “create system and fit it” to include the naive drug switches. Loosely speaking the 4 naive condition switches are simple Boolean functions added to all rules of each FIS, so that upon simulation they are evaluated at a value with the sole purpose of outputting either 1 or 0, thereby neglecting the parameters learned in the conditions that are not currently simulated. **Equation 3.2** and **equation 3.3** were included in the code by adding 1 input with 2 trapezoidal membership functions parameterized as Boolean functions for each one of the 4 conditions. Formally, as shown in **figure 4.11D**, the parameter reduction strategy yielded 2 rules per system per dataset. Hence, to include all parameters trained for the 4 datasets, the multi-treatment model for each species in the signaling network consisted of 8 rules. Consider for illustration the model  $f(x)$  encoding the transcription factor cJUN, which according to **figure 4.13A** is regulated by one only intermediate i.e. JNK. Following **equation 4.2**, the model including the 3 naive condition switches  $f(x, d_1, d_2, d_3)$  for a value  $x$  of JNK is shown in **equation 3.4**:

$$f(x, d_1, d_2, d_3) = \frac{(p_i x + q_i) \omega_i}{\sum_{i=1}^8 \omega_i} \quad (3.4)$$

, where  $\omega_1 = \mu_{low}(x)\alpha(d_1)\alpha(d_2)\alpha(d_3)$ ,  $\omega_2 = \mu_{high}(x)\alpha(d_1)\alpha(d_2)\alpha(d_3)$ ,  
 $\omega_3 = \mu_{low}(x)\rho(d_1)\alpha(d_2)\alpha(d_3)$ ,  $\omega_4 = \mu_{high}(x)\rho(d_1)\alpha(d_2)\alpha(d_3)$ ,  
 $\omega_5 = \mu_{low}(x)\alpha(d_1)\rho(d_2)\alpha(d_3)$ ,  $\omega_6 = \mu_{high}(x)\alpha(d_1)\rho(d_2)\alpha(d_3)$ ,  
 $\omega_7 = \mu_{low}(x)\alpha(d_1)\alpha(d_2)\rho(d_3)$ ,  $\omega_8 = \mu_{high}(x)\alpha(d_1)\alpha(d_2)\rho(d_3)$ ,  

$p$  and  $q$  are the fitted parameters and  $d$  is a discrete value that will let the switches output the combination of zeroes and ones that will neglect all but the parameters learned in the conditions being simulated. Hence, when no inhibitor was indicated to be present, the parameters used were the ones estimated in control conditions. For more details on the simulation process, the reader is referred to the next section.

### 3.4.5 Full network simulation

For model simulation, values were defined for each naive condition switch corresponding to the current simulation. Simulation was performed by automatically assigning to each upstream node the experimental value measured at a given time point. No model was implemented for the upstream models because no experimental measurement was acquired upstream of them. An exception to this was the benchmark simulation, where the upstream nodes were a model was implemented to encode their behavior as a function of time, analogously to the benchmark method. Subsequently, models downstream were evaluated, thereby propagating the signal via the SIMULINK model. The network states in a logic model can be updated in a synchronous and deterministic manner or asynchronously [Wynn et al., 2012]. Here, the state of each node in the network was synchronously determined by the state of the nodes upstream at a specific time point.

# 4

## Results

### 4.1 Modeling interactions of heterogeneous data in apoptosis

#### 4.1.1 Integration of mitochondrial and apoptotic measurements in response to diverse stimuli

##### Detection and classification of mitochondrial morphology states

To investigate the relationship between mitochondrial morphology and apoptotic events, a pipeline was established to detect different morphological states by high resolution imaging as presented in [Reis et al., 2012]. Human MCF-7 breast cancer cells stably expressing mitochondrial targeted GFP (Mito-GFP) were imaged by high-resolution, wide field fluorescence microscopy. To trigger different morphological states, three conditions were initially considered with enriched networked, fragmented and swollen phenotypes (**figure 4.1**).

Networked states were obtained under full medium (FM) conditions. Fragmentation was induced by the pro-apoptotic lipid second messenger ceramide [Parra et al., 2007] and swelling was induced using the mitochondrial uncoupler CCCP (carbonyl cyanide m-chlorophenylhydrazone) [Ganote and Armstrong, 2003]. In order to analyze a significant amount of cells and measure mitochondrial morphology states, the above-mentioned imaging pipeline included the use of CellProfiler image analysis software, which enabled feature extraction [Carpenter et al., 2006]. Feature sets extracted included mitochondrial area and volume, average number per cell and distribution within the cell to a total of 69 features per cell. These extracted features were the basis for building an

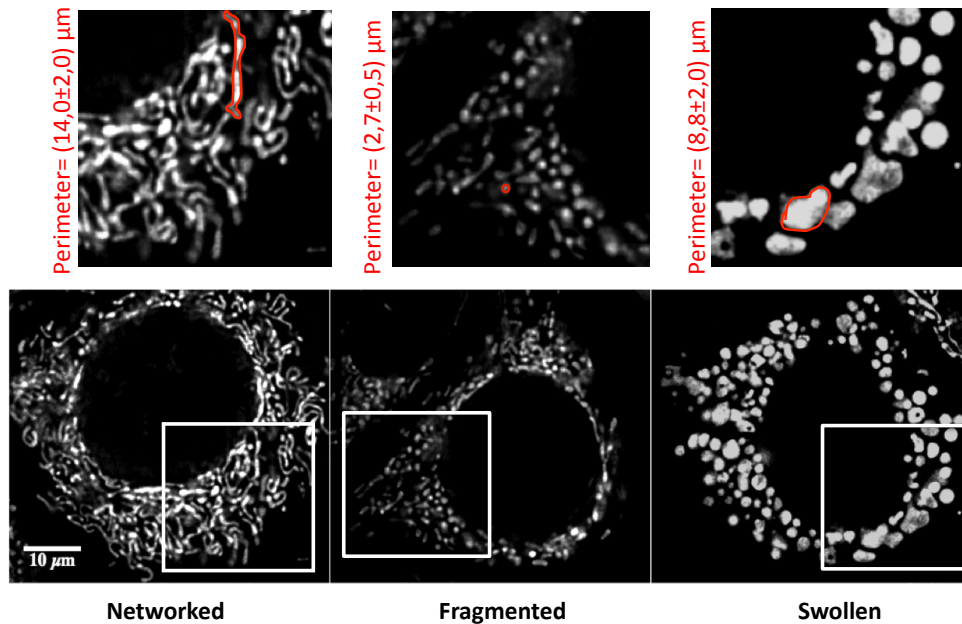


**Figure 4.1: Differential morphological states of mitochondria were imaged by high resolution fluorescence microscopy.** MCF-7 cells stably expressing Mito-GFP were incubated 6 hours under conditions known to induce networked (FM), fragmented (ceramide,  $300\mu\text{M}$ ) and swollen (CCCP,  $20\mu\text{M}$ ) mitochondria. Average perimeter values (in red) were measured from 10 mitochondria present in the zoomed region. Images correspond to the middle slice from 3D stacks. Adapted from [Reis et al., 2012]

automated classifier algorithm.<sup>1</sup> Subsequently, a supervised learning approach was developed using an image set of cells,<sup>2</sup> which were individually cropped and manually classified as networked, fragmented or swollen. These images were obtained under the above-mentioned control conditions and submitted to the imaging pipeline for feature extraction. The features were used to build a Random Forest classifier, which is a standard method in machine learning techniques and consists of a collection of classification trees [Breiman, 2001]. Two training sets of manually classified cells were used to build the classifier. In order to compare manual classification with the random forest classification, one class was assigned per cell, as it was impossible to clearly define intermediate classes within a single cell manually. Training sets were cross-validated and resulted in 92% overall accuracy. Inspection of the features used

<sup>1</sup>Experiments to acquire differential states of mitochondrial morphology were performed by Yara Reis. The imaging pipeline was established by Yara Reis and Daniela Richter.

<sup>2</sup>The random forest classification algorithm was developed by Thomas Wolf.

for classification led to the observation that *Zernicke* and *mitochondrial area and shape* were the most relevant for class distinction. For further details on the random forest classification algorithm, the reader is referred to [Reis et al., 2012]. Once the imaging and classification pipeline was established, we next sought to quantify redistributions of morphology subpopulations in response to various pro-apoptotic stimuli. Cells were treated with compounds known to impact mitochondrial bioenergetics and induce mitochondrial apoptosis. Drugs were selected which initiate mitochondrial apoptosis in a spatially heterogeneous manner. Death receptor (DR) ligands  $\text{TNF}\alpha$  (43 ng/mL) and TRAIL (20 ng/mL) activate the mitochondrial death pathway via caspase 8-mediated cleavage of Bid [Li et al., 1998]. The ER calcium pump inhibitor thapsigargin (1 mM) induces ER stress, cytosolic calcium, and subsequent activation of BH3- only proteins [Puthalakath et al., 2007]. Camptothecin (2 mM), a DNA topoisomerase I inhibitor induces mitochondrial apoptosis [Shimizu and Pommier, 1997]. Bioenergetic perturbations were induced with oligomycin (10 mM), which inhibits oxidative phosphorylation at the mitochondrial ATP synthase [Penefsky, 1985] (**figure 4.2**).

Images were acquired following 6 hours treatment and approximately 300 cells per condition were classified (**figure 4.3**). Plotted results reflect the drug impact on mitochondrial subpopulations, as (N/F/S) percentages are all taken into account and averaged through whole cell population. In addition to the apoptotic conditions, cells were incubated with two control conditions, i.e. FM and BSS.

To sum up, the imaging and classification pipeline was able to quantify the mitochondrial morphology response as a function of shifts of networked, fragmented and swollen subpopulations in images containing multiple cells. To investigate the relationship between changes in mitochondrial morphology and apoptosis, the impact of the above-mentioned drugs was subsequently measured in certain apoptotic events.

### **Mitochondrial permeability transition as a measure of apoptosis**

Tetra-methyl rhodamine methyl-ester (TMRM), a fluorescent lipophilic cation that electrophoretically accumulates in mitochondria [Métivier et al., 1998], can be photoactivated to generate reactive oxygen species (ROS) levels within

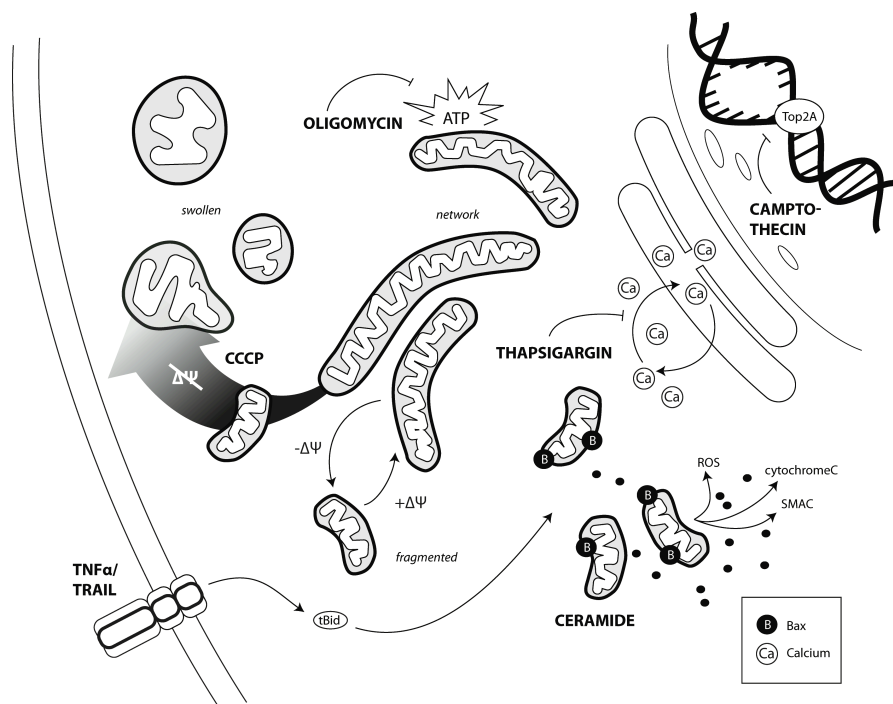


**Figure 4.2: Apoptotic drugs for population analysis of mitochondrial morphology.** The cartoon scheme shown here represents the tested apoptotic drugs and its targets. MCF-7 stably expressing Mito-GFP were incubated for 6 hours at 37uC with 7 different apoptotic drugs inducing a variety of cellular stress: calcium overload (thapsigargin, 1 mM); DNA synthesis inhibition (camptothecin, 2 mM); ATP synthesis inhibition (oligomycin, 10 mM); death receptor (DR) pathway activation (TNF $\alpha$ , 43 ng/mL and TRAIL, 20 ng/mL); mitochondrial fragmentation (ceramide, 300 mM); as well as a mitochondrial uncoupler (CCCP, 20 mM). The scheme summarizes the subcellular impact of our drug selection and depicts the three possible morphologic states of mitochondria: networked, fragmented and swollen. For example, DR activation activates pro-apoptotic tBid, which leads to Bax activation at the mitochondria. Mitochondria are shown in a fragmented state during cytosolic release of pro-apoptotic signaling factors and related to a swollen stated upon loss of  $\Delta\psi_m$  (gradient arrow). Cartoon by Daniela Richter.

the mitochondrial matrix that are sufficient to trigger Mitochondrial Permeability Transition (MPT) [Bradham et al., 1998]. Analogous to the acquisition of morphological states of mitochondria, cells were loaded with TMRM (25 nM) and continuous fluorescence imaging was performed following to 6 hours incubation with pro-apoptotic compounds. The use of continuous fluorescence imaging induced ROS-dependent MPT [Brady et al., 2004], hence we could measure the corresponding change in membrane potential, i.e.  $\Delta\psi_m$ . The time of  $\Delta\psi_m$  loss reports the threshold for MPT induction, and can be used as an



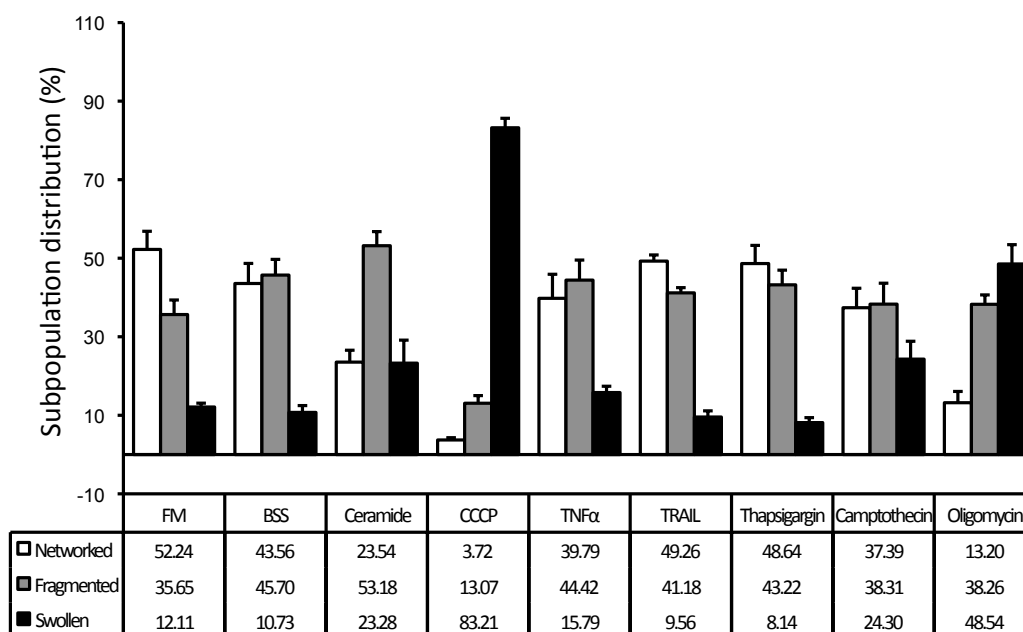


**Figure 4.3: Population analysis of mitochondrial morphology.** Mitochondrial morphologic classes were quantified in response to apoptotic stimuli. Bar plot shows the random forest classification into networked, fragmented and swollen for the different conditions. Values are given as mean percentage  $\pm$  s.e.m. per cell for each N (N=3, approx. 300 cells per condition). \*,  $P \leq 0.05$ , \*\*,  $P \leq 0.01$ , t-test against BSS). Adapted from [Reis et al., 2012].

indicator for mitochondrial sensitivity to specific stress [Neuspiel et al., 2005].<sup>3</sup> Quantification of TMRM kinetics was undertaken by considering the whole cell area and extracting a standard deviation value [Toescu and Verkhatsky, 2000] per cell. Approximately 400 cells per condition were analyzed per condition and the mean value was plotted. Signal dissipation curves were represented as heatmaps to ease comparison between drugs (**figure 4.4A**). Expectedly, signal dissipation occurred at the latest time point under FM (negative control), i.e. approximately 232 seconds. Next, the signal dissipation curves for the two controls and the 7 pro-apoptotic stimuli were submitted to euclidean clustering, which suggested 3 main groups: (i) conditions not impacting initial  $\psi_m$ , drugs sensitizing mitochondria to depolarization and drugs that depolarized mitochondria (**figure 4.4B**). To establish the role of mitochondrial morphology in apoptosis, an additional data set was acquired.

<sup>3</sup>Experiments to measure mitochondrial permeability transition were performed by Yara Reis.

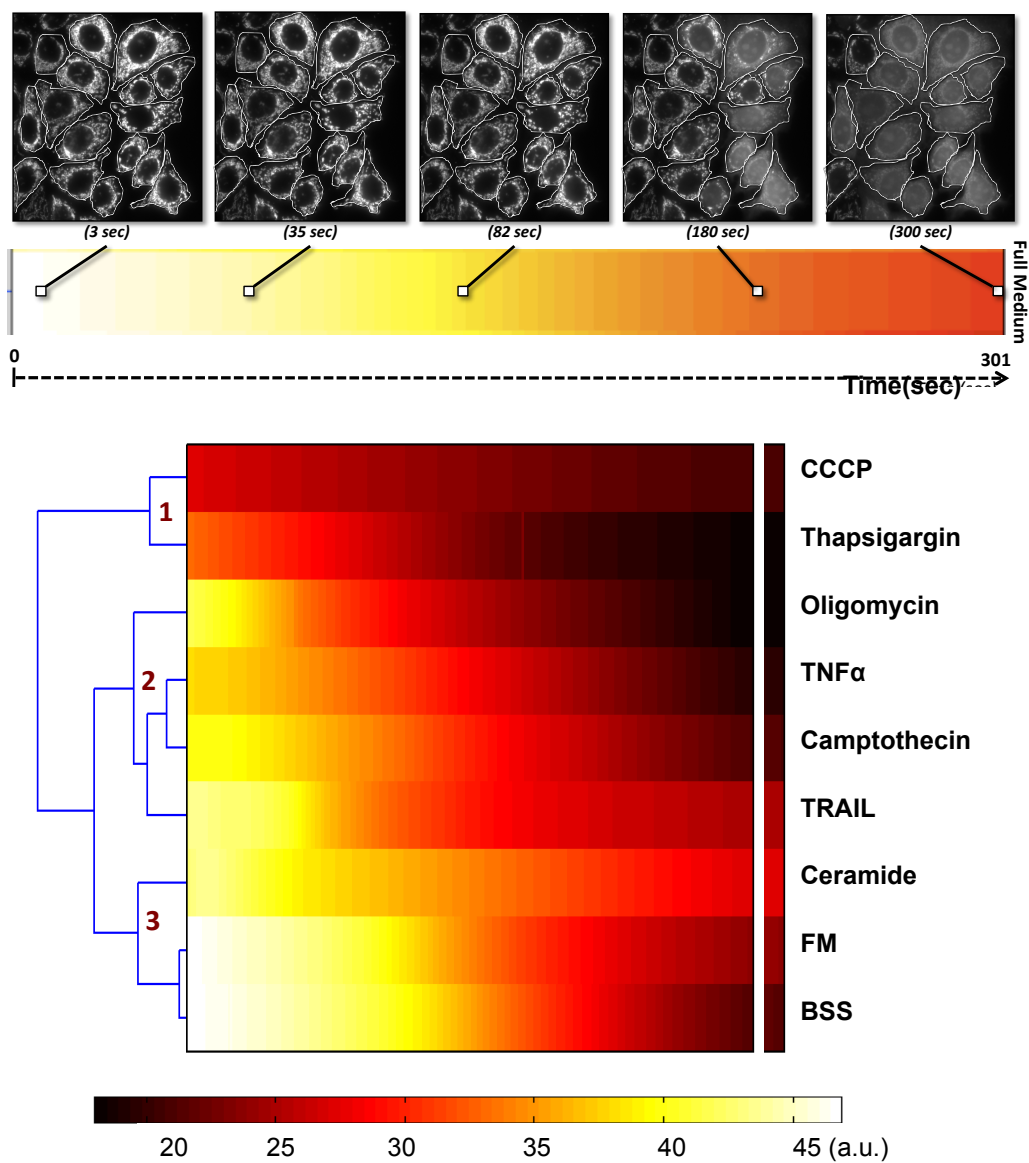


**Figure 4.4: Dataset acquired for  $\Delta\psi_m$  loss.** (A) Standard deviation of TMRM signal as a heatmap. Mean values of standard deviation were translated into a heatmap (color scaled from 0 to 50 in arbitrary units, a.u.). (B) Heatmap of standard deviation values over time for all conditions. Conditions were clustered using euclidean clustering, which revealed three main groups of similar patterns in signal dissipation. Adapted from [Reis et al., 2012].

### Apoptotic compounds result in different levels of Bax activation

Bax, a pro-apoptotic member of the Bcl-2 family of proteins is thought to be crucial for inducing permeabilization of the outer mitochondrial membrane [Youle and Strasser, 2008]. Importantly, Bax has been shown to participate in fragmentation events [Desagher and Martinou, 2000] and promote mitochondrial fusion [Conradt, 2006]. Here, we measured Bax activity in response to the above-mentioned panel of pro-apoptotic conditions and control conditions.<sup>4</sup>. To that end, MCF-7 cells were stably transfected with GFP-Bax, which forms clusters of high molecular weight when activated [Nechushtan et al., 2001] In BSS control conditions, GFP-Bax was homogeneously distributed within the cytosol, with low basal activation of 5% (**figure 4.5**). In response to apoptotic perturbations, GFP-Bax exhibited a punctuated pattern and clustered at the mitochondria (**figure 4.5**). Taken together, the described datasets of states of mitochondrial morphology, MPT over time and Bax activation were used for modeling of heterogeneous datasets to infer potential relationships during activation of apoptosis under matched conditions. For further measurements, the reader is referred to [Reis et al., 2012], where we show further analysis of Bax activation pattern, measurements of cell death and loss of cytochrome c under matched conditions.

### Data normalization and scaling enables integration of heterogeneous datasets for data-derived modeling

We next sought to use mathematical modeling to infer relationships between the morphological and the functional features of mitochondria from the datasets acquired. Because of their high accuracy and prediction power, physicochemical models such as ordinary differential equations are well suited to encode chemical reactions over time. However, two reasons hindered the use of such approaches in this study, namely (i) the heterogeneous nature of the described datasets, which did not measure protein concentration but morphological and functional features of mitochondria and (ii) the fact that there are no underlying interactions at the molecular level known between said events. Hence, we aimed at establishing an approach which was based on Fuzzy Logic (FL), a rule-based approximate reasoning method suitable for investigating hetero-

---

<sup>4</sup>Experiments to assess level of Bax activation were performed by Yara Reis

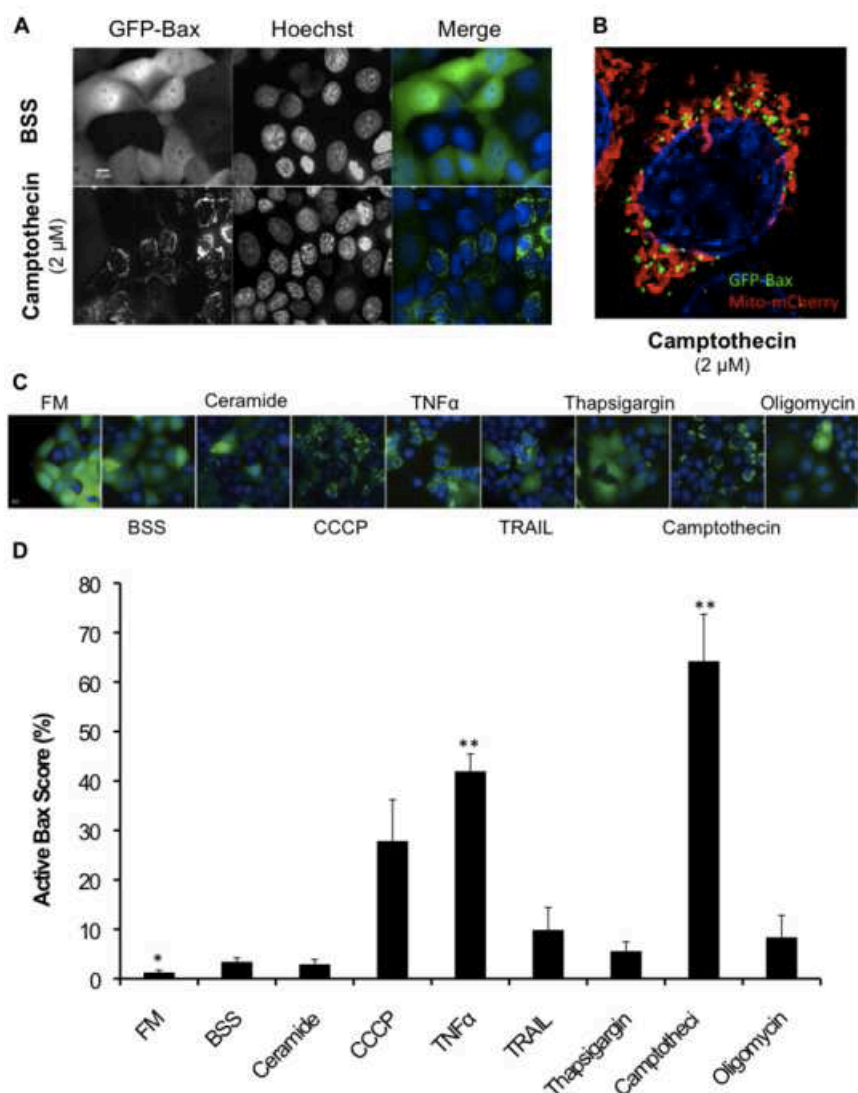


**Figure 4.5: Dataset acquired to capture Bax clustering under apoptotic stress.** (A) Bax clustering. MCF-7 cells stably expressing GFP-Bax were incubated 6 hours with the different conditions and nuclei were stained with Hoechst (100 ng/mL). Here is shown a representative example of basal levels of Bax activation (BSS) and an example of Bax activation under camptothecin (2 mM). (B) Active Bax translocates to the mitochondria. MCF-7 cells stably expressing GFP-Bax were transiently transfected with mito-mCherry and incubated 6 hours with camptothecin (2 mM) (Hoechst for nuclei). The 3D rendering (ImageJ) image shows GFP-Bax (green) translocated to mitochondria (in red). (C) Bax clustering. Representative microscope region for each pro-apoptotic condition is shown. (D) Bax levels. Cells with GFP-Bax clusters were scored as “positive” for Bax activation. Values are presented as mean percentage  $\pm$  s.e.m. (N = 5, approx. 500 cells/condition; \*:  $P \leq 0.05$ , \*\*:  $P \leq 0.01$ , t-test). Images were acquired with a DVRT scope and a 406 Objective. Figure from [Reis et al., 2012].

geneous datasets of signal transduction pathways [Aldridge et al., 2009]. To enable the analysis described below, the TMRM dissipation curves shown in (figure 4.4B) were described by extracting three secondary metrics which represented the dynamic response: (i) the half time for the decay of the signal, i.e.  $t_{1/2}decay$ , (ii) the spread of the signal ( $Yspread$ ) and the maximum initial signal (MAX) (figure 4.6). This transformation enabled use of a modeling approach, which did not incorporate the role of time as an explicit component.

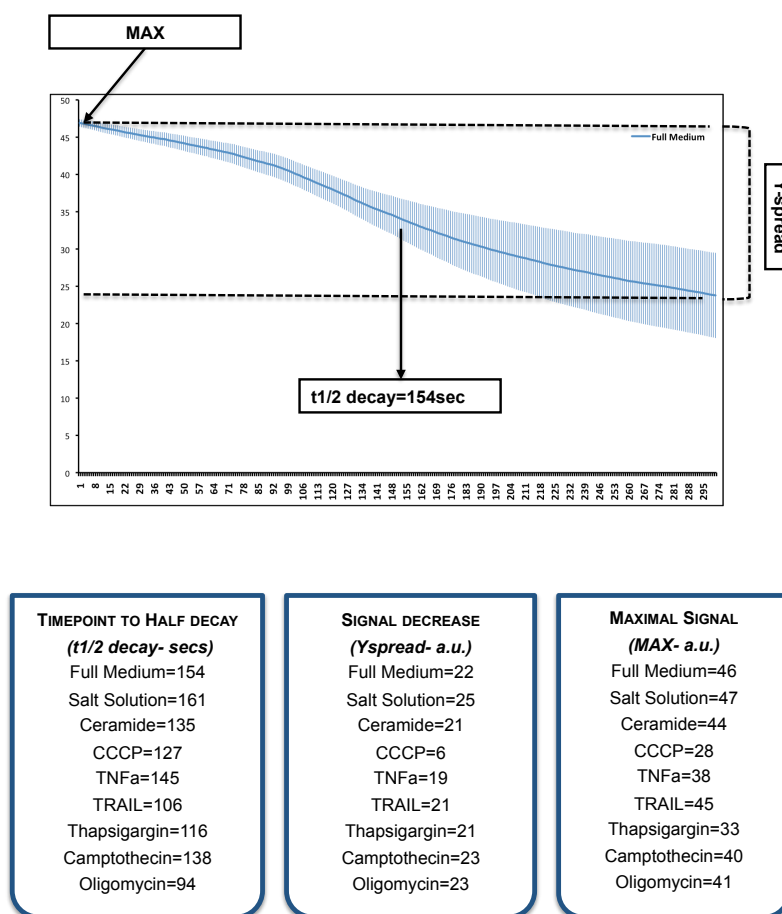


**Figure 4.6: Secondary dataset derived from acquired data** Three parameters were extracted per each signal dissipation curve: (i)  $t_{1/2}decay$ : time that takes for the signal to reach half of its initial value, (ii)  $Yspread$ : Total decrease of the signal over time and (iii) MAX: The initial maximum value. For better illustration, the box shows one representative curve example for the standard deviation curve of FM over time (301 seconds), and the extraction of secondary metrics was performed for all conditions. Mean values  $\pm$  s.e.m. per drug are shown; experiments  $N = 4$ , approx. 400 cells per condition were followed. Modified from [Reis et al., 2012].

Finally, raw data from the various experimental procedures was scaled. The

reasons for that are two: (i) as introduced in **section 1.3**, the aim of scaling is to adjust for dissimilarities in fold differences in each variable measured; (ii) furthermore, the measurement of model performance used here-forth i.e. the root-mean-squared error is scale-dependent, as it measures the distance between model simulation and data point. Here, scaling of each dataset was performed by normalizing to the maximum value measured per variable and condition. It is noteworthy that different data pretreatment methods have different impact on the data and each pretreatment method has advantages and disadvantages such as as inflation of small values, sensitivity to large fold changes or focus on the differences instead of the similarities.

### 4.1.2 Single interaction modeling encodes nonlinear regulation

In **section 4.1.1** we have described the reasons to base the modeling approach presented here on a neuro-fuzzy framework. A neuro-fuzzy model is a fuzzy logic model which can be trained using optimization algorithms common in neural networks. As such, the qualities of a FL model that can be trained are the premise and consequent membership function parameters [Übeyli, 2009], the variables related in each logic rule [Chiu, 1994] and the number of rules [Wang and Palade, 2011]. Here, we established an exhaustive search for all possible interactions between morphological and functional features of mitochondria by constructing 30 single input-single output (SISO) fuzzy logic (FL) models. Each interaction represents a potential cause and consequence relationship, and amongst those the best models indicated events that were likely to be related. This initial approach has the characteristic that such a metric is not absolute but relative to other models, which was enabled by using the same setup for all models. In further work we investigated different modeling setups, a strategy to reduce the number of free parameters and the contribution of the model qualities to the sensitivity of the model to establish an absolute measure of performance (see **section 4.2**). In order to implement a SISO FL model, logic rules need to be determined that relate input to outputs e.g. IF concentration of protein  $X$  is **high**, THEN protein  $Y$  is **highly inhibited**. However, said rules do not relate directly the experimental data but the so-called fuzzy sets such as *high*. To establish the degree of membership (DOM) of the data points

to said fuzzy sets, we used two membership functions [Zadeh, 1968] of gaussian shape as shown in **equation 4.1**.

$$\mu_{low}(x) = e^{-\frac{(x-a)^2}{2\sigma^2}} \quad (4.1)$$

, where  $\sigma$  is the width of the membership function centered at  $a$ . Several types of fuzzy inference systems are possible [Takagi and Sugeno, 1985, Mamdani and Assilian, 1999]. To enable the use of neuro-fuzzy training algorithms, we chose a first order Takagi-Sugeno system [Übeyli, 2009] and distributed the parameters as a neural network (see **figure 4.7**).

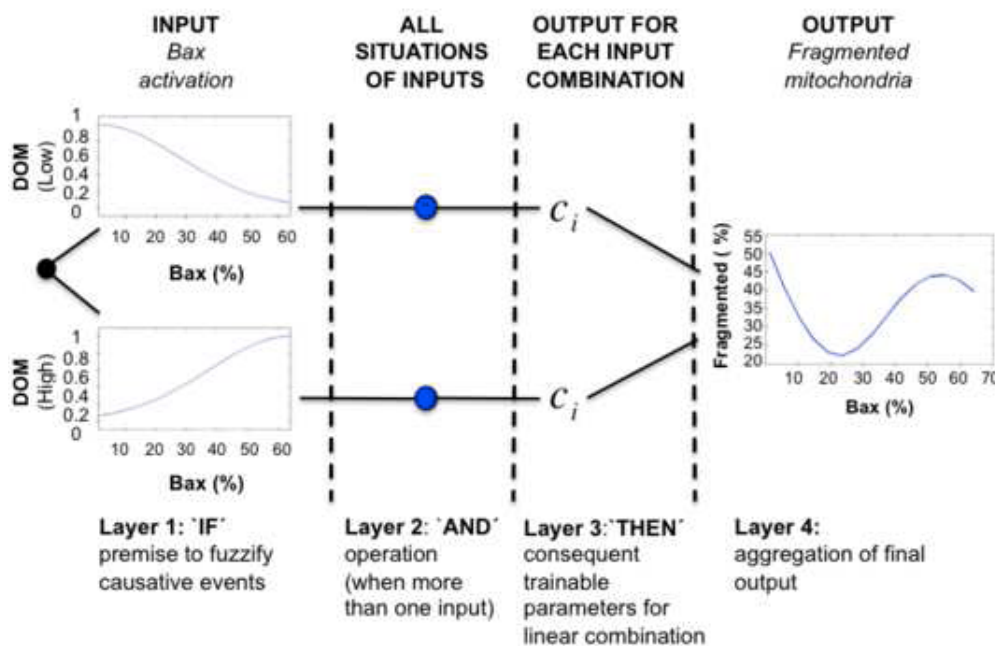


**Figure 4.7: Representative Single input-single output (SISO) model.** Example of one model built upon the hypothesis that Bax activation caused fragmented mitochondria. The parameters of the model are distributed following a neural network structure. In the first layer are shown the parameters of the membership functions (MFs) that fuzzified Bax activation, mapping the degree of membership (DOM) of its measurements into 2 fuzzy sets. These fuzzy sets represent “low” and “high” levels of Bax activation. The second layer has scalability purposes: it would contain the rules to combine all the inputs if the model had more than 1 input. The third layer contains parameters ( $c$ ) to linearly combine the  $i$  input MFs. Input and output MF parameters were fitted to the data. The fourth layer aggregates the values from layer 3 to finally model the behavior of “fragmented” mitochondria as a function of “Bax”. Figure from [Reis et al., 2012].

The SISO model was then fit to the data via standard algorithms [Übeyli,

2009]. Importantly, estimating the parameters of the system from the data eliminated the bias inherent to manually implementing the systems. An advantage of this method is that it is straight-forward to extend the approach to a multiple input-single output model. For more details on the implementation of a single model for this first approach, the reader is referred to **section 3.3**. For more details on how to extend and evaluate this approach, the reader is referred to **section 4.2**, in which we further extended the approach and applied it to analyze the evolution of signaling networks.

### 4.1.3 Modeling suggests a hierarchy for mitochondrial apoptotic events

#### Exhaustive search of potential interactions

To determine directionality of all interactions, i.e. relationships between morphological and functional events of mitochondrial regulation, we analyzed each model in a pair-wise manner as shown in **figure 4.8A**. The two analogous models encoding the two potential senses were termed *mirror-models*, e.g. the models which considered Bax influence on mitochondrial morphology were compared against the models in which mitochondrial morphology classes influenced Bax activity. From each pair of *mirror-models*, the one with a root-mean-squared error (RMSE) higher than a threshold value of 15 were excluded (threshold in **figure 4.8A**). Thereby we obtained a set of models with a defined directionality of input-output. From the remaining models, those with the least error within each *mirror-model* were selected and its direction represented in **figure 4.8B** and **C** (black arrows for the smaller RMSE).

#### Potential hierarchy of mitochondrial apoptotic events

Our exhaustive search results suggest that Bax activation was strongly related to both  $\Delta\psi_m$  and mitochondrial fragmentation, which in turn strongly influenced  $\Delta\psi_m$  dynamics together with the swollen mitochondrial morphologic state **figure 4.8B**. In summary, Bax is suggested to be upstream of mitochondrial depolarization and mitochondrial fragmentation **figure 4.8C**. In turn, mitochondrial morphology and  $\Delta\psi_m$  are closely related in both directions, although with different intensities revealed by a smaller error on the direction



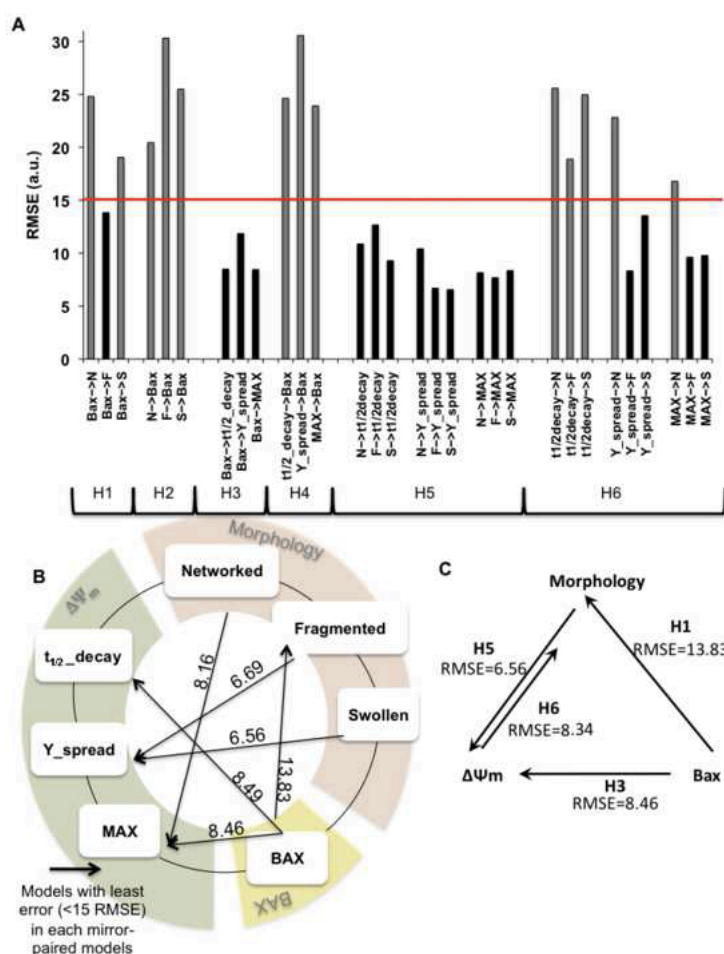


**Figure 4.8: Hierarchy of apoptotic events suggested by exhaustive search.** (A) Root-mean-square error (RMSE) of all 30 models. A Single Input-Single Output (SISO) model was trained with the data for each corresponding interaction, thereby parameterizing 30 different models. Model accuracy was measured and expressed as RMSE. Here are plotted the RMSE for all possible hypothesis (H): H1. "Individual mitochondrial morphology classes cause Bax"; H2. "Bax is responsible for morphology classes"; H3. "Bax causes each of mitochondrial membrane potential ( $\Delta\psi_m$ ) subset"; H4. " $\Delta\psi_m$  subset induces Bax"; H5. "Mitochondrial morphology induces  $\Delta\psi_m$  subset"; H6. "Each of the  $\Delta\psi_m$  subset is responsible for the morphologic classes". First selection was made by discarding all models with a  $RMSE > 15$  (threshold in red). Next, the least errors between "mirror-models" were chosen (black bars). For clarity, H1-model is the "mirror-model" of the H2-model as H3-model is the opposite of H4-model and as H5-model is for H6-model. (B) Detailed causality predictions between datasets. Scheme representing the final 6 most relevant predictions out of the 30 models. To assign these directional arrows, associated RMSE errors of the individual "mirror-models" were compared, e.g. H1-RMSE against H2-RMSE. Arrow direction was chosen based on the smaller error between "mirror-models" per dataset: Morphology, Bax and  $\Delta\psi_m$ . The numeric values associated with the arrows correspond to the actual RMSE value resultant for the directional model prediction. (C) Simplified scheme summarizing main interactions and causality suggested by our modeling results. Figure adapted from [Reis et al., 2012]

from mitochondrial fragmented states, i.e. fragmented and swollen to  $\Delta\psi_m$ .

#### 4.1.4 Literature validation of hierarchy suggested by model

The results presented above suggested that Bax is actively involved in causing mitochondria fragmentation, consistent with reports that its interaction with mitochondrial fission protein Drp1 regulates fragmented states (see **table 4.1**). Additionally, it was suggested by modeling that mitochondrial morphological states are tightly linked to MPT dynamics. In fact, the model proposed a strong connection between  $\Delta\psi_m$  and non-networked states of mitochondrial morphology, fragmentation in particular. Studies in the literature showed that by inhibiting mitochondrial fragmentation, a delay in MPT is observed (**table 4.1**). Finally, the model indicated that Bax activation is upstream of MPT, which is also supported by literature as shown in the studies compiled in the center row of **table 4.1**.

Here we have presented exclusively the results of this study, which were directly involved in or derived from the modeling process. For further results on the experimental branch of this work, the reader is referred to [Reis et al., 2012]. The modeling method presented here was designed and established for the specific experimental question described. Next, this approach was further developed to study the question presented in **section 4.2**.

**Table 4.1: Studies in literature supporting hierarchy of morphological and functional features of mitochondria suggested by the model.**

<b>Causality</b>	<b>Last error parameters (RMSE<sup>a</sup>)</b>	<b>Reported interactions</b>
Bax $\rightarrow$ Mitochondrial morphology	Fragmented (13.83)	Active Bax redistributes to the mitochondria and stimulates Drp1-mediated fission during apoptosis, leading to fragmentation. [Karbowski and Youle, 2003, Frank et al., 2001, Desagher and Martinou, 2000, Karbowski et al., 2002, Bossy-Wetzler et al., 2003, Arnoult, 2007]
Bax $\rightarrow \Delta\Psi_m^b$	Max (8.46); $t_{1/2}$ decay (8.49)	Bax undergoes conformational changes and oligomerization resulting in loss of $\Delta\Psi_m$ and subsequent MOMP <sup>c</sup> . [Wolter et al., 1997, Wasiak et al., 2007, Pastorino et al., 1998, Nechushtan et al., 2001, Waterhouse et al., 2001, Kuwana et al., 2002, Kim et al., 2009]
Bax $\rightarrow \Delta\Psi_m(Y_{spread})$	Fragmented (6.69), Swollen (6.56)	Inhibition of fragmentation has been shown to delay MOMP. Disruption of the mitochondrial outer membrane and consequent loss of $\Delta\Psi_m$ can result from intensive swelling. [Vander Heiden et al., 1997, Petit et al., 1998, Minamikawa et al., 1999, Scarlett et al., 2000]

<sup>a</sup>RMSE: root mean square error

<sup>b</sup> $\Delta\Psi_m$ : mitochondrial membrane potential

<sup>c</sup>MOMP: mitochondrial outer membrane permeability

## 4.2 Modeling evolution of MAPK signaling

### 4.2.1 Study of signal transduction to identify signaling rearrangements

#### Phosphoplex study of MAPK signaling

A-375, a melanoma cell line featuring constitutive activation of the MAPK pathway due to the activating mutation V600E [Polzien et al., 2011] was submitted to treatment using 3 pharmacological kinase inhibitors<sup>5</sup>. The transduction of the signal through the pathway was measured as level of phosphorylated protein for 10 signaling intermediates and transcription factors involved in the MAPK pathway at 8 time points spanning over 4 days. These signaling intermediates and transcription factors include mitogen-activated protein kinase 1 (MEK1), extracellular signal-regulated kinase 1/2 (ERK1/2), cAMP response element-binding protein (CREB), protein kinase B/Akt (Akt), c-jun n-terminal kinase (JNK), the JNK substrate cJUN, IKK, p38, p53 and ATF2. In such a long time scale, expression and degradation events play an important role in the dynamics of the system [Terfve and Saez-Rodriguez, 2012], hence abundance of the proteins was also measured. As a representative example, **figure 4.9A** shows measurements of total levels of ERK 1/2 in control conditions and the level of the phosphorylated protein measured in the same sample is shown in **figure 4.9B**.

#### Idea behind developed method

Using the acquired phosphorylation profiles as a signature of signal transduction, we sought to develop a method based on mathematical modeling to test the canonical pathway and, in the event of finding it invalid, to identify potential signaling rearrangements. Along these lines, we expected that if the experimental data disagreed with the reported interactions after a certain point in time and onwards, a model based solely on a prior knowledge network and trained to the relevant data would exhibit an increase of error that would suggest such rearrangement. This idea is described in **figure 4.10**.

---

<sup>5</sup>Experimental measurements of total and phosphorylated protein levels were performed by Stefan Maßen

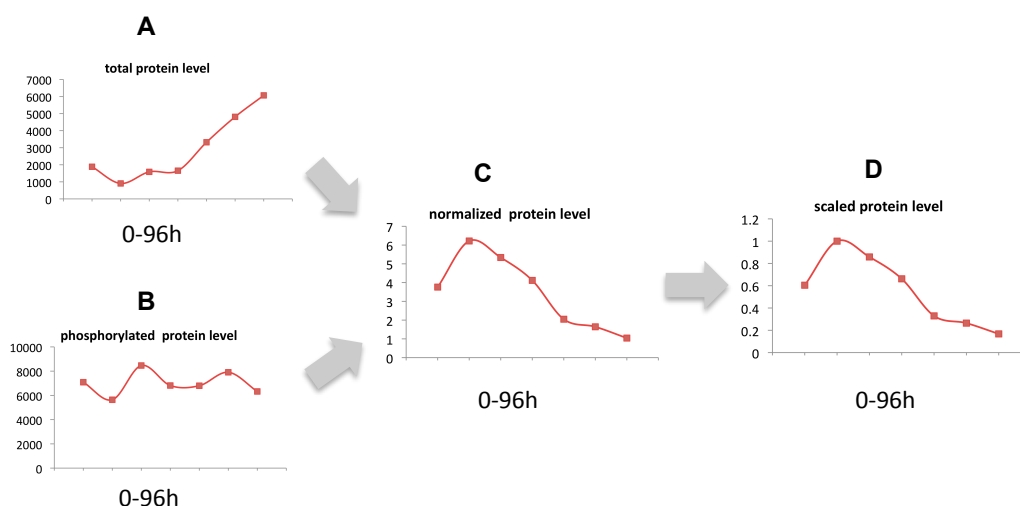


**Figure 4.9: Study of phosphorylation profiles to enable identification of signaling rearrangements.** (A) At the indicated times, A-375 melanoma cell line was measured to acquire total protein level of 10 signaling intermediates and transcription factors involved in MAPK signaling. Here, ERK is depicted for representation. (B) As a signature of signal transduction, phosphorylated levels were measured at same time points. (C) Phosphorylated protein levels were normalized to total for all measurements, to account for total protein loss. (D) To enable model fitting and comparison amongst species, measurements were scaled to maximum protein value for each condition.

### Data scaling and normalization

Data scaling was performed as mentioned in [section 4.1.1](#). To that end, phosphorylated protein levels were normalized to total in order to remove apparent loss of activation due to loss of total protein ([figure 4.9C](#)). In the last step of our data processing pipeline, normalized values were scaled to the maximum value across all measurements in the same condition to free the data-driven model from artifacts in which higher intensity values could dominate the modeling process ([figure 4.9D](#)). Due to the V600E mutation, the pathway was expected to exhibit a high phosphorylation profile, potentially with oscillatory behavior as it has been shown in silico that the combination of a negative feedback loop and ultrasensitivity can bring about sustained biochemical oscillations [Kholodenko, 2000].

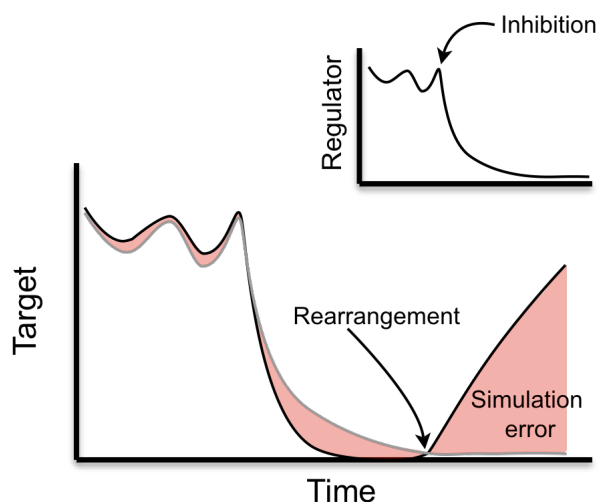


**Figure 4.10: Phosphorylation profiles suggest signaling plasticity.** Cartoon illustrating the aim of the method presented here to identify a rearrangement in the expected behavior of the phosphorylation profile (black curve, upper panel) exhibited by a member of the MAPK pathway in A-375, a melanoma cell line with a constitutive activation driven by V600E mutation. When treated with a specific inhibitor, the phosphorylation of a regulatory kinase should be completely inhibited. The regulated downstream target (black curve, lower panel) should be analogously down-modulated. In the case of a signaling rearrangement, the regulated protein should stop responding to regulatory behavior, and a mathematical model (grey curve) assuming the original situation should exhibit a high error (increased red area under the curve).

#### 4.2.2 Data-derived single model implementation and parameter reduction

We next aimed at developing a method to mine the acquired data set, thereby enabling identification and understanding of dynamical changes and differences between the established topology and the regulatory network of interactions in the specific cell line of interest. To illustrate the modeling process established in this work to encode a single intermediate and its behavior as a component of a signaling network, consider the interaction between cJUN and JNK. The reason for this specific choice is that JNK is a member of the MAPK pathway that has been shown to be tyrosine and threonine phosphorylated as part of the stress and inflammatory response. Phosphorylated JNK can translocate to the nucleus to activate a number of transcription factors including cJUN [Liu et al., 2007]. Thereby, the aim to express the behavior of cJUN as a function of JNK was justified. To enable mapping of input data into output data, IF-THEN

logic rules lay at the core of logic models such as *if phosphorylation of JNK is high then activity of cJUN is high*. Here, sets such as *high*, *medium*, or *low* are fuzzy sets to which the continuous experimental data belongs. Conversely to Boolean logic, fuzzy sets have unsharp boundaries; that is, measurements do not either belong to them or not. Instead, measurements can belong to the fuzzy sets to a certain degree, requiring a transformation known as fuzzification performed by the so-called membership function [Zadeh, 1968].

### Model definition

In **section 4.1** we used Gaussian functions to fuzzify measurements of mitochondrial morphology and apoptotic signaling in order to explore their non-linear relationships in human breast carcinoma. Analogously, input membership functions were defined here as shown in **equation 4.1** and used to establish the degree of membership of the JNK measurements –here represented as  $x$ – to the sets *low* and *high* (**figure 4.11B**).

Output membership functions were defined as a first order polynomial, as established in first order Takagi-Sugeno systems (see methods for further detail). In this framework, logic rules establish which combination of input and output membership functions are connected. Hence, the two-rules FL model or fuzzy inference system (FIS)  $f(x)$  illustrated in **figure 4.11C** can be expressed as the summation of the products of the normalized outputs from the rule premise and a first-order polynomial for each rule as shown in **equation 4.2**.

$$f(x) = \sum_{i=1}^2 \bar{\omega}_i f_i = \frac{e^{-\frac{x^2}{2\sigma^2}}(p_1x + q_1) + e^{-\frac{(x-1)^2}{2\sigma^2}}(p_2x + q_2)}{e^{-\frac{x^2}{2\sigma^2}} + e^{-\frac{(x-1)^2}{2\sigma^2}}} \quad (4.2)$$

, where  $\sigma$  is the width of the membership function centered at 0 or 1 and  $p$  and  $q$  are parameters of the polynomial. In **section 4.1.2**, we established our first modeling approach, in which premise and consequent membership function parameters of a FL model were learned from the data as shown in [Übeyli, 2009]. In said approach, the focus was at exhaustively searching amongst all measured events the best model, as a relative metric indicating events that were likely to be related. Conversely, in this work we sought to evaluate the accuracy of the models in a more absolute manner.

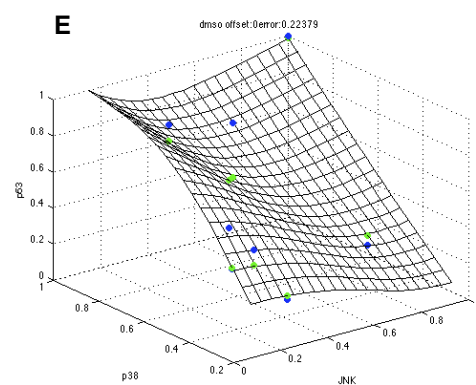
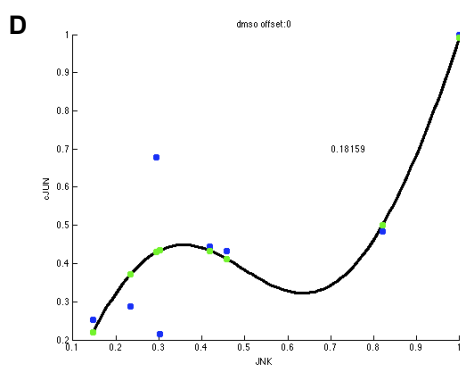
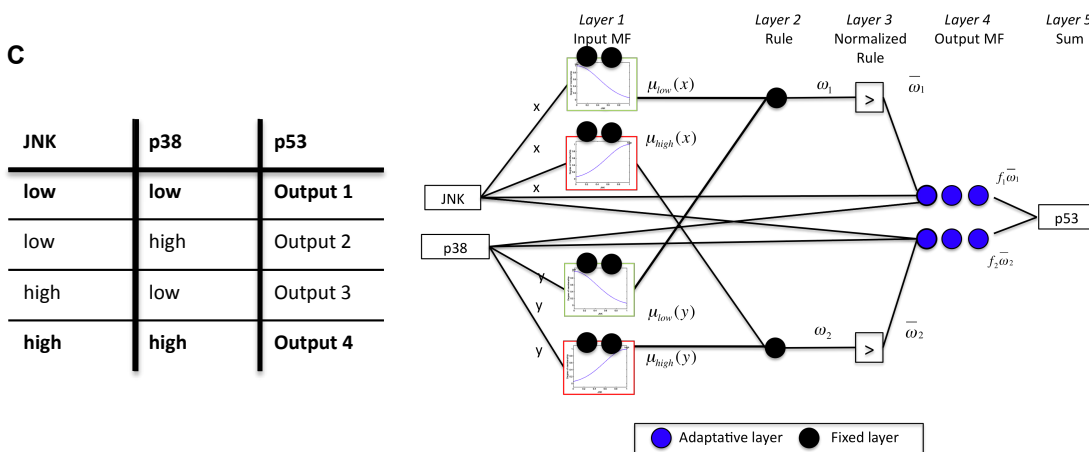
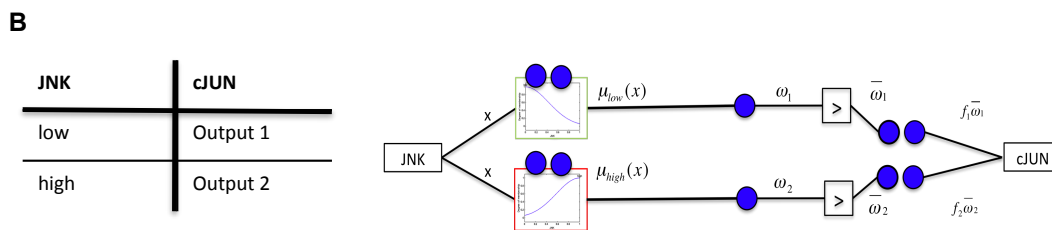
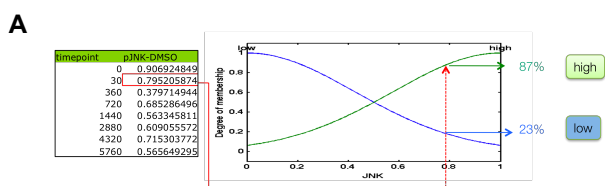
Additionally, in the model shown in **equation 4.2**, it would be necessary

to fit 8 parameters exclusively for the definition of the membership functions. Additionally, a list of model qualities can be learned from the data, namely variables related in each rule [Chiu, 1994], number of rules [Wang and Palade, 2011] and type of membership functions, increasing the number of parameters even orders of magnitude [Huang and Hahn, 2009]. Importantly, such a high complexity of the model becomes a problem when one wants to gain insight on the data based on its reproducibility by the model. Hence, it was crucial in this work to establish a strategy to reduce the number of parameters.

---

**Figure 4.11 (following page): Parameter reduction strategy and data-derived model implementation.** As an example, the strategy for model implementation is illustrated using JNK regulation of cJUN. **(A)** A fuzzy inference system was built to model the JNK-cJUN relationship. To enable fuzzy inference, as a first step experimental data needs to be fuzzified into the logic sets used in logic rules. Here, JNK data was transformed into fuzzy sets via 2 Gaussian input membership functions. **(B)** A logic rule such as IF phosphorylation of JNK is *low*, THEN activity of cJUN is *low* is in practical terms a placeholder here represented as a horizontal line, that maps certain values of JNK -e.g. those classified as *low* by the membership functions- to those values of cJUN classified as e.g. *low*. In a simple FL system with two rules, even when the number of rules has been determined, 10 free parameters are required. Displayed as blue circles, 8 free parameters are required for the membership functions. The input membership functions could require even more parameters, depending on the type of function. In turn, the number of parameters in the output membership functions depends on the number of model inputs. Another step to implement such a system is to determine the input functions involved in each logic rule, here depicted as an additional parameter in the center of each rule. **(C)** Implementation of a FL model encoding the regulation of p53 by p38 and JNK to illustrate the parameter reduction strategy. A traditional fuzzy logic features many qualities that are usually trained. In the Takagi-Sugeno framework, the number of consequent parameters depends on the number of rules, which in turn depend on the number of inputs. The setup described in **(C)** would yield 4 rules (see left panel), which would require 20 parameters altogether. To reduce the number of free parameters, we fixed the number of input-output combinations (left, in bold), which yielded a reduced system of 2 rules and 14 parameters (right). By fixing the premise parameters, the number of parameters to be estimated was reduced to 6, i.e. below the number of experimental time points. **(D)** The minimal set of parameters free for training proved to be sufficient to capture the trend in the data (blue dots, RMSE=0.181) upon simulation (green dots), here illustrated in control conditions. The black curve shows the simulation of the model at 100 interpolated data points distributed uniformly. The same reduced model was later readily fitted to the measurements of JNK and cJun in all inhibition conditions (see Results). **(E)** To illustrate modeling of a transcription factor regulated by two upstream intermediates, p53 model is depicted here as a mesh showing high accuracy as well (RMSE=0.223). To better display the deviation of the model, training data points are depicted in blue and the simulation at the same data point is depicted in green, while the black curve shows the simulation of the model at 100 interpolated data points distributed uniformly.





• experimental data    • data point simulation    — interpolated simulation

### Parameter reduction strategy

We fixed the number of fuzzy sets – and thereby the number of input membership functions – to 2, i.e. measurements were separated into being *low* and *high* to a certain degree. Next, the number of rules was fixed: as the number of rules depends on the number of inputs, consider for illustration of the reduction strategy an upgrade to a FL system with two inputs, implemented to model the behavior of p53. p53 has been shown to be activated by p38 kinase [Bulavin et al., 1999] and via JNK signaling [Fuchs et al., 1998]. Given that two fuzzy sets are defined for each input, the number of input membership function combinations is  $2^n = 4$ , where  $n$  is the number of inputs, i.e. 4 rules were necessary to accommodate the 4 combinations. Importantly, in Takagi-Sugeno systems, parameters of output MFs cannot be shared. Instead, in classical training different parameters are learned for each output MF [Jang, 1993]. Therefore, the above-mentioned system of rules would yield 3 consequent parameters for the linear combination of 2 inputs for each rule, i.e.  $2^n(n + 1) = 12$  output parameters. Together with the 8 parameters for the input membership functions, such a rule setup yields a total of 20 parameters. Therefore, as part of the reduction strategy only those combinations for the extreme cases *low-low* and *high-high* were taken into account (**figure 4.11D**), yielding a system of 2 rules, 8 parameters of the input membership functions and 6 parameters for the different output membership functions to a total of 14 parameters. In the last step of the parameter reduction strategy, we aimed at fixing the parameters themselves, as opposed to the above-mentioned steps to fix the number of parameters. Because the consequent parameters of each rule cannot be shared, we fixed the premise parameters. Hence, the final number of parameters fitted is  $2(n + 1) = 6$  where  $n$  is the number of inputs. The system following the example shown in **figure 4.11D** is expressed as  $f(x, y)$ :

$$\begin{aligned}
 f(x, y) &= \sum_{i=1}^2 \bar{\omega}_i f_i = \\
 &= \frac{e^{-\frac{x^2}{2*0.4247^2}} e^{-\frac{y^2}{2*0.4247^2}} (p_1 x + q_1 + r_1) + e^{-\frac{(x-1)^2}{2*0.4247^2}} e^{-\frac{(y-1)^2}{2*0.4247^2}} (p_2 x + q_2 + r_2)}{e^{-\frac{x^2}{2*0.4247^2}} e^{-\frac{y^2}{2*0.4247^2}} + e^{-\frac{(x-1)^2}{2*0.4247^2}} + e^{-\frac{(y-1)^2}{2*0.4247^2}}}
 \end{aligned} \tag{4.3}$$

Subsequently, we sought to assess whether the free parameters sufficed to capture the patterns in the data. Upon training, the JNK-cJUN system (equation 4.2, illustrated in figure 4.11C) showed a noteworthy accuracy, RMSE= 0.181 (figure 4.11E). For the JNK-p38-p53 system illustrated in figure 4.11D), high accuracy was achieved as well (0.223, figure 4.11F). Due to the high flexibility of the fuzzy inference system, several solutions could be found during the fitting process. The reader is referred to the methods section for a detailed description on the objective function defined to select fits with best interpolation power. Hence, the method established enabled to satisfactorily fit exclusively  $2(n + 1)$  premise parameters, where  $n$  is the number of inputs, thereby avoiding estimating (i) the number of rules, (ii)  $4n$  premise parameters and (iii) up to  $2^n(n + 1)$  consequent parameters. For further details on the strategy followed to fix the number of free parameters, the reader is referred to the methods.

### Data-derived sensitivity analysis

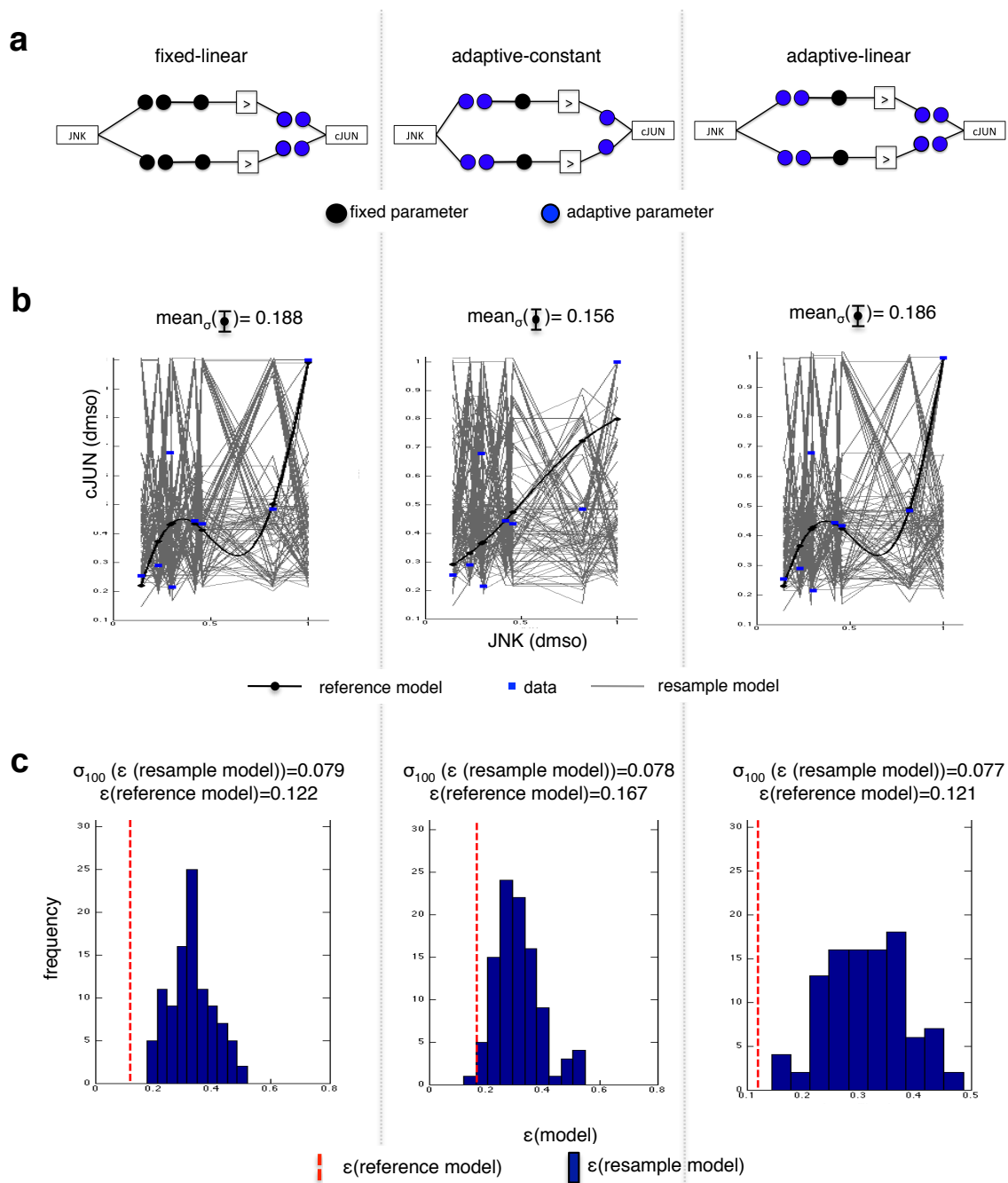
In spite of the number of free parameters being greatly reduced, we expected the system to keep its flexibility, a key feature in a data-derived model. To validate this, the effect on parameter changes was studied here to determine its impact on the system implemented via the presented reduction strategy. Sensitivity of a systems output to certain parameters can be used to determine which parameters of a model should be estimated when modeling signal transduction [Zi et al., 2005, Huang and Hahn, 2009]. In general, during sensitivity analysis the parameters of the model are directly modified. Instead, to continue with the data-derived nature of this approach, here the training data was resampled, which in turn led to a modification of the fitted parameters. To study the effect of the presented reduction strategy on the flexibility of the system, the analysis was performed on the established setup (represented in figure 4.12A, left) and two comparisons where the model's complexity was only partially reduced by fixing the number of rules and MFs but not the premise parameters: (i) the equivalent 0-order Takagi-Sugeno system (figure 4.12A, center), featuring free parameters for the premise and free constant parameters instead of linear for the consequence clause [Takagi and Sugeno, 1985] and (ii) the system shown in equation 4.2, which features free premise and consequent

parameters (**figure 4.12A**, right).

Consequently, the fixed-linear setup rendered 4 free parameters, as opposed to 6 in the adaptive-constant and 8 in the adaptive-linear. The three systems were trained using the JNK-cJUN measurements in control conditions –the reference model– and 100 resampled versions of the same dataset –the resample models– (**figure 4.12B**). Resampling was performed following the method introduced in [Efron, 1979]. Dependency on the data was calculated by simulating the resampled models and computing the standard deviation at the datapoints across models (**figure 4.12B**). Fixed-linear and adaptive-linear setups varied greatly ( $\text{mean}_\sigma(\text{fixed-linear}) = 0.188$  and  $\text{mean}_\sigma(\text{adaptive-linear}) = 0.186$ ), while adaptive-constant setup showed a smaller dependency on the

---

**Figure 4.12 (following page): Data-derived sensitivity analysis validates accuracy and flexibility of approach.** The training dataset was resampled and the impact in the proposed setup was compared to two alternative setups in order to test whether the parameter reduction strategy hindered flexibility or accuracy of the model. **(A)** Three approaches were compared. The schematic left represents the above-proposed approach, with the corresponding fixed premise parameters (black circles) and free linear consequent parameters. A simpler, established 0 order Takagi-Sugeno fuzzy logic system is represented in the center schematic. Such a system features the same input MFs –with free parameters here for comparison– and simpler consequent MFs with a free single parameter, i.e. a constant. The right-hand schematic shows the same setup as the left schematic, with the difference that no parameter was fixed, i.e. both premise and consequent parameters were adaptive. **(B)** Models implemented via the 3 setups were trained with 100 bootstrapped datasets, i.e. resampled with repetition. Thereby, 100 models per setup were created, here shown as grey curves. The reference model was trained to the full original dataset (black curves for the model, blue dots for the experimental data). As a signature of flexibility, the standard deviation  $\sigma$  for the model simulation at each data point was calculated across the 100 bootstrapped models. The mean of the deviation mean for all data points was next calculated. While both the adaptive-linear and fixed-linear show an ability to adapt to the different datasets ( $\text{mean}(\text{fixed-linear})=0.188$  and  $\text{mean}(\text{adaptive-linear})=0.186$ ), the adaptive-constant setup exhibited a less flexible performance (center,  $\text{mean}(\text{adaptive-constant})=0.156$ ) confirming that the consequent parameters outweigh the premise parameters in impact on performance. **(C)** As a signature of accuracy, the RMSE for the fully-trained i.e. reference model was calculated for each setup. While the fixed-linear and adaptive-linear setups exhibit similar accuracy (0.122 and 0.121 RMSE error respectively), the loss of accuracy is more important in the adaptive-constant setup (RMSE error 0.167). Additionally, the RMSE for each bootstrapped model was calculated and depicted here as a histogram against the error of the model fitted to the full dataset (blue bars and red line respectively). The standard deviation of the error was calculated to be similar in all setups, indicating that the RMSE error did not change differently for each method. These findings in performance and ranking of the 3 approaches were reproduced across the measurements upon the 3 inhibitors (see **table 4.2**). Taken together, these analyses indicate that the parameter reduction strategy renders a system that is not importantly compromised neither in flexibility nor in accuracy.



data ( $\text{mean}_\sigma(\text{adaptive-linear}) = 0.156$ ). To study the evolution of accuracy across resampled models, the RMSE error  $\epsilon$  for the reference model in each setup was calculated, and contrasted to the frequency of resample errors  $\sigma_{100}\epsilon$  (**figure 4.12C**). No important loss of accuracy was observed when comparing the fixed-linear model ( $\epsilon(\text{reference model}) = 0.122$ ,  $(\sigma_{100}\epsilon(\text{resample model}) = 0.079$ ) to the adaptive-linear model ( $\epsilon(\text{reference model}) = 0.121$ ,  $\sigma_{100}\epsilon(\text{resample model}) = 0.077$ ). On the contrary, the adaptive-constant setup showed a noteworthy loss of accuracy ( $\epsilon(\text{reference model}) = 0.167$ ,  $\sigma_{100}\epsilon(\text{resample model}) = 0.078$ ), indicating that most of the information on the data is captured by the consequent parameters.

These results were reproduced when performing the analysis on the 3 additional datasets acquired upon treatment with MAPK inhibitors (**table 4.2**). To that end, the analysis resampling the data to evaluate flexibility and accuracy of the approach, as described in **figure 4.12** for control conditions, was performed for all conditions. The model implementation and training setup featuring fixed premise parameters and adaptive linear consequent parameters was contrasted to two established setups: (i) A system with adaptive premise parameters and adaptive zero-order consequent parameters and (ii) a system with adaptive premise parameters and adaptive linear consequent parameters, i.e. the same setup as the fixed-linear system with the difference that here the premise parameters were not fixed. For each condition, a reference system was created which was trained to all data points acquired in said condition. The RMSE  $\epsilon$  was calculated for the reference model as a metric of accuracy. The training data set was resampled 100 times via bootstrapping and the standard deviation of the simulations  $\xi_{100}(t_i)$  at each data point  $t_i$  was calculated as a metric of flexibility. The error of every bootstrapped model was calculated, and the deviation for all 100 models  $\sigma_{100}(\epsilon)$  is shown. Ranking the calculations for the metrics of the setups for each condition shows that the first in accuracy, i.e. the setup with least references error, is the adaptive-linear closely followed by the fixed-linear. The most robust setup is the adaptive-constant, and the fixed-linear and adaptive-linear perform similarly, indicating that neither accuracy nor flexibility are greatly compromised by using the parameter-reduced setup.

Because neither flexibility nor accuracy seemed to be compromised, we con-

cluded that the parameter reduction strategy rendered a valid system. Therefore, the approach here presented enabled implementation and training of a model to encode the nonlinear behavior of a signaling intermediate or transcription factor as a function of the upstream activity. Next, this method was used as the cornerstone of our pipeline to model the dynamic behavior of the full network containing the 10 above-mentioned measurements upon 4 experimental scenarios.

**Table 4.2: Results of sensitivity analysis were reproduced upon inhibition conditions.**

	metric	control	rank	U0126	rank	AZD6244	rank	Sorafenib	rank
<b>Fixed linear</b>	$\xi_{100}(t_i)$	0.188	3	0.193	3	0.165	2	0.249	3
	$\sigma_{100}(\epsilon)$	0.079	3	0.076	3	0.073	2	0.084	3
	$\epsilon$	0.122	2	0.197	2	0.212	2	0.191	2
<b>Adaptive constant</b>	$\xi_{100}(t_i)$	0.156	<b>1</b>	0.126	<b>1</b>	0.112	<b>1</b>	0.191	<b>1</b>
	$\sigma_{100}(\epsilon)$	0.078	2	0.056	<b>1</b>	0.060	<b>1</b>	0.065	<b>1</b>
	$\epsilon$	0.167	3	0.223	3	0.230	2	0.211	3
<b>Adaptive linear</b>	$\xi_{100}(t_i)$	0.186	2	0.169	2	0.174	3	0.234	2
	$\sigma_{100}(\epsilon)$	0.077	1	0.057	2	0.073	3	0.075	2
	$\epsilon$	0.121	<b>1</b>	0.194	<b>1</b>	0.208	<b>1</b>	0.188	<b>1</b>

### 4.2.3 Prior knowledge and literature-based definition of initial topology

In order to use the described approach to implement a model for each experimental measurement, it was necessary to determine the subset of data to use for model training. Therefore, a signaling network containing all measurements was implemented as first step for simulation (**figure 4.13**). **Table 4.3** references the sources used for each interaction included. For a global view of the pathway map, the reader is referred to [Johnson and Lapadat, 2002] and the corresponding entry of the KEGG database (<http://www.genome.jp>). Once implemented, the topology shown became the hypothesis to be either confirmed or to reveal dynamic mismatches between prior knowledge and experimental data.

Consider for clarification a transcription factor TF.

Specifically, as stated in the previous section, implementation into the initial topology of transcription factor TF as being regulated by MAPK1 and MAPK2 implied linking data for measurements of MAPK1 and MAPK2 to measurements of TF under the same conditions. Subsequently, this data subset was used to fit the corresponding generalized FIS, thereby determining the specific parameter set for model TF under a single condition (**figure 4.13**).

### Multi-scenario simulation

The process to fit a single model under one condition was iterated using the generalized sFIS as initial function for all conditions (**figure 4.13**), and each parameter set was used to create a multi-scenario model (here termed msFIS). In order to allow evaluation of the model upon a chosen condition, a “naive condition switch” was introduced a posteriori in the FIS equation (**figure 4.13**), thereby avoiding an increase in the number of parameters required for training. See materials and methods for the mathematical definition, which features the requirements of a TKS fuzzy logic system and enables the use of said new variable in the msFIS. Finally, once all multi-scenario models in our signaling

---

**Figure 4.13 (following page): Workflow for network definition, fitting and simulation. Definition of starting topology.** The initial step was the implementation of a network topology. Grey nodes are measured in our experimental assay, here connected by vertexes representing interactions reported in literature. Blue nodes are not modeled due to not being measured and are depicted here solely to enable understanding of network as a whole. **FIS implementation.** Schematic representation of a 2-rule fuzzy inference system. Each horizontal line represents a rule and its elements (see **figure 4.11**). The method presented here enabled generalization: Following a parameter reduction strategy (**figure 4.11** and **4.12**), all parameters were fixed to the same value for all models and conditions with the exception of the consequent parameters here represented by question marks. **Condition-dependent FIS training.** A generalized FIS was trained using each condition-dependent dataset to determine the parameter set specific for each condition. **Multi-treatment FIS implementation.** The condition-dependent parameters were then used to create a multi-scenario model, including a naive condition switch to enable choice of corresponding parameters in the simulation of each specific treatment scenario. **Network simulation.** Upstream species could not be fitted to further upstream regulators. Hence, to reduce propagation of unnecessary error, upstream species were not simulated. Instead, an input node consisting of a simple mapping function specified the measured value of the upstream species at the simulated time point. Thereby, the propagation of time as a signal was enabled. In turn, the fitted models were evaluated at the upstream-simulated value. The discontinuous arrow represents the possibility, that signaling intermediates and transcription factors can be modeled as a function of multiple regulators upstream of them.



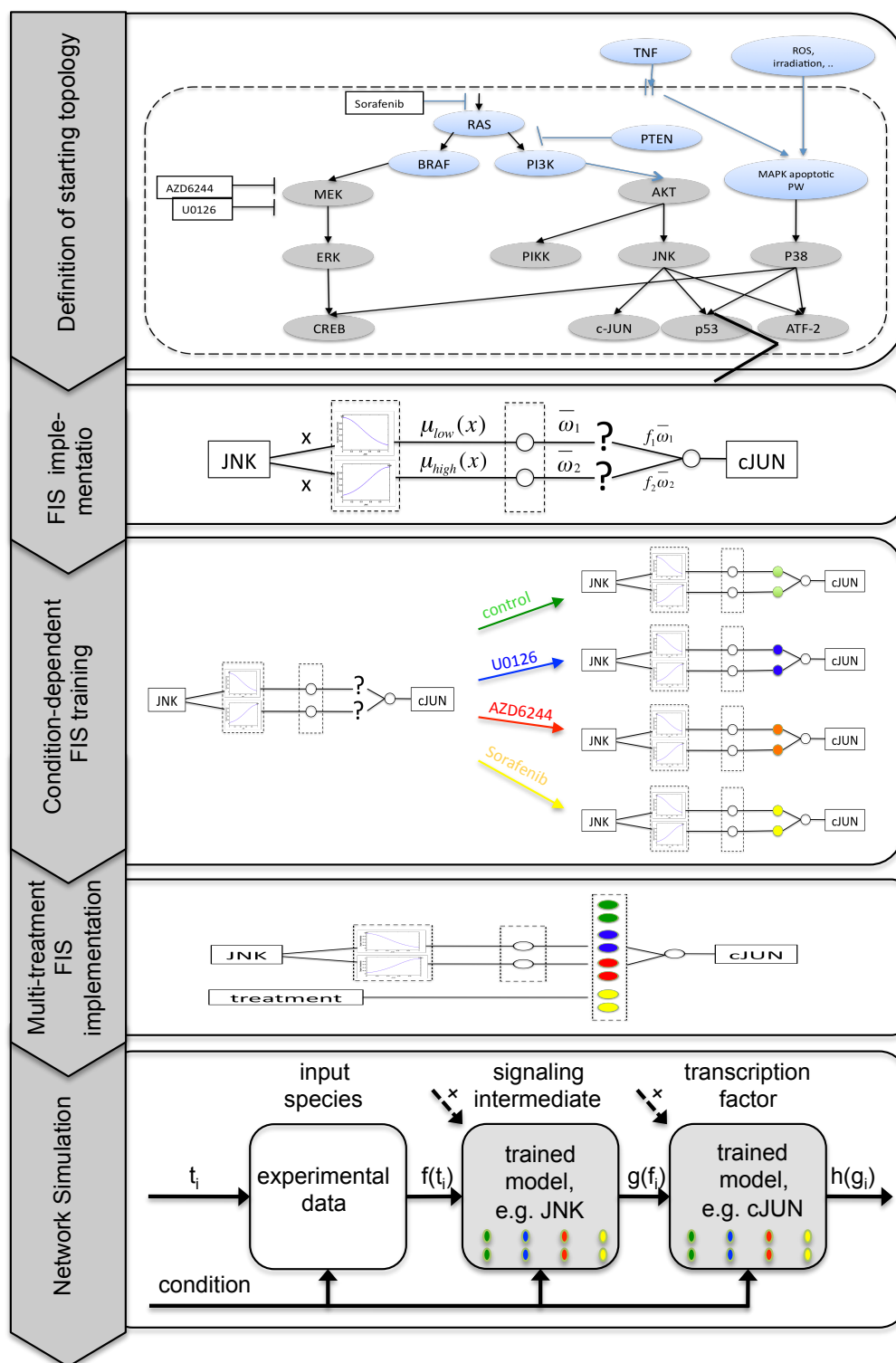


**Table 4.3: References used to determine interactions used for model fitting**

Regulation	Reference
MEK $\rightarrow$ ERK1/2	[Roberts and Der, 2007]
ERK1/2 $\rightarrow$ CREB	[Park and Cho, 2006]
p38 $\rightarrow$ CREB	[Iordanov et al., 1997]
Akt $\rightarrow$ JNK	[Aikin, 2004]
Akt $\rightarrow$ IKK	[Vivanco and Sawyers, 2002]
JNK $\rightarrow$ cJUN	[Liu et al., 2007]
JNK $\rightarrow$ ATF2	[Liu et al., 2007]
JNK $\rightarrow$ p53	[Fuchs et al., 1998]
p38 $\rightarrow$ p53	[Bulavin et al., 1999]
p38 $\rightarrow$ ATF2	[Liu et al., 2007]
PTEN $\rightarrow$ JNK	[Vivanco et al., 2007]

network were defined, simulation of full network behavior was performed. For those measurements being most upstream of the network, i.e. with no measurements upstream in the defined topology such as Akt, a mapping function was used to establish its value at each time point. Subsequently, propagation of the signal at each time point was achieved by evaluating each downstream model at the simulated output of those models defined as being upstream of it (**figure 4.13**). Reproducibility as RMSE below 0.2 could be considered very high taking into the account that the behavior of the network is derived from data and did not require mechanistic information.

#### 4.2.4 Benchmarking approach

To further evaluate goodness of network behavior and benchmark the accuracy of the propagated signal, we compared the performance of our method with the one of the method successfully established in [Aldridge et al., 2009]. To that end, the method described here was used to implement each model in the benchmark network and subsequently the data presented in [Gaudet et al., 2005] was used for parameter estimation (see **figure 4.14**).

**Figure 4.15** shows that high accuracy, i.e. up to 10 fold increase, was achieved with the method presented here. Additionally, this comparison em-

phasizes the reusability of the modeling approach, which can readily be used in different datasets. Interestingly, the comparison also revealed limitations of the method in terms of data-density requirements. For further insight learned from benchmarking, the reader is referred to the discussion.

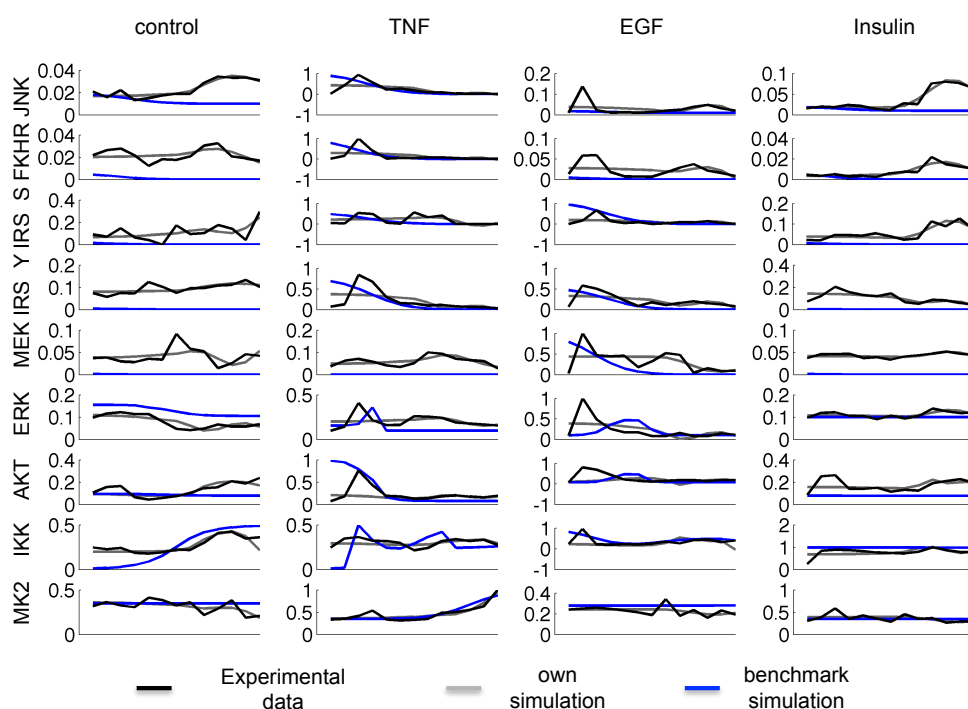


**Figure 4.14: Benchmarking our method shows high reproducibility, reduced bias and increased reusability at the cost of drastic increase of data requirements.** Model simulation (grey line) shows up to 10 fold increase of accuracy with respects to benchmarking method (blue line) presented by Aldridge et al in [Aldridge et al., 2009] and an improvement in capturing the trend over the 24 hours of measurement in the benchmarking data (black line). This improvement was enabled by the described modeling approach over the 4 conditions out of 10 in the benchmark dataset (columns) selected to enable comparison. The application of the approach presented here to an additional dataset revealed that parameters can be readily estimated, thereby easing the process of model implementation and simulation to encode the behavior of a signaling network. This is an advantage over methods that require manual model implementation. Challenges revealed by benchmarking in terms of data density requirements are extensively described in the discussion.

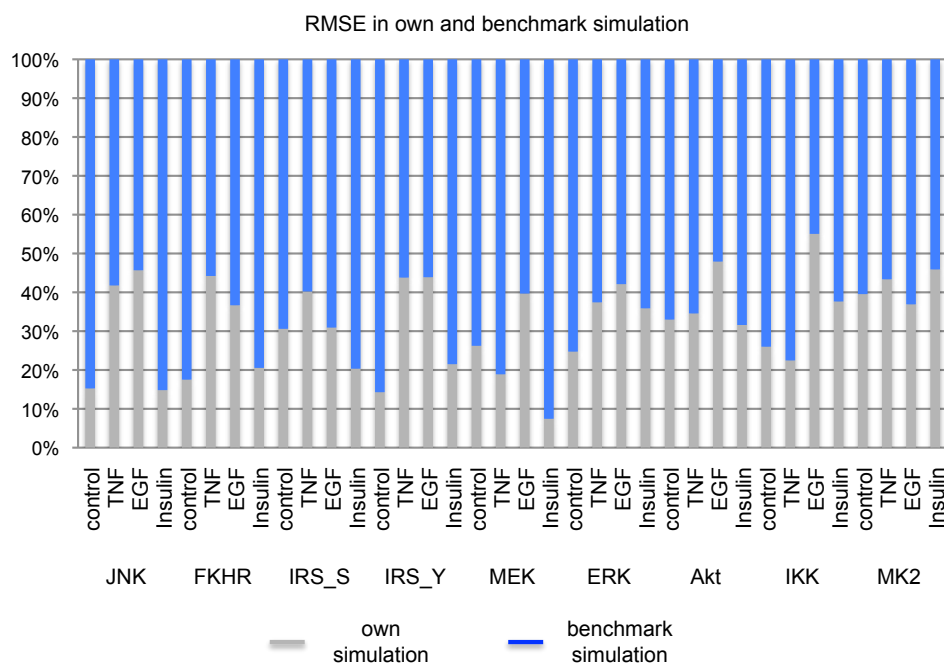


**Figure 4.15: Own method error against benchmark method error.** Comparing the performance of our method (root-mean-squared error in grey) against the benchmark method (root-mean-squared error in blue) shows that high accuracy i.e. up to 10 fold increase was achieved with the method presented here. Both models were trained to the same dataset, presented in [Gaudet et al., 2005].

### 4.2.5 Analysis of model evolution

Having established and tested a method to encode the behavior of the given signaling network, we next sought to identify potential signaling rearrangements. Therefore, we created new training data subsets by removing late time points in a stepwise manner, i.e. new datasets contained only measurements from 0 to 72h and analogously for 0 to 48h. The full training process was repeated and the newly trained network was simulated and evaluated (see **figure 4.16** and **4.17**).

We expected that if a signaling rearrangement occurred at a certain time point, the agreement between the involved intermediate and its substrate or substrates should greatly decrease after said time point. Such disagreement should be revealed by an increase of the RMSE calculated for the model downstream of the rearrangement. For those models fitted to control conditions with a high error already at the period 0-48 hours, this indicated that the

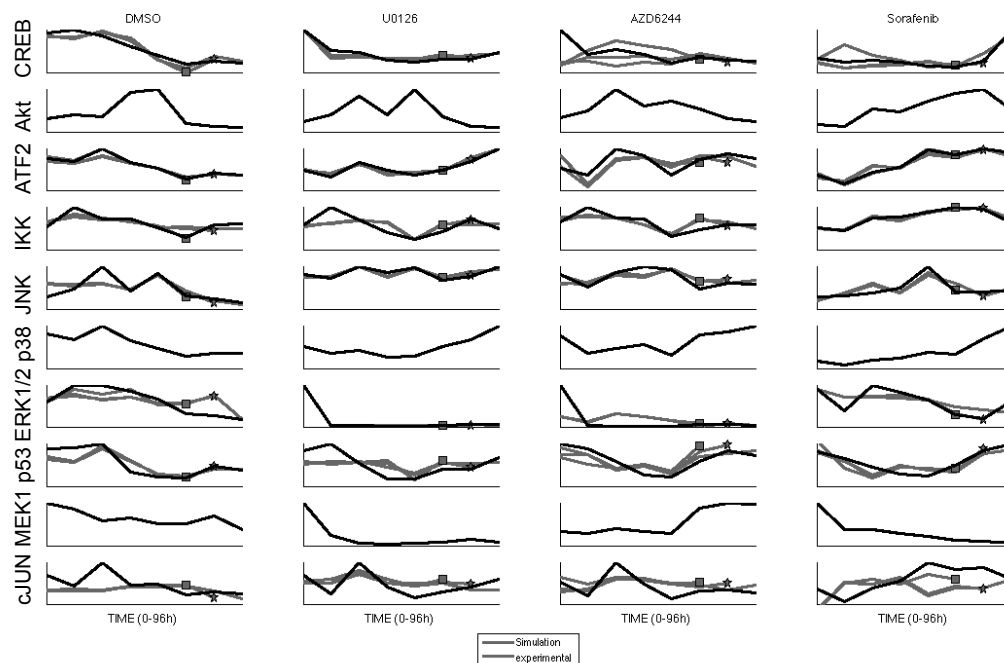


**Figure 4.16: Experimental data and model simulations for time-defined training subsets according to initial prior knowledge network.** Each species in the network is shown as rows for each treatment used (columns). Simulations are shown in grey upon training to data subsets containing measurements from 0 to 96h, up to 72h (indicated with a star) and 48h (indicated with a square). Experimental measurements are shown as black lines.

topology was wrongly assumed from the beginning. This was the case of JNK (error 96h=0.18921 vs error 72h=0.20094) and cJUN (error 96h=0.28357 vs error 72h=0.30519), which was emphasized when displaying the 96h error versus the 48h error (**figure 4.18A**). Plotting the trajectories for said models and data as implemented in the context of the prior knowledge network confirms that the reason for the JNK-cJUN misbehavior is that in our measurements Akt seems not to be driving their behavior (**figure 4.18B**), contrary to the topology introduced in the prior knowledge network.

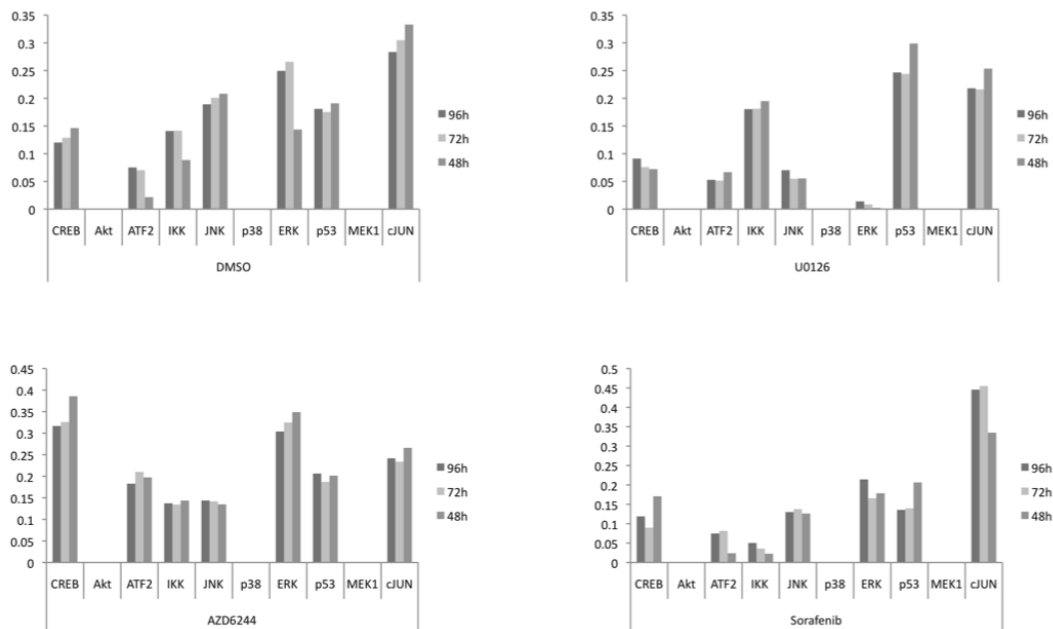


**Figure 4.17: Root-mean-squared error for time-defined model simulations according to initial prior knowledge network.** Root-mean-squared error was calculated for each simulation for all treatments. Control conditions show a high error for the Akt-JNK-cJUN pathway implemented in the prior knowledge network. This observation led to literature-based reimplementations of the network topology.

#### 4.2.6 Reimplementation of starting topology to account for emerging behavior

To take into account the Akt-JNK mismatch that emerged in control conditions, we modified our starting topology. In [Vivanco et al., 2007], the authors show that the JNK signaling pathway is itself a functional target of PTEN in prostate cancer cells, meaning that Akt and JNK can be activated independently from each other. Hence, we implemented JNK as being regulated independently from Akt by turning it into an input node (**figure 4.18C**). The behavior of cJUN was then strongly associated to JNK (new cJUN error at

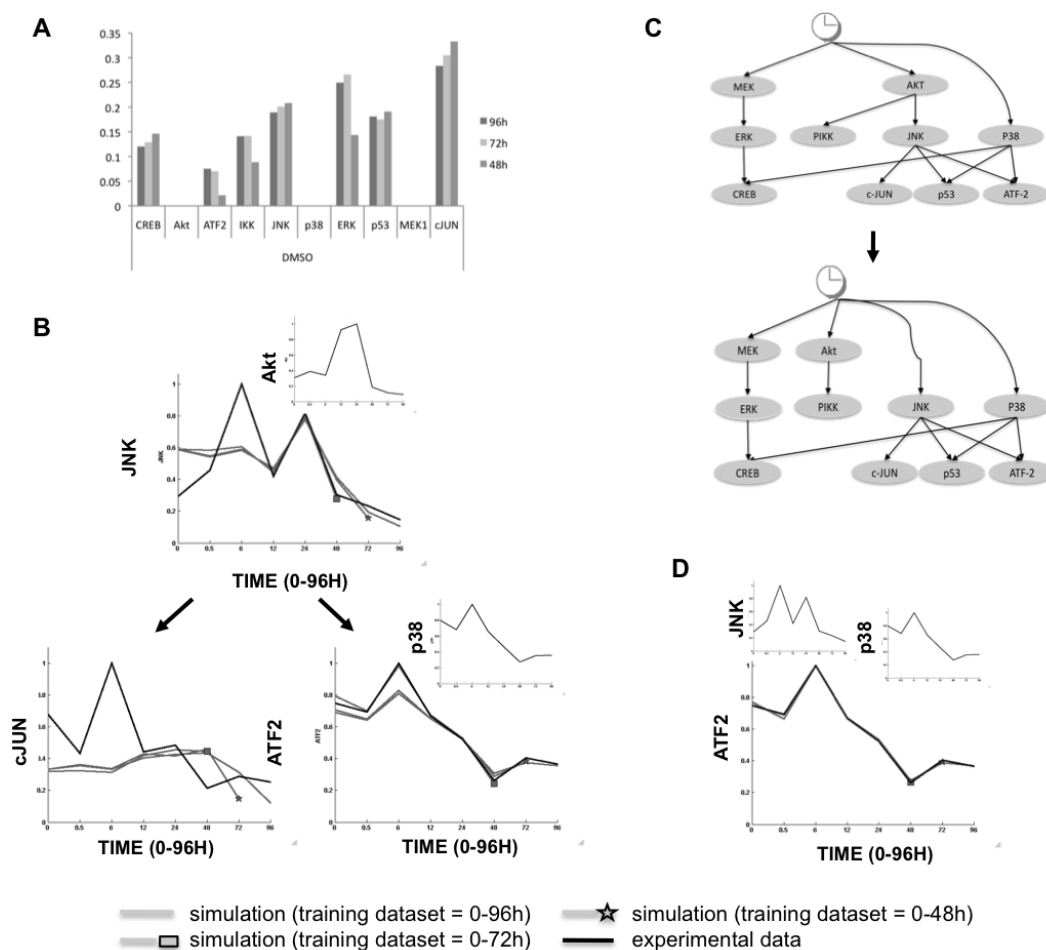


**Figure 4.18: Model-suggested reimplementations of topology addresses emerging behavior.** Using the described method, the behavior of all the species in the model was simulated in the context of the prior knowledge network specified. **(A)** Upon whole-network simulation, RMSE was calculated for models fitted to corresponding training measurements up to 48, 72 and 96 hours. The input nodes Akt, p38 and MEK1 were not simulated and are shown here as a reminder. The model cJUN shows a high error already at 48h and no improvement over time in control conditions (see **figure 4.16** and **4.17** for all models). **(B)** Plotting cJUN simulation in the context of the signaling network (trajectory of input species in smaller time course) for the models trained to measurements up to 48, 72 and 96h (grey curves, for better differentiation of models a star and a square indicate the last training data point used in 72 and 48 hour models respectively) shows that the reason for failed simulation is the error propagated from JNK, which in turn could not be modeled as regulated by Akt because the experimental data (black line) are indeed not related. On a neighbor branch of the prior knowledge network, ATF2 successfully reproduces the behavior of p38 but is also suffering from error propagation from Akt to JNK. **(C)** As a solution, literature search suggested an alternative topology in which Akt signaling is parallel to JNK. This alternative topology is depicted here, and was introduced in the model to account for this emerging behavior by turning JNK into an input node independent from Akt. **(D)** The reimplemented topology corrected JNK-regulated cJUN simulation (see **figure 4.19** and **4.20** for all models) and as there was no error propagation from JNK, simulation of ATF2 (grey lines) was then able to correctly follow p38 signaling.

96h=0.12241, see **figure 4.19** and **4.20**), and the misbehavior of ATF2 at early time points shown in (**figure 4.18B**) was corrected as well (**figure 4.18D**).

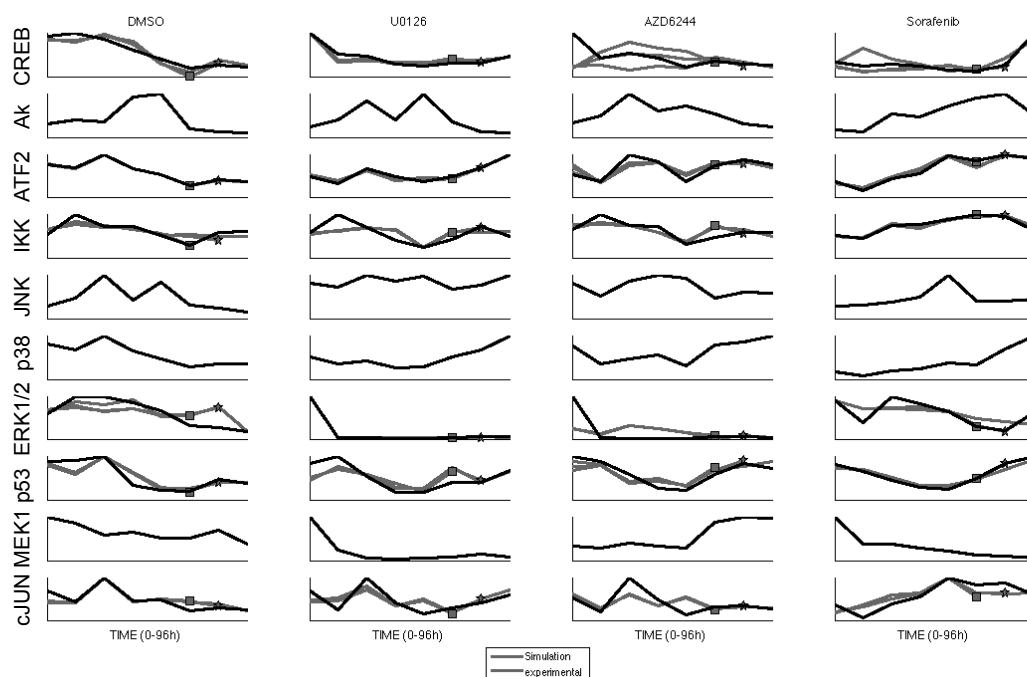


**Figure 4.19: Simulation after reimplementing of the initial prior knowledge network to account for emerging behavior.** Each species in the network is shown as rows for each treatment used (columns). Simulations are shown in grey upon training to data subsets containing measurements from 0 to 96h, up to 72h (indicated with a star) and 48h (indicated with a square). Experimental measurements are shown as black lines.

### 4.2.7 Identification of signaling rearrangement and literature validation

**Different mechanism of action of two specific MEK1 inhibitors** The study of network evolution using the newly implemented topology revealed poor model behavior in ERK regulation upon treatment with MEK inhibitor AZD6244 -ERK1/2 error at 96h=0.30386- but not U0126 -ERK1/2 error at 96h=0.013945- (see **figure 4.21**). This error then propagated to CREB. Taken together, this indicated that the invalid regulation of ERK1/2 by MEK1 suggested by the model was due to the presence of AZD6244. This was noticeable by plotting the



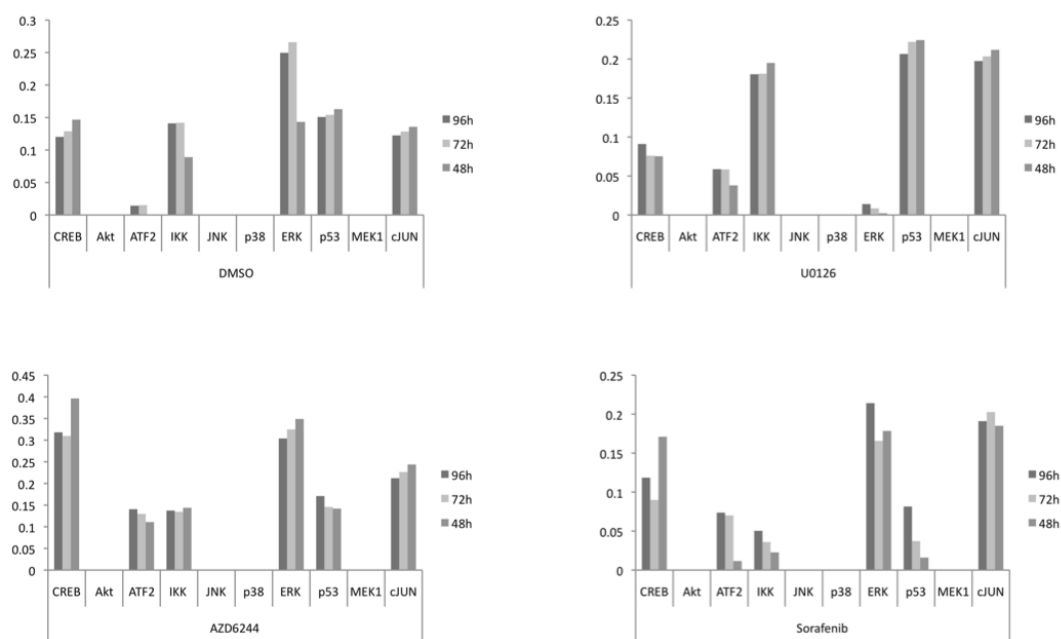


**Figure 4.20: Root-mean-squared error for simulation after reimplementing of the initial prior knowledge network.** Root-mean-squared error was calculated for each time-defined simulation for all treatments, enabling analysis of network evolution. This analysis revealed a potential rearrangement upstream of ERK1/2, which could be specific for A-375 melanoma cell line. Additionally, high error in ERK1/2 simulation upon AZD6244 but no U0126 suggested differential mechanism of action of the two specific MEK1 inhibitors

trajectories of ERK1/2 as implemented in the context of the prior knowledge network for U0126 (figure 4.22A) and AZD6244 (see figure 4.22B). Indeed, literature search showed that U0126 is a specific MEK1 inhibitor [Wilhelm et al., 2004], which prevents its phosphorylation, while AZD6244 was presented in [Yeh et al., 2007] and reported as an inhibitor of ERK1/2 phosphorylation by selectively inhibiting enzymatic activity of MEK1. Its mechanism of action is documented in [Davies et al., 2007].

### Signaling rearrangement in classic MAPK pathway in A-375 melanoma cell line.

Analysis of the error evolution led to the identification of ERK upon Sorafenib treatment (error 96h=0.2141 vs error 48h=0.17851) as a potential rearrangement in the region of confidence (figure 4.21). Closer observation of ERK1/2 upon Sorafenib treatment showed that the reason for this model prediction was the late activation of ERK1/2 at 96h in spite of the decreasing trend of its regulator MEK1 (figure 4.21 and upper 4.22C). A disagree-

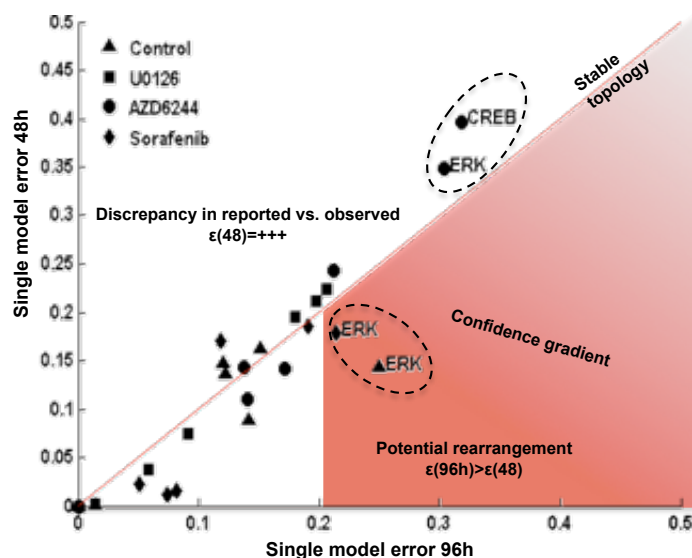


**Figure 4.21: Analysis of error evolution with upgraded topology reveals A-375-specific signaling rearrangement.** Error evolution displayed as errors for models trained with 0-96h dataset (abscissas) against errors for models trained with 0-48h dataset (ordinates). The condition in which the data for model training was acquired is represented by a triangle (DMSO), a square (U0126), a circle (AZD6244) and a diamond (Sorafenib). All models with errors at 96h and 48h below 0.1 RMSE capture the trend in the data accurately (see 4.19 and 4.20 for simulations and error calculations). Hence, models above 0.1 RMSE suggest a topological disagreement to a certain degree. The diagonal shows the models, whose errors exhibited no change upon retraining and simulation. CREB and ERK upon treatment with specific MEK1 inhibitor AZD6244 show a high error both at 48h and 96h, indicating that a disagreement in MEK1-ERK1/2 regulation is present from the first acquirement onwards. This disagreement is not present with specific MEK1 inhibitor U0126. The region of confidence constrains the models that have simultaneously a low error at 48h and a high error at 96h. This is the case of ERK both in control conditions and Sorafenib, thereby suggesting a potential rearrangement in the canonical MAPK pathway.

ment was also shown to arise at 72h in control conditions (figure 4.22C, lower panel) and was also noticeable at 6h in both control and Sorafenib (figure 4.21 and 4.22A). Sorafenib is a RAF kinase and VEGFR-2 inhibitor and thereby prevents phosphorylation of MEK1/2 (Wilhelm et al., 2004). Because RAF is upstream of MEK1 and ERK1/2 as shown in [Roberts and Der, 2007] and [Fukuda et al., 1997], the MEK1-independent increase of ERK1/2 activity at 6h and 96h upon Sorafenib treatment was unexpected. However, the A-375 melanoma cell line used in this study has been shown to be more resistant than other melanomas to apoptosis. For instance, it has been shown that Sorafenib down-modulates the levels of Bcl-2 and Bcl-XL, and such down-modulation was shown to be MAPK-independent in A2058 and SKMEL5 melanoma cells

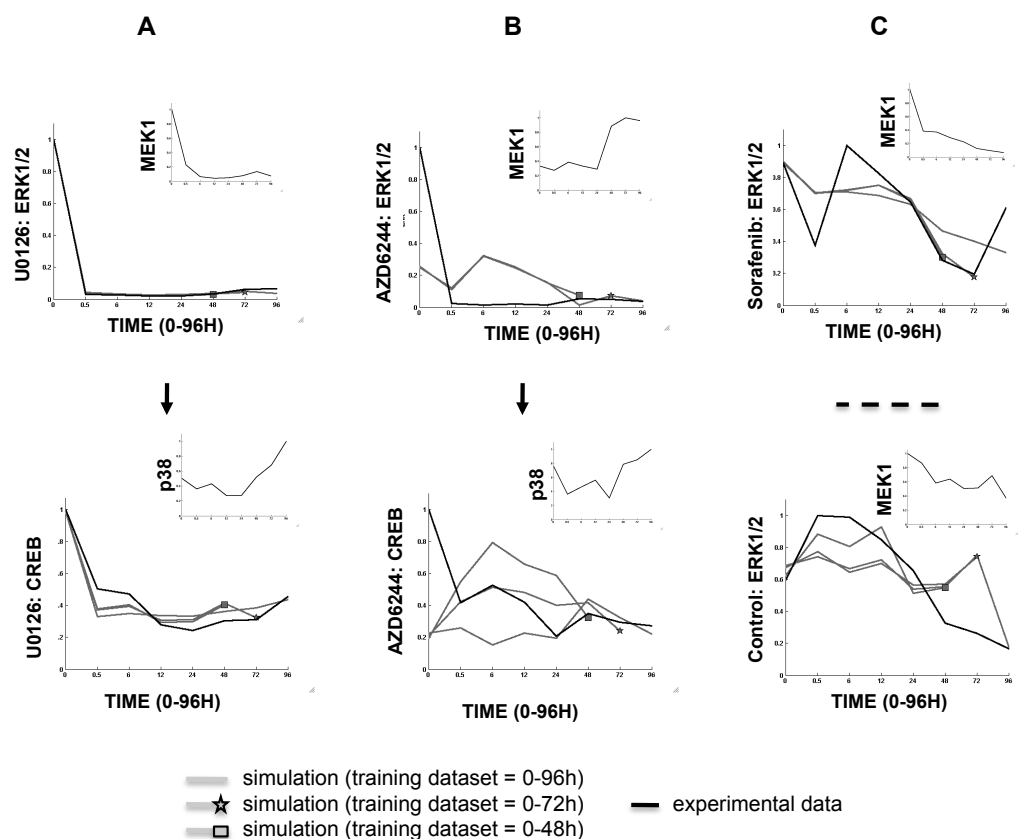


**Figure 4.22: Model analysis provides rationale for hits identified.** (A) Based on the disagreement suggested by the model, plotting of ERK1/2 trajectory for retrained simulations and experimental data supports the finding that MEK1 regulation follows canonical pathway implemented in the prior knowledge network upon treatment with specific inhibitor U0126, but (B) not upon specific MEK1 inhibitor AZD6244, suggesting differential mechanisms of action of both inhibitors. (C) Trajectory plot for ERK1/2 confirms lack of regulation by MEK1 throughout early and late time points upon treatment with both Sorafenib inhibitor (upper panel) and control conditions (lower panel). The observation that canonical MEK1-ERK1/2 regulation is present upon U0126 suggests that the rearrangement is upstream of ERK1/2, and as supported by literature it could be specific in A-375 melanoma cell line.

but not in A-375 cells [Panka, 2006]. From this we conclude that the model prediction is suggestive of an A-375-specific rearrangement. This rearrangement could potentially be upstream of MEK1, consistent with the above-mentioned ERK1/2 response upon MEK1 specific inhibition with U0126 and AZD6244.

# 5

## Discussion

### 5.1 On the biological findings

#### 5.1.1 Modeling suggests a hierarchy of morphological and functional features of mitochondria

In the first part of this work, we sought to elucidate the role of mitochondrial morphology during apoptosis. To that end, high resolution imaging was used to access signatures of apoptosis not only at the sub-cellular but also at the population level during stress induced with a panel of pro-apoptotic stimuli. The heterogeneous response of mitochondria to stress allowed for identification of three mitochondrial morphologies. To directly assess the apoptotic mitochondrial state, we measured the activation of the pro-apoptotic protein Bax, which has been reported in the literature as a clear apoptotic marker [Wolter et al., 1997]. Furthermore, mitochondrial permeability transition was measured.

Direct analysis of the three datasets revealed no existing linear relationship between the measured events [Reis et al., 2012]. Here, we established an exhaustive search to identify non-linear relationships by fitting non-linear FL models to the data and determining those with best performance. The resulting models suggest a hierarchy of apoptotic events: upon Bax activation, mitochondria become fragmented; in turn, different states of mitochondrial morphology closely relate to mitochondrial permeability transition. These results are in accordance with published studies, and taken together, demonstrate that the integrated response of mitochondria to stimuli is rarely linear. In fact, cell-to-cell variability constitutes a rich source of information, in which the challenge lies in detection and quantification. Here, we used high-content

biosensors to extract and quantify spatio-temporal sub-cellular mitochondrial features, thereby identifying single cell dynamics and phenotype distributions in cell populations. Along these lines, the exhaustive search presented here is scalable and can be readily extended to include further datasets to investigate the possibility of multiple simultaneous events causing single phenotypes. We acknowledge that the exhaustive search established here determines the most related events as a metric solely relative to all other measurements acquired. The further development of the method to attempt to establish an absolute measure of performance was undertaken in the second part of this work: therefore, we incorporated temporal and topological structure and investigated different modeling setups, a strategy to reduce the number of free parameters and the contribution of the model qualities to the sensitivity of the model.

### **5.1.2 MAPK signaling is rearranged in A-375 melanoma cell line**

In the second part of this work, we described the establishment and evaluation of a data-derived method to identify discrepancies in signaling networks and pathway rearrangements that grant tumors their plasticity in order to predict putative targets for personalized therapy. The pipeline discussed above rendered a generalized system that we termed gFIS. Based on literature, we defined a signaling network containing our experimental measurements, and subsequently a gFIS could be trained to the data corresponding to each model in the network. Next, a multi-scenario model (msFIS) was created for each single experimental measurement that could reproduce its nonlinear behavior upon the 4 conditions of our experimental setup. We showed that evaluation of the network's performance revealed a mismatch in the MAPK stress response pathway, i.e. Akt-JNK-cJUN as reported in [Vivanco and Sawyers, 2002, Aikin, 2004] with the experimental data in control conditions, indicating alternative regulation to the canonical pathway implemented in the topology expected. By introducing an alternative topology reported in the literature [Vivanco et al., 2007], we could take this emerging behavior into account thereby improving the simulation. However, this manual literature search and implementation of modified network motifs can introduce a bias and be tedious when upscaled.

We anticipate that methods that can identify potential signaling rearrangements in a prior knowledge network and then use automated optimization to identify new interactions that improve the fit to data will be a key advance. In principle, this might be achieved via a combination of the objective function used here with the one presented in [Saez-Rodriguez et al., 2009], which was developed to assemble Boolean logic models from a prior knowledge network and determine the optimal topology by quantifying the difference between data and global simulation while penalizing model size.

We acknowledge that there should be more rigorous definitions of the optimization process to account for models fitted to different number of time points to analyze network evolution. Hence, we propose that the exploration of the objective function mentioned above would be highly interesting. Once the topology was modified according to the model performance, analysis of the evolution of the resulting model revealed a potential signaling rearrangement: while Sorafenib is a RAF kinase and VEGFR-2 inhibitor and thereby prevents phosphorylation of MEK1/2 [Wilhelm et al., 2004], the observed phosphorylation profile of ERK was not consistently inhibited. This lack of regulation of ERK1/2 by MEK1 was also present in the model in control conditions, suggesting non-canonical MAPK signaling in the cell line used in this study. Indeed, it has been reported that A-375 melanoma cell lines show higher resistance to apoptosis than other melanoma cell lines, where anti-apoptotic proteins are down-modulated in a MAPK-independent manner [Panka, 2006]. Additionally, the analysis of model evolution described here led to observation of different mechanisms of action of the two specific MEK1 inhibitors used in this work. Such differential mechanisms were consistent with literature. Taken together, the fact that specific targeting of MEK1 led to consistent inhibition of ERK1/2 indicated that the above-mentioned potential signaling rearrangement developed in A-375 melanoma cell line should be upstream of MEK1. The confirmation of said rearrangement requires further experimentation and would thereby close the interplay between experiments and theory in the classic circle of systems biology, in which modeling is supposed to suggest experiments, which in turn improve the understanding of the phenomena at study.

## 5.2 Advantages and shortcomings of the methods presented

### 5.2.1 Benchmarking

#### High accuracy and reusability

To further evaluate the method presented here, the dataset presented in [Gaudet et al., 2005] was used to benchmark it against the method described in [Aldridge et al., 2009]. Thereby, it was possible to show that our method achieved high accuracy -up to 10 fold increase- and, due to the establishment of the general process for automation of model building, the model can readily be adapted to different datasets, importantly without the bias of manual implementation. This comparison also served as proof of principle for the parameter reduction strategy presented here. In turn, increased high accuracy was a crucial property of the model which then led to identification of differences in model simulation arising at specific time points, therefore enabling study of network evolution.

#### Data requirements to predict optimal treatment combination in cancer treatment and resistance

Additionally, benchmarking revealed that high accuracy and reusability came at the cost of increased number of parameters. While the method by Aldridge et al. could successfully encode experimental data measured upon 10 combinations of TNF/EGF/Insulin at different concentrations, no direct comparison to our method was possible. The reason for that is that to account for different treatment concentrations, the treatment themselves should be implemented in the model as a regulatory event. While in a manual approach one can include the treatment as an input to only its *a priori* targets, we instead aimed at inferring regulatory behavior from training. Thus, in our approach one should include all treatments as inputs to all FIS models thereby enabling quantification of its contribution. This immediately increases the density of the dataset required: each individual species implemented in the model contains  $2(n + 1)$  free parameters, where  $n$  is the number of upstream regulatory intermediates for this specific species defined in the prior knowledge network. For instance, this implies that if a species regulated by e.g. 3 upstream signaling intermedi-



ates was to be included in a network measured upon 3 treatments, more than  $2(6+1)=14$  data points should be acquired in order to maintain the number of free parameters below it. Here only those measurements in control conditions and maximum concentrations of treatment were selected from the dataset presented in [Gaudet et al., 2005] in order to perform the benchmarking, thereby preventing the need of including treatments as inputs in the model. Hence, to enable use of the method presented here to elucidate network evolution upon combinatorial treatment, high-density datasets should be acquired. Although costly, such an extension should be feasible, as there currently is a wealth of experimental methods in the field of proteomics that enable high-throughput measurement of signal transduction signatures [Saez-Rodriguez et al., 2011]. An additional obvious challenge to use the modeling approach presented here to identify signaling rearrangements in the context of acquired resistance and subsequently predict optimal treatment is the following: while processes exist which are faster than genetic mechanisms such as mutation to acquire resistance [Di Nicolantonio et al., 2005], the later are the common, most important mechanisms. Hence, to investigate them, chronic treatment experiments spanning over months are required [Villanueva et al., 2010].

### 5.2.2 Network structure

In [Hanahan and Weinberg, 2011], the authors of this highly instructive review article state that the advantages to tumor cells of activating signaling at the receptor level versus downstream level remain obscure, as does the functional impact of crosstalk between the multiple pathways radiating from growth factor receptors. Regarding the second part of this statement and the role of crosstalk, it has been proposed that combinatorial assemblies and spatiotemporal dynamics are the cell's strategy to achieve a number of functions higher than the number of genes responsible of performing them [Kholodenko et al., 2010]. Here, the authors state that the next question is to explain why evolution chose combinatorial assemblies over single pathway deterministic solutions; an answer being that successful designs can be recycled and adapted for new purposes. Along these lines, in **sections 1.1.2** and **1.3.2** we review mechanisms that have been reported to grant specificity of signaling when crosstalk is present between pathways regulating different responses; a number of this

mechanisms rely on network structure, such as negative feedback loops. We therefore argue that methods to identify signaling rearrangements from data such as the one presented here could be used as a first line of analysis in studies that seek to understand spatio-temporal dynamics of crosstalk regulation.

The first question raised above, why do cancers preferentially activate proliferative signaling at the receptor level, is potentially related to the network structure, i.e. the topology of signaling networks regulating proliferation such as the MAPK signaling cascade. In a letter titled "Why do protein kinase cascades have more than one level", the authors show that the property of having multiple levels in a cascade can itself cause high sensitivity [Brown et al., 1997], i.e. by having multiple levels the sensitivity of the target to the signal is increased. Therefore, it is possible that the higher upstream an activating mutation occurs, the more the proliferative response could be increased. Conversely, one could argue that there are also advantages to activating proliferative signaling downstream, which are also related to network structure. Indeed, in **section 1.3.2** we review mechanisms that are used by the cell to provide a robust response in pathways regulated by proteins with fluctuating levels, due to e.g. cell-to-cell variability. In [Fritsche-Guenther et al., 2011], the authors perturb the protein levels of the effector MAPK ERK and find that activation, i.e. phosphorylation of ERK is very robust against fluctuating protein levels; they also show that one single strong feedback from Erk to Raf-1 accounts for the observed robustness. Other motifs exist that can differentially shape network structure to provide robustness to the pathway [Blüthgen and Legewie, 2012]. It is therefore also possible that an activating mutation downstream could be harder to compensate via robustness mechanisms, or crosstalk to other pathways, due to the more direct proximity -in number of signaling levels- to the effector signaling intermediate that will translocate to the nucleus and up- or down-regulate the transcription of the gene that will ultimately cause increase in proliferation. Along these lines, an advantage of the methods presented here is that evaluation of the signaling structure present at the experimental cell line is possible. The limitation is then, that identification of discrepancies in reported vs. experimental cellular signaling does not directly imply understanding how this rearrangement has been achieved. We argue that to better understand said rearrangement, an improvement of

the objective function used here as discussed in **section 5.1.2** would enable prediction of novel crosstalk interactions. Again, this would not imply understanding which mechanism was the cause of the modification in the network structure identified by the modeling -for a list of potential causal mechanisms, the reader is referred to **table 1.2**-. We expect that in the future, elucidation of the mechanisms that regulate emergence or impairing of crosstalk between pathways and thereby shape network structure will aid to quantify the interest as treatment targets of individual signaling intermediates depending on the specific network motif of their location. We further discuss this concept in the outlook.

### 5.2.3 Use of literature data

Evidence on interactions amongst signaling intermediates across cell lines accumulates vastly [Kiel and Serrano, 2011]. Theoretical systems biology approaches exist that use experimental data reported in the literature in three different ways:

1. Model relationships in own experimental data in an unsupervised manner, i.e. with no assumption or use of literature data whatsoever.
2. Use only topological information from the literature, i.e. without assuming that the spatio-temporal and kinetic regulation in the particular cell line at study coincides with those of literature. Subsequently analyze its validity or evolution in own experimental data.
3. Use topological information and physicochemical detail in the literature regarding the chemical reaction underlying said interactions, e.g. using protein concentration or kinetic constants in addition to the link itself between the species at study.

#### **Novel mechanistic insight comes at the prize of assuming prior knowledge**

The stated in point 3 is the basis for physicochemical modeling approaches such as ordinary and partial differential equations. Ordinary differential equations are based on mass action kinetics and able to describe the concentration of

reactants in continuous time, thereby aiding to achieve insight at a mechanistic level. The spatial component can be added to the model by using partial differential equations, thereby enabling to represent the system in time and space. However, it might be invalid to assume that the interactions between said reactants are regulating the pathway of study in own experimental systems analogously as they do in the literature. The reason for that is that the presence of said interactions is generally cell type specific and dynamically modified both in disease and physiological conditions. In disease, it has been shown that cancers can preferentially express alternate transcripts to maintain abnormal proliferation [Kurada et al., 2009] or escape specific drug targeting [Villanueva et al., 2010]. In physiological conditions, it has been shown that network structures are spatially and temporally regulated in order to enable cells to integrate information to determine specific biological functions [Kholodenko et al., 2010] and grant robustness to systems regulating key processes [Blüthgen and Legewie, 2012]. For example, in [Kiel and Serrano, 2009] the authors show that kinetic rates can be cell-type specific.

### **Data-derived modeling: less bias from prior knowledge at the cost of less mechanistic insight**

Modeling approaches exist that prevent the bias in point 3. However, the more qualitative and phenomenological the approach, the less mechanistic the insight achieved by employing it [Spencer and Sorger, 2011]. An example of formalism, which complies with point 1 are data-driven approaches. Data-driven approaches build models based solely on analyzing the data itself; examples of such formalisms are clustering, principal component analysis and partial least squares. For a comprehensive review on said techniques, the reader is referred to [Janes and Yaffe, 2006]. The limitation in such analysis techniques is that they are reductionist approaches, able to emphasize variables and their difference in the data. In the first part of this work, we employed a non-reductionist approach, which also followed point 1. In the second part of this work, we aimed at using available information and analyzing its validity in own experimental measurements, in an attempt to benefit from available information without introducing a bias. This approach then followed point 2. To describe both approaches we coined the term data-derived, i.e. the models are to a

great extent derived from data. This term then applies for the two formalisms presented in this work, although the first one is also data-driven, i.e. solely based on the data.

The results presented in the first and second part of this work are discussed below in detail (see **Section 5.1.1 and 5.1.2**). Overall, from the results described in the first part of this work we can conclude that mutual relationships can be derived from heterogeneous measurements of high-content e.g. bioenergetic, morphological and functional signatures of signal transduction using an approach based on data-derived logic models. Further, the results presented in the second part of this work show that by incorporating temporal and topological structure to the approach, changes in network topology can be inferred from the training and simulation of time-defined fuzzy logic models, thus providing a tool to facilitate understanding of the dynamic signaling mechanisms that grant melanoma its molecular plasticity. In addition, we argue that in the future the method presented here could be combined with ODE-based modeling approaches for increased mechanistic insight. Thereby, a physicochemical model could be prevented to rely on kinetic rates, initial conditions or interactions shown in literature but identified as not valid by data-derived fuzzy logic model, due to e.g. different stimuli, signaling rewiring or cell-type-specific signaling.

#### **5.2.4 Number of free parameters**

In the second part of this work, we established a training setup to fit the parameters of a Fuzzy Inference System (FIS) to experimental time-defined measurements. In training fuzzy inference systems, a number of model qualities and parameters can be learned that can vary orders of magnitude [Huang and Hahn, 2009]. Using a parameter reduction strategy, the number of qualities that are traditionally trained in a fuzzy inference system was importantly reduced to increase interpretability. In doing so, the contribution of the model features to the flexibility and accuracy of the output was calculated, and we could conclude that circumventing training of a number of model qualities without greatly compromising accuracy is possible. Thereby, the number of free parameters was reduced to below the threshold of our 8 data points acquired in our dataset per kinase or transcription factor measured. As previously intro-

duced, in FL the parameters can be abstract, unrelated to or not representing kinetic rates. The conclusions presented here raise the possibility that sensitivity analysis derived from data -e.g. resampling the training set- aids to elucidate the meaning and impact of the model parameters, thereby improving its interpretability.

### 5.2.5 Temporal activation

#### **Time rules... and there are rules to time**

To include the role of time in network topology, we based our method on the assumption that the behavior of each single model trained was the consequence of the behavior upstream of it. Therefore, to simulate the behavior of the whole network, only the upstream models were simulated and its predicted value was used to propagate the signal throughout each level of the signaling cascade. For in-depth review of the role of time in logic models, the reader is referred to [Wynn et al., 2012, Morris et al., 2010]. Along the line of the role of time in the approach presented here, it has been shown that transient ERK activation in PC12 cells upon EGF stimulation induced proliferation, whereas sustained ERK activation by NGF induced differentiation [Marshall, 1995]. In the future, data-derived logic models should be a key step forward to facilitate identifying the events in which duration of activation i.e. transient versus sustained is critical for cell signaling decisions. In principle this should be straightforward to achieve by including time as input analogously to the inclusion of signaling intermediates as inputs shown in this work, with same constraints regarding dataset density. Thereby, direct quantification of the contribution of time as a signal would be enabled. Thus, bringing together high-density datasets and data-derived modeling would create a framework to directly investigate events in which duration of activation is critical for cell signaling decisions. In other -loose-: such combination of experimental and theoretical approaches would be a rule to elucidate the specific role of time... in those events in which time rules.

## 5.3 Outlook

In this chapter we have discussed the advantages and limitations of the methods presented in the course of this work. Looking forward, it seems likely that the above-proposed solutions to the limitations discussed will aid these methods to prove even more effective in the analysis of cell-type specific network evolution from heterogeneous datasets. In short, we have discussed the use of the presented data-derived modeling formalism to elucidate non-linear signaling from high-content heterogeneous datasets. We reported a hierarchy of morphological and functional features of mitochondrial regulation during apoptosis in MCF-7 breast cancer cell line, and reviewed the limitations of doing so by means of an algorithm lacking temporal and topological structure. We further discussed how this specific aim was solved in the second part of this work, thereby enabling elucidation of network evolution and providing a means to facilitate understanding of the mechanisms that grant melanoma its molecular plasticity. We anticipate that once identified, these rearrangements might be better characterized by combining the approach presented here with physicochemical modeling such as ordinary differential equations. In addition, we anticipated strategies to validate the potential signaling rearrangement specific in A-375 melanoma cell line. We also have discussed the important advantages of our method learned from benchmarking, and we suggested experimental strategies to enable use of the method in order to provide a quantitative measure of interest as treatment target of each signaling intermediate over time. Along these lines, we anticipate that exploration of the objective function landscape should enable the method presented here to better characterize signaling rearrangements; this might be achieved by analyzing evolution of not only discrepancies in interactions present, but also novel interactions added which could decrease the objective function, resulting in improved model behavior.

Nevertheless, the exploration of network evolution as discussed above immediately raises several possibilities as to what mechanism originates the rearrangement, ranging from genetic mechanisms such as mutations to tight spatio-temporal pathway regulation (see **table 1.2**). In the future, heterogeneous datasets combining measurements of post-translational modifications with other data should provide a stronger basis to elucidate the mechanisms of topological complexity. To that end, the current major advance in sequencing

technologies could be exploited, to the point that patient-specific next generation sequencing data could be acquired [Desai and Jere, 2012] and combined to elucidate impact of specific mutations in signaling. While statistical approaches such as dynamic Bayesian networks can be used to infer signaling networks from time series of genetic data [Markowitz and Spang, 2007], application of data-derived logic modeling should enable combination with post-translational modification and single-cell imaging data; in turn, single-cell imaging data might facilitate understanding of spatio-temporal pathway regulation [Grecco et al., 2011]. In the event of integrating such a dataset, when using data-derived logic modeling an added computational challenge would be arising from the heterogeneity of the experimental data. In the first part of this work (see **section 4.1**), we have used an exhaustive search of data-derived fuzzy models to identify nonlinear relationships in heterogeneous measurements of mitochondrial morphological, apoptotic, and energetic states by high-resolution imaging of human breast carcinoma MCF-7 cells [Reis et al., 2012]. This raises the possibility that, in the future, further exploration of data-derived logic and other modeling approaches fitted to heterogeneous datasets should yield valuable insights into the sources of the mechanisms granting specific tumors its plasticity, thereby contributing to facilitate personalized therapy.



# Appendix 1

## Example of Matlab functions for model implementation and fitting

```
1 %*****
2 %maxtime: number of datapoints to temporally define training
3 %varlist: measurements used to train model
4 %h: figure for cumulative plotting
5 %(for more details, see methods)
6 %*****
7
8 function [zpred] =FitAndEuclidean1kGauss (maxtime, varlist, h)
9
10
11 %*****
12 % General variables
13 Nodes={'CREB', 'Akt', 'ATF2', 'IKK', 'JNK', 'p38', 'ERK', 'p53', 'MEK1',
14         'cJUN'};
15 %NodesBenchmark={'MK2', 'JNK', 'FKHR', 'IRS_S', 'IRS_Y', 'MEK', 'ERK',
16                 'Akt', 'IKK', 'clv-c8', 'pro-c3'};
17 %conditionsBenchmark=struct('name', {'control', 'TNF', 'EGF', '
18                               Insulin'}, 'position', {'1:13', '27:39', '40:52', '79:91'});
19
20 conditions=struct('name', {'dms0', 'U0', 'AZ', 'Sor'});
21
22 output=char(Nodes(varlist(end)));
23
24 NumInputs=1; %this is the function for the case: only 1 kinase
25                upstream, or only time as input
26
27 NumInputMFs=2;
28 mfType=str2mat('gausmf');
29
30 NumOutputMFs=power(NumInputMFs, NumInputs);
31
32 OutputMFs=struct('name', {}, 'params', {});
33
34 numConditions=4;
35
36 %*****
37 %model-specific variables
38
```

---

```

29 nparams = 4;
30 condIndex=1;
31 OutputMFindex=1;
32 %p0=(rand(1,nparams)*200)-100;
33 %p0 = [-1 -1 -1 -1]/5
34 options=optimset('Display','Iter','MaxFunEvals',3000);
35 %options=optimset('Display','Iter','PlotFcns',{@optimplotx,
    @optimplotfval},'MaxFunEvals',3000);
36 %*****#
37
38 while condIndex<=numConditions
39
40     data=orgaDataFullMelanoma(varlist,condIndex,maxtime);
41     nruns = 100;
42     p = zeros(nruns, nparams);
43     offsetList = zeros(nruns,1);
44
45     %-----
46     %loop to randomize initial parameters
47     indexParams=1;
48     for indexParams=1:nruns
49         p0=(rand(1,nparams)*200)-100;
50
51         % [p(indexParams,1:4), pen(indexParams)] = lsqnonlin(
52             @evaluateFIS,p0,[],[],options);
53
54         [p(indexParams,:), pen(indexParams)] = fminunc(
55             @evaluateFIS,p0,options);
56         offsetList(indexParams) = offset;
57         %indexParams=indexParams+1;
58     end
59     [valParam, positionParam]=min(pen);
60     %-----
61 %plot relevant models, here MEK1 (9) and cJUN (10), see above
62
63
64     if varlist==[0 9]
65
66         figure(h);
67         xForPrediction = linspace(min(data(:,1)),max(data(:,1)))

```

```

        ,100);
68 prediction=FuzzyLogicSystem1k(p(positionParam,1:4),
    xForPrediction);
69 zpred = FuzzyLogicSystem1k(p(positionParam,1:4),data
    (:,1));
70
71 subplot(3,4,condIndex)
72 plot(xForPrediction,prediction,'-')
73 hold on;
74 plot(data(:,1),data(:,2),'bo','MarkerFaceColor','b'); %
    plot data
75 plot(data(:,1),zpred,'go','MarkerFaceColor','g'); %plot
    prediction for datapoints
76 box off;
77 if varlist(1)==0
78     xlabel(char('TIME'));
79 else xlabel(char(Nodes(varlist(1))));
80 end
81 ylabel(char(Nodes(varlist(2))));
82
83 ResVector=num2str(residuals(:));
84 title([char(conditions(condIndex).name),'_offset:',
    num2str(offsetList(positionParam))]);
85 text(0.7,0.7,[ResVector])
86 end
87
88 if varlist==[5 10]
89     figure(h);
90     xForPrediction = linspace(min(data(:,1)),max(data(:,1))
        ,100);
91     prediction=FuzzyLogicSystem1k(p(positionParam,1:4),
        xForPrediction);
92     zpred = FuzzyLogicSystem1k(p(positionParam,1:4),data
        (:,1));
93
94     plot(xForPrediction,prediction,'k-','LineWidth',2)
95     hold on;
96     plot(data(:,1),data(:,2),'bo','MarkerFaceColor','b'); %
        plot data
97     plot(data(:,1),zpred,'go','MarkerFaceColor','g'); %plot
        prediction for datapoints
98     box off;

```

---

```

99         if varlist(1)==0
100             xlabel(char('TIME'));
101         else xlabel(char(Nodes(varlist(1))));
102         end
103         ylabel(char(Nodes(varlist(2))));
104
105         ResVector=num2str(residuals(:));
106         title ([char(conditions(condIndex).name), '□offset:',
107             num2str(offsetList(positionParam))]);
108         text (0.7,0.7,[ResVector])
109     end
110
111
112     OutputMF(OutputMFindex).name=strcat(char(conditions(
113         condIndex).name),num2str(OutputMFindex));
114     OutputMF(OutputMFindex).params(1)=p(positionParam,1);
115     OutputMF(OutputMFindex).params(2)=p(positionParam,2);
116     OutputMFindex=OutputMFindex+1;
117     OutputMF(OutputMFindex).name=strcat(char(conditions(
118         condIndex).name),num2str(OutputMFindex));
119     OutputMF(OutputMFindex).params(1)=p(positionParam,3);
120     OutputMF(OutputMFindex).params(2)=p(positionParam,4);
121     OutputMFindex=OutputMFindex+1;
122
123     condIndex=condIndex+1;
124 end
125 %defining the final FIS with all estimated parameters
126
127 %general
128
129 %e=genfis1(data,NumInputMFs,mfType);%the default for outputmf
130 is linear
131
132 e.name=strcat(output,char('final'));
133 e.type='sugeno';
134 e.andMethod='prod';
135 e.orMethod='probor';
136 e.defuzzMethod='wtaver';
137 e.impMethod='prod';
138 e.aggMethod='sum';

```

---

```

136
137
138 if ( varlist (1)==0)
139     e.input(1).name='TIME';
140 else e.input(1).name=char(Nodes(varlist(1)));
141 end
142 e.input(1).range=[0 1];
143 e.input(1).mf(1).name='l';
144 e.input(1).mf(1).type=mfType;
145 e.input(1).mf(1).params(1)=0.4247;
146 e.input(1).mf(1).params(2)=0;
147
148 e.input(1).mf(2).name='mL';
149 e.input(1).mf(2).type=mfType;
150 e.input(1).mf(2).params(2)=1;
151 e.input(1).mf(2).params(1)=0.4247;
152
153 %create FIS inputs for dummy vars
154
155 condIndex=2; %control is already default, hence not
    implementing a dummy var for control
156 while condIndex<=numConditions
157
158     %e.input(condIndex).name=char(conditionsBenchmark(condIndex
        ).name);
159     e.input(condIndex).name=char(conditions(condIndex).name);
160     e.input(condIndex).range=[0 1];
161     e.input(condIndex).mf(1).name='no';
162     e.input(condIndex).mf(1).type='trapmf';
163     e.input(condIndex).mf(1).params=[-1 0 0.5 0.51];
164     e.input(condIndex).mf(2).name='yes';
165     e.input(condIndex).mf(2).type='trapmf';
166     e.input(condIndex).mf(2).params=[0.5 0.51 1 1.5];
167     condIndex=condIndex+1;
168 end
169
170
171
172
173 %output
174 %defining output MFS to be used by rules under each condition
175 e.output(1).name=output;

```

---

```

176 e.output(1).range=[0 1];
177 condIndex=1;
178
179 OutputMFindex=1;
180 while OutputMFindex <= times(NumOutputMFs,numConditions)
181     e.output(1).mf(OutputMFindex).name=streat(char(conditions(
        condIndex).name),num2str(OutputMFindex));
182     e.output(1).mf(OutputMFindex).name=streat(char(conditions(
        condIndex).name),num2str(OutputMFindex));
183
184     e.output(1).mf(OutputMFindex).type='linear';
185     e.output(1).mf(OutputMFindex).params= [OutputMF(
        OutputMFindex).params(1) 0 0 0 OutputMF(OutputMFindex).
        params(2)];
186
187     if (mod(OutputMFindex,NumOutputMFs)==0) && condIndex<
        numConditions
188         condIndex=condIndex+1;
189     end
190     OutputMFindex=OutputMFindex+1;
191
192 end
193
194
195
196
197 %rules
198 %expanding rules

```

---

```

199 %rules for dms0
200 e.rule(1).antecedent=[1 1 1 1];
201 e.rule(1).consequent=[1];
202 e.rule(1).weight=1;
203 e.rule(1).connection=1;
204
205 e.rule(2).antecedent=[2 1 1 1];
206 e.rule(2).consequent=[2];
207 e.rule(2).weight=1;
208 e.rule(2).connection=1;
209
210
211 %defining rules to be used by rules upon U0

```

---

```

212 e.rule(3).antecedent=[1 2 1 1];
213 e.rule(3).consequent=[3];
214 e.rule(3).weight=1;
215 e.rule(3).connection=1;
216
217 e.rule(4).antecedent=[2 2 1 1];
218 e.rule(4).consequent=[4];
219 e.rule(4).weight=1;
220 e.rule(4).connection=1;
221
222
223 %defining rules to be used by rules upon AZ
224
225 e.rule(5).antecedent=[1 1 2 1];
226 e.rule(5).consequent=[5];
227 e.rule(5).weight=1;
228 e.rule(5).connection=1;
229
230 e.rule(6).antecedent=[2 1 2 1];
231 e.rule(6).consequent=[6];
232 e.rule(6).weight=1;
233 e.rule(6).connection=1;
234
235
236 %defining rules to be used by rules upon Sorafenib
237 e.rule(7).antecedent=[1 1 1 2];
238 e.rule(7).consequent=[7];
239 e.rule(7).weight=1;
240 e.rule(7).connection=1;
241
242 e.rule(8).antecedent=[2 1 1 2];
243 e.rule(8).consequent=[8];
244 e.rule(8).weight=1;
245 e.rule(8).connection=1;
246
247 fprintf( '\n————\nthe FIS %s was created\n————', strcat(
    output, char(' final ')));
248
249 writefis(e, strcat(output, char(' final ')));
250
251
252 function objective = evaluateFIS(params)

```

---

```

253     nInterpPoints = 100;
254     x = data(:,1);
255     offset = 0;
256     %weight = x; weight(1) = 1e-5;
257     %minPenalty=0.1;
258     %maxPenalty=0.1;
259     %
260     %     p1 = params(1);
261     %     q1 = params(2);
262     %     p2 = params(3);
263     %     q2 = params(4);
264
265     zpred = FuzzyLogicSystem1k(params,x);
266     residuals = sqrt((sum((zpred - data(:,2)).^2))./maxtime
267         );% compute the differences to penalize bad fits
268     %calcualte offset to later penalize for out of range
269         simluation
270     % To that end, first calculate solution for a larger
271         number of data points
272     xExtended = linspace(min(x),max(x),nInterpPoints);
273     zforRange = FuzzyLogicSystem1k(params,xExtended);
274     zforRange=zforRange(:);
275
276     offset = sqrt(sum(( [ zforRange(zforRange<0); zforRange(
277         zforRange>1) ] ).^2) ./ numel(zforRange));
278
279
280     objective=residuals + offset;
281
282 end
283 end

```



# Appendix 2

## Example of Matlab functions for generalized model

```
1 %*****
2 %F: simulation of the reduced single input FIS
3 %p: parameters estimated
4 %x: experimental data
5 %(for more details , see methods)
6 %*****
7
8
9 function F = FuzzyLogicSystem1k (p,x)
10     F = (exp(-(x.^2) ./ (2.*(0.4247).^2)) .* (p(1) .* x+p(2))+exp
        ( -((x-1).^2) ./ (2.*(0.4247).^2)) .* (p(3) .* x+p(4))) ./ (
        exp(-(x.^2) ./ (2.*(0.4247).^2))+exp(-((x-1).^2)
        ./ (2.*(0.4247).^2)));
11
12     end
```



# Appendix 3

## Example of Matlab function for temporally defined network simulation

```
1
2
3 %*dataset-specific variables defined*****
4 clear ;
5 maxtime=8; %number of datapoints used for training, which will
   be used for simulation
6 %NodesBenchmark={ 'MK2', 'JNK', 'FKHR', 'IRS(S)', 'IRS(Y)', 'MEK', 'ERK', 'Akt', 'IKK', 'clv-c8', 'pro-c3' };
7 Nodes={ 'CREB', 'Akt', 'ATF2', 'IKK', 'JNK', 'p38', 'ERK', 'p53', 'MEK1',
   'cJUN' };
8 NumNodes=10;
9 %conditionsBenchmark=struct('name',{ 'control', 'TNF', 'EGF', 'Insulin' }, 'position', { '1:13', '27:39', '40:52', '79:91' });
10 conditions=struct('name',{ 'control', 'U0126', 'AZD6244', 'Sorafenib' });
11
12 **definition of network model
13 numCond=4;
14
15 CREBfinal=readfis('CREBfinal');
16 Aktfinal=readfis('Aktfinal');
17 ATF2final=readfis('ATF2final');
18 IKKfinal=readfis('IKKfinal');
19 JNKfinal=readfis('JNKfinal');
20 p38final=readfis('p38final');
21 ERKfinal=readfis('ERKfinal');
22 p53final=readfis('p53final');
23 MEK1final=readfis('MEK1final');
24 cJUNfinal=readfis('cJUNfinal');
25
26 modelfile='mapktopology10Penalty'
```

---

```

27 modelfile='mapkAlternativeTopologyLookUp2'; %simulink model,
    see appendix 2
28 % modelfile='mapktopology10LookUp2';
29 %modelfile='mapktopology10rangeDecay2'
30 %modelfile='mapktopology10DecayPenalty'
31 %modelfile='model2benchAllcond';
32 %modelfile='model2bench1condFeedback';
33 % modelfile='mapkmodelfeedback';
34
35 % %drug input values
36 yes=[0 1; 0 1]; %1
37 no=[0 0; 0 0]; %0
38
39 %expoDecay=[];%it is 1, the input used will be real time. If it
    is 0, exponential decay.
40 %UpstreamChoice=[];%This switch is implemented in the simulink
    model.
41 %Range=[0 0; 0 0];
42
43
44 timepoints=[0 30 360 720 1440 2880 4320 5760]; %for own dataset
45 %timepoints=[0 5 15 30 60 90 120 240 480 700 960 1200 1440];%
    for benchmarcking
46 endtime=timepoints(maxtime);
47 normatime=timepoints(:)/endtime;
48
49 %declare output vars
50 totalactivity=zeros(maxtime,40);
51 % activitydmso=[];
52 % activityU0=[];
53 % activityAZ=[];
54 % activitySor=[];
55 %*****
56
57
58 condIndex=1; %drug index
59
60 while condIndex<=numCond
61     if condIndex==1
62         U0=no
63         AZ=no
64         Sorafenib=no

```

---

```

65     UpstreamChoice=[0 0; 0 0]
66     %if UpstreamChoice is >0.5, upstream FIS models
        specified in simulink model will be simulated for
        exponential decay of time and otherwise for time
67 elseif condIndex==2
68     U0=yes
69     AZ=no
70     Sorafenib=no
71     UpstreamChoice=[0 1; 0 1]
72 elseif condIndex==3
73     U0=no
74     AZ=yes
75     Sorafenib=no
76     UpstreamChoice=[0 0; 0 0]
77 elseif condIndex==4
78     U0=no
79     AZ=no
80     Sorafenib=yes
81     UpstreamChoice=[0 1; 0 1]
82 end
83
84
85 i=1; %timepoint index
86 j=1; %index for global simulation
87
88 while i<=maxtime
89
90     if condIndex==1
91         k=1; %index for separation of results in array
            according to drug simulation
92
93     elseif condIndex==2
94         k=11;
95     elseif condIndex==3
96         k=21;
97     elseif condIndex==4
98         k=31;
99     end
100
101     %         TIME=[0 normatime(i); 0 normatime(i)];
102     %         expoDecay=[0 exp(times(normatime(i),-50)); 0
            exp(times(normatime(i),-50))];

```

---

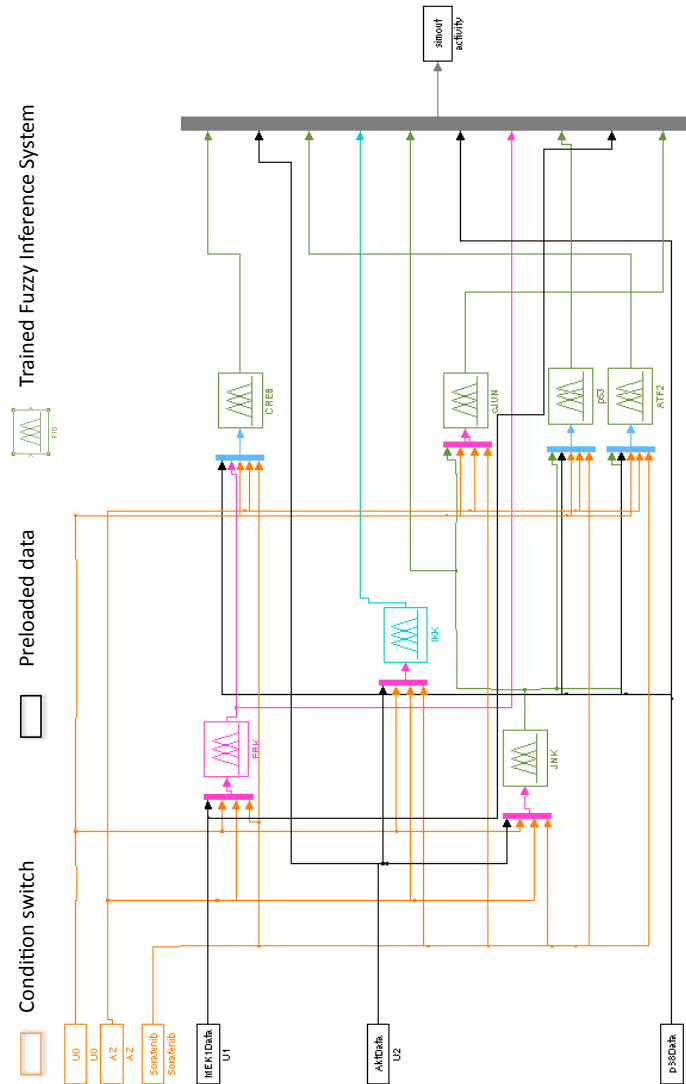
```

103     MEK1Data = MEK1DataLoader(i, condIndex, maxtime);
104     AktData = AktDataLoader(i, condIndex, maxtime);
105     p38Data = p38DataLoader(i, condIndex, maxtime);
106     JNKData = JNKDataLoader(i, condIndex, maxtime);
107     %MEK1Data= [0 1; 0 1]
108     %AktData=[0 1; 0 1]
109     %p38Data=[0 1; 0 1]
110
111
112     [t, x, y]=sim(modelfile);
113
114     %activitydms0=[activitydms0; simout.signals.values];
115
116     while j<=NumNodes
117         totalactivity(i, k)=simout.signals.values(j);
118         %name=char(NodesBenchmark(j));
119         name=char(Nodes(j));
120
121         %fprintf('***** the simulation
122                 is %s upon %s\n', name, conditionsBenchmark(
123                 condIndex).name);
124         fprintf('***** the simulation
125                 is %s upon %s\n', name, conditions(condIndex).
126                 name);
127
128         j=j+1;
129         k=k+1;
130     end
131
132     fprintf('***** the timepoint is %g\n', normatime(i) )
133     ;
134     i=i+1;
135     j=1;
136 end
137
138 totalactivity %#ok<NOPRT>

```

# Appendix 4

## Example of Simulink network







# Bibliography

- [Aikin, 2004] Aikin, R. (2004). Cross-Talk between Phosphatidylinositol 3-Kinase/AKT and c-Jun NH2-Terminal Kinase Mediates Survival of Isolated Human Islets. *Endocrinology*, 145(10):4522–4531.
- [Albeck et al., 2006] Albeck, J. G., MacBeath, G., White, F. M., Sorger, P. K., Lauffenburger, D. A., and Gaudet, S. (2006). Collecting and organizing systematic sets of protein data. *Nature Reviews Molecular Cell Biology*, 7(11):803–812.
- [Aldridge et al., 2006] Aldridge, B. B., Burke, J. M., Lauffenburger, D. A., and Sorger, P. K. (2006). Physicochemical modelling of cell signalling pathways. *Nature Cell Biology*, 8(11):1195–1203.
- [Aldridge et al., 2009] Aldridge, B. B., Saez-Rodriguez, J., Muhlich, J. L., Sorger, P. K., and Lauffenburger, D. A. (2009). Fuzzy Logic Analysis of Kinase Pathway Crosstalk in TNF/EGF/Insulin-Induced Signaling. *PLoS Computational Biology*, 5(4):e1000340.
- [Arnoult, 2007] Arnoult, D. (2007). Mitochondrial fragmentation in apoptosis. *Trends in cell biology*, 17(1):6–12.
- [Baehrecke, 2011] Baehrecke, E. H. (2011). The Grand Finale. *Cell*, 144(4):463–464.
- [Batchelor et al., 2011] Batchelor, E., Loewer, A., Mock, C., and Lahav, G. (2011). Stimulus-dependent dynamics of p53 in single cells. *Molecular Systems Biology*, 7:1–8.
- [Bleris et al., 2011] Bleris, L., Xie, Z., Glass, D., Adadey, A., Sontag, E., and Benenson, Y. (2011). Synthetic incoherent feedforward circuits show adaptation to the amount of their genetic template. *Molecular Systems Biology*, 7:1–12.
- [Blüthgen and Legewie, 2012] Blüthgen, N. and Legewie, S. (2012). Robustness of signal transduction pathways. *Cellular and Molecular Life Sciences*.
- [Bogoyevitch et al., 2010] Bogoyevitch, M. A., Ngoei, K. R. W., Zhao, T. T., Yeap, Y. Y. C., and Ng, D. C. H. (2010). c-Jun N-terminal kinase (JNK) signaling: recent advances and challenges. *Biochimica et biophysica acta*, 1804(3):463–475.
- [Bosl, 2007] Bosl, W. J. (2007). Systems biology by the rules: hybrid intelligent systems for pathway modeling and discovery. *BMC Systems Biology*, 1:13.
- [Bossy-Wetzel et al., 2003] Bossy-Wetzel, E., Barsoum, M. J., Godzik, A., Schwarzenbacher, R., and Lipton, S. A. (2003). Mitochondrial fission in apoptosis, neurodegeneration and aging. *Current opinion in cell biology*, 15(6):706–716.

- [Bradham et al., 1998] Bradham, C. A., Qian, T., Streetz, K., Trautwein, C., Brenner, D. A., and Lemasters, J. J. (1998). The mitochondrial permeability transition is required for tumor necrosis factor alpha-mediated apoptosis and cytochrome c release. *Molecular and cellular biology*, 18(11):6353–6364.
- [Brady et al., 2004] Brady, N. R., Elmore, S. P., van Beek, J. J. H. G. M., Krab, K., Courtoy, P. J., Hue, L., and Westerhoff, H. V. (2004). Coordinated Behavior of Mitochondria in Both Space and Time: A Reactive Oxygen Species-Activated Wave of Mitochondrial Depolarization. *Biophysical Journal*, 87(3):2022–2034.
- [Breiman, 2001] Breiman, L. (2001). Random forests. *Machine Learning*, pages 5–32.
- [Brini, 2003] Brini, M. (2003). Ca(2+) signalling in mitochondria: mechanism and role in physiology and pathology. *Cell calcium*, 34(4-5):399–405.
- [Brown et al., 1997] Brown, G. C., Hoek, J. B., and Kholodenko, B. N. (1997). ScienceDirect.com - Trends in Biochemical Sciences - Guy C. Brown, Jan B. Hoek, Boris N. Kholodenko. *Trends in biochemical . . .*
- [Bulavin et al., 1999] Bulavin, D. V., Saito, S., Hollander, M. C., Sakaguchi, K., Anderson, C. W., Appella, E., and Fornace, A. J. (1999). Phosphorylation of human p53 by p38 kinase coordinates N-terminal phosphorylation and apoptosis in response to UV radiation. *The EMBO Journal*, 18(23):6845–6854.
- [Cargnello and Roux, 2011] Cargnello, M. and Roux, P. P. (2011). Activation and Function of the MAPKs and Their Substrates, the MAPK-Activated Protein Kinases. *Microbiology and Molecular Biology Reviews*, 75(1):50–83.
- [Carpenter et al., 2006] Carpenter, A. E., Jones, T. R., Lamprecht, M. R., Clarke, C., Kang, I. H., Friman, O., Guertin, D. A., Chang, J. H., Lindquist, R. A., Moffat, J., Golland, P., and Sabatini, D. M. (2006). CellProfiler: image analysis software for identifying and quantifying cell phenotypes. *Genome biology*, 7(10):R100.
- [Chen et al., 1992] Chen, R. H., Sarnecki, C., and Blenis, J. (1992). Nuclear localization and regulation of erk- and rsk-encoded protein kinases. *Molecular and cellular biology*, 12(3):915–927.
- [Chiu, 1994] Chiu, S. L. (1994). Fuzzy model identification based on cluster estimation. *Journal of intelligent and Fuzzy systems*.
- [Conradt, 2006] Conradt, B. (2006). Cell biology: mitochondria shape up. *Nature*, 443(7112):646–647.
- [Coulombe and Meloche, 2007] Coulombe, P. and Meloche, S. (2007). Atypical mitogen-activated protein kinases: structure, regulation and functions. *Biochimica et biophysica acta*, 1773(8):1376–1387.
- [Cuadrado and Nebreda, 2010] Cuadrado, A. and Nebreda, A. R. (2010). Mechanisms and functions of p38 MAPK signalling. *The Biochemical journal*, 429(3):403–417.

- [Davies et al., 2007] Davies, B. R., Logie, A., McKay, J. S., Martin, P., Steele, S., Jenkins, R., Cockerill, M., Cartlidge, S., and Smith, P. D. (2007). AZD6244 (ARRY-142886), a potent inhibitor of mitogen-activated protein kinase/extracellular signal-regulated kinase kinase 1/2 kinases: mechanism of action in vivo, pharmacokinetic/pharmacodynamic relationship, and potential for combination in preclinical models. *Molecular cancer therapeutics*, 6(8):2209–2219.
- [Davies et al., 2002] Davies, H., Bignell, G. R., Cox, C., Stephens, P., Edkins, S., Clegg, S., Teague, J., Woffendin, H., Garnett, M. J., Bottomley, W., Davis, N., Dicks, E., Ewing, R., Floyd, Y., Gray, K., Hall, S., Hawes, R., Hughes, J., Kosmidou, V., Menzies, A., Mould, C., Parker, A., Stevens, C., Watt, S., Hooper, S., Wilson, R., Jayatilake, H., Gusterson, B. A., Cooper, C., Shipley, J., Hargrave, D., Pritchard-Jones, K., Maitland, N., Chenevix-Trench, G., Riggins, G. J., Bigner, D. D., Palmieri, G., Cossu, A., Flanagan, A., Nicholson, A., Ho, J. W. C., Leung, S. Y., Yuen, S. T., Weber, B. L., Seigler, H. F., Darrow, T. L., Paterson, H., Marais, R., Marshall, C. J., Wooster, R., Stratton, M. R., and Futreal, P. A. (2002). Mutations of the BRAF gene in human cancer. *Nature*, 417(6892):949–954.
- [Davies and Samuels, 2010] Davies, M. A. and Samuels, Y. (2010). Analysis of the genome to personalize therapy for melanoma. *Oncogene*, 29(41):5545–5555.
- [Desagher and Martinou, 2000] Desagher, S. and Martinou, J. C. (2000). Mitochondria as the central control point of apoptosis. *Trends in cell biology*, 10(9):369–377.
- [Desai and Jere, 2012] Desai, A. N. and Jere, A. (2012). Next-generation sequencing: ready for the clinics? *Clinical Genetics*, 81(6):503–510.
- [Di Nicolantonio et al., 2005] Di Nicolantonio, F., Mercer, S. J., Knight, L. A., Gabriel, F. G., Whitehouse, P. A., Sharma, S., Fernando, A., Glaysher, S., Di Palma, S., Johnson, P., Somers, S. S., Toh, S., Higgins, B., Lamont, A., Gulliford, T., Hurren, J., Yiangou, C., and Cree, I. A. (2005). Cancer cell adaptation to chemotherapy. *BMC cancer*, 5:78.
- [Dumont et al., 2001] Dumont, J. E., Pécasse, F., and Maenhaut, C. (2001). Crosstalk and specificity in signalling. Are we crosstalking ourselves into general confusion? *Cellular signalling*, 13(7):457–463.
- [Efron, 1979] Efron, B. (1979). Bootstrap methods: another look at the jackknife. *The annals of Statistics*, 7(1):1–26.
- [Fadeel et al., 1999] Fadeel, B., Orrenius, S., and Zhivotovsky, B. (1999). Apoptosis in human disease: a new skin for the old ceremony? *Biochemical and biophysical research communications*, 266(3):699–717.
- [Fey et al., 2012] Fey, D., Croucher, D. R., Kolch, W., and Kholodenko, B. N. (2012). Crosstalk and signaling switches in mitogen-activated protein kinase cascades. *Frontiers in physiology*, 3:355.
- [Fisher et al., 2010] Fisher, D. E., Barnhill, R., Hodi, F. S., Herlyn, M., Merlino, G., Medrano, E., Bastian, B., Landi, M. T., Landi, T. M., and Sosman, J. (2010). Melanoma

- from bench to bedside: meeting report from the 6th international melanoma congress. In *Pigment cell & melanoma research*, pages 14–26. Massachusetts General Hospital, MA, USA. dfisher3@partners.org.
- [Frank et al., 2001] Frank, S., Gaume, B., Bergmann-Leitner, E. S., Leitner, W. W., Robert, E. G., Catez, F., Smith, C. L., and Youle, R. J. (2001). The role of dynamin-related protein 1, a mediator of mitochondrial fission, in apoptosis. *Developmental Cell*, 1(4):515–525.
- [Fritsche-Guenther et al., 2011] Fritsche-Guenther, R., Witzel, F., Sieber, A., Herr, R., Schmidt, N., Braun, S., Brummer, T., Sers, C., and thgen, N. B. u. (2011). Strong negative feedback from Erk to Raf confers robustness to MAPK signalling. *Molecular Systems Biology*, 7:1–13.
- [Fuchs et al., 1998] Fuchs, S. Y., Adler, V., Pincus, M. R., and Ronai, Z. (1998). MEKK1/JNK signaling stabilizes and activates p53. *Proceedings of the National Academy of Sciences of the United States of America*, 95(18):10541–10546.
- [Fukuda et al., 1997] Fukuda, M., Gotoh, Y., and Nishida, E. (1997). Interaction of MAP kinase with MAP kinase kinase: its possible role in the control of nucleocytoplasmic transport of MAP kinase. *The EMBO Journal*, 16(8):1901–1908.
- [Ganote and Armstrong, 2003] Ganote, C. E. and Armstrong, S. C. (2003). Effects of CCCP-induced mitochondrial uncoupling and cyclosporin A on cell volume, cell injury and preconditioning protection of isolated rabbit cardiomyocytes. *Journal of molecular and cellular cardiology*.
- [Gaudet et al., 2005] Gaudet, S., Janes, K. A., Albeck, J. G., Pace, E. A., Lauffenburger, D. A., and Sorger, P. K. (2005). A compendium of signals and responses triggered by prodeath and prosurvival cytokines. *Molecular & cellular proteomics : MCP*, 4(10):1569–1590.
- [Grecco et al., 2011] Grecco, H. E., Schmick, M., and Bastiaens, P. I. H. (2011). Signaling from the living plasma membrane. *Cell*, 144(6):897–909.
- [Green, 2011] Green, D. R. (2011). Means to an End: Apoptosis and Other Cell Death Mechanisms. Cold Spring Harbor, N.Y: Cold Spring Harbor Laboratory Press.
- [Hanahan and Weinberg, 2011] Hanahan, D. and Weinberg, R. A. (2011). Hallmarks of Cancer: The Next Generation. *Cell*, 144(5):646–674.
- [Hendrix et al., 2003] Hendrix, M. J. C., Seftor, E. A., Hess, A. R., and Seftor, R. E. B. (2003). Molecular plasticity of human melanoma cells. *Oncogene*, 22(20):3070–3075.
- [Huang and Hahn, 2009] Huang, Z. and Hahn, J. (2009). Fuzzy modeling of signal transduction networks. *Chemical Engineering Science*, pages 1–13.
- [Iordanov et al., 1997] Iordanov, M., Bender, K., Ade, T., Schmid, W., Sachsenmaier, C., Engel, K., Gaestel, M., Rahmsdorf, H. J., and Herrlich, P. (1997). CREB is activated by UVC through a p38/HOG-1-dependent protein kinase. *The EMBO Journal*, 16(5):1009–1022.

- [Janes, 2005] Janes, K. A. (2005). A Systems Model of Signaling Identifies a Molecular Basis Set for Cytokine-Induced Apoptosis. *Science*, 310(5754):1646–1653.
- [Janes et al., 2004] Janes, K. A., Kelly, J. R., Gaudet, S., Albeck, J. G., Sorger, P. K., and Lauffenburger, D. A. (2004). Cue-signal-response analysis of TNF-induced apoptosis by partial least squares regression of dynamic multivariate data. *Journal of computational biology : a journal of computational molecular cell biology*, 11(4):544–561.
- [Janes and Yaffe, 2006] Janes, K. A. and Yaffe, M. B. (2006). Data-driven modelling of signal-transduction networks. *Nature Reviews Molecular Cell Biology*, 7(11):820–828.
- [Jang, 1993] Jang, J. S. R. (1993). ANFIS: adaptive-network-based fuzzy inference system. *IEEE Transactions on Systems, Man, and Cybernetics*, 23(3):665–685.
- [Johnson and Lapadat, 2002] Johnson, G. L. and Lapadat, R. (2002). Mitogen-activated protein kinase pathways mediated by ERK, JNK, and p38 protein kinases. *Science*, 298(5600):1911–1912.
- [Karasarides et al., 2004] Karasarides, M., Chiloeches, A., Hayward, R., Niculescu-Duvaz, D., Scanlon, I., Friedlos, F., Ogilvie, L., Hedley, D., Martin, J., Marshall, C. J., Springer, C. J., and Marais, R. (2004). B-RAF is a therapeutic target in melanoma. *Oncogene*, 23(37):6292–6298.
- [Karbowski et al., 2004] Karbowski, M., Arnoult, D., Chen, H., Chan, D. C., Smith, C. L., and Youle, R. J. (2004). Quantitation of mitochondrial dynamics by photolabeling of individual organelles shows that mitochondrial fusion is blocked during the Bax activation phase of apoptosis. *The Journal of Cell Biology*, 164(4):493–499.
- [Karbowski et al., 2002] Karbowski, M., Lee, Y.-J., Gaume, B., Jeong, S.-Y., Frank, S., Nechushtan, A., Santel, A., Fuller, M., Smith, C. L., and Youle, R. J. (2002). Spatial and temporal association of Bax with mitochondrial fission sites, Drp1, and Mfn2 during apoptosis. *The Journal of Cell Biology*, 159(6):931–938.
- [Karbowski and Youle, 2003] Karbowski, M. and Youle, R. J. (2003). Dynamics of mitochondrial morphology in healthy cells and during apoptosis. *Cell Death and Differentiation*, 10(8):870–880.
- [Kennady et al., 2004] Kennady, P. K., Ormerod, M. G., Singh, S., and Pande, G. (2004). Variation of mitochondrial size during the cell cycle: A multiparameter flow cytometric and microscopic study. *Cytometry. Part A : the journal of the International Society for Analytical Cytology*, 62(2):97–108.
- [Kholodenko, 2000] Kholodenko, B. N. (2000). Negative feedback and ultrasensitivity can bring about oscillations in the mitogen-activated protein kinase cascades. *European journal of biochemistry / FEBS*, 267(6):1583–1588.
- [Kholodenko et al., 2010] Kholodenko, B. N., Hancock, J. F., and Kolch, W. (2010). Signalling ballet in space and time. *Nature Reviews Molecular Cell Biology*, 11(6):414–426.

- [Kholodenko and Kolch, 2008] Kholodenko, B. N. and Kolch, W. (2008). Giving Space to Cell Signaling. *Cell*, 133(4):566–567.
- [Kiel and Serrano, 2009] Kiel, C. and Serrano, L. (2009). Cell Type-Specific Importance of Ras-c-Raf Complex Association Rate Constants for MAPK Signaling. *Science Signaling*, 2(81):ra38–ra38.
- [Kiel and Serrano, 2011] Kiel, C. and Serrano, L. (2011). Challenges ahead in signal transduction: MAPK as an example. *Current Opinion in Biotechnology*, pages 1–10.
- [Kim et al., 2009] Kim, H., Tu, H.-C., Ren, D., Takeuchi, O., Jeffers, J. R., Zambetti, G. P., Hsieh, J. J.-D., and Cheng, E. H.-Y. (2009). Stepwise activation of BAX and BAK by tBID, BIM, and PUMA initiates mitochondrial apoptosis. *Molecular Cell*, 36(3):487–499.
- [Kober et al., 2011] Kober, A. M. M., Legewie, S., Pforr, C., Fricker, N., Eils, R., Krammer, P. H., and Lavrik, I. N. (2011). Caspase-8 activity has an essential role in CD95/Fas-mediated MAPK activation. *Cell Death and Disease*, 2(10):e212–10.
- [Kollmann et al., 2005] Kollmann, M., Løvdok, L., Bartholomé, K., Timmer, J., and Sourjik, V. (2005). Design principles of a bacterial signalling network. *Nature*, 438(7067):504–507.
- [Korsmeyer, 1999] Korsmeyer, S. J. (1999). BCL-2 Gene Family and the Regulation of Programmed Cell Death. *Cancer Research*.
- [Korsmeyer et al., 2000] Korsmeyer, S. J., Wei, M. C., Saito, M., Weiler, S., Oh, K. J., and Schlesinger, P. H. (2000). Pro-apoptotic cascade activates BID, which oligomerizes BAK or BAX into pores that result in the release of cytochrome c. *Cell Death and Differentiation*, 7(12):1166–1173.
- [Kurada et al., 2009] Kurada, B. R. V., Li, L. C., Mulherkar, N., Subramanian, M., Prasad, K. V., and Prabhakar, B. S. (2009). MADD, a Splice Variant of IG20, Is Indispensable for MAPK Activation and Protection against Apoptosis upon Tumor Necrosis Factor-Treatment. *Journal of Biological Chemistry*, 284(20):13533–13541.
- [Kuwana et al., 2002] Kuwana, T., Mackey, M. R., Perkins, G., Ellisman, M. H., Latterich, M., Schneider, R., Green, D. R., and Newmeyer, D. D. (2002). Bid, Bax, and lipids cooperate to form supramolecular openings in the outer mitochondrial membrane. *Cell*, 111(3):331–342.
- [Kuznetsov and Margreiter, 2009] Kuznetsov, A. V. and Margreiter, R. (2009). Heterogeneity of mitochondria and mitochondrial function within cells as another level of mitochondrial complexity. *International journal of molecular sciences*, 10(4):1911–1929.
- [Kyriakis and Avruch, 1996] Kyriakis, J. M. and Avruch, J. (1996). Sounding the alarm: protein kinase cascades activated by stress and inflammation. *The Journal of biological chemistry*, 271(40):24313–24316.
- [Lemmon and Schlessinger, 2010] Lemmon, M. A. and Schlessinger, J. (2010). Cell signaling by receptor tyrosine kinases. *Cell*, 141(7):1117–1134.

- [Ley et al., 2005] Ley, R., Ewings, K. E., Hadfield, K., and Cook, S. J. (2005). Regulatory phosphorylation of Bim: sorting out the ERK from the JNK. *Cell Death and Differentiation*, 12(8):1008–1014.
- [Li et al., 1998] Li, H., Zhu, H., Xu, C. J., and Yuan, J. (1998). Cleavage of BID by caspase 8 mediates the mitochondrial damage in the Fas pathway of apoptosis. *Cell*, 94(4):491–501.
- [Liaw and Wiener, 2002] Liaw, A. and Wiener, M. (2002). Classification and Regression by randomForest. *R news*.
- [Liu et al., 2007] Liu, Y., Shepherd, E. G., and Nelin, L. D. (2007). MAPK phosphatases — regulating the immune response. *Nature Reviews Immunology*, 7(3):202–212.
- [Ma et al., 2009] Ma, W., Trusina, A., El-Samad, H., Lim, W. A., and Tang, C. (2009). Defining Network Topologies that Can Achieve Biochemical Adaptation. *Cell*, 138(4):760–773.
- [Maiuri et al., 2007] Maiuri, M. C., Zalckvar, E., Kimchi, A., and Kroemer, G. (2007). Self-eating and self-killing: crosstalk between autophagy and apoptosis. *Nature Reviews Molecular Cell Biology*, 8(9):741–752.
- [Mamdani and Assilian, 1999] Mamdani, E. H. and Assilian, S. (1999). An experiment in linguistic synthesis with a fuzzy logic controller. *International journal of human-computer studies*, 51(2):135–147.
- [Markowetz and Spang, 2007] Markowetz, F. and Spang, R. (2007). Inferring cellular networks – a review. *BMC Bioinformatics*, 8(Suppl 6):S5.
- [Marshall, 1995] Marshall, C. J. (1995). Specificity of receptor tyrosine kinase signaling: transient versus sustained extracellular signal-regulated kinase activation. *Cell*, 80(2):179–185.
- [Martinou and Youle, 2006] Martinou, J. C. and Youle, R. J. (2006). Which came first, the cytochrome c release or the mitochondrial fission? *Cell Death and Differentiation*, 13(8):1291–1295.
- [McBride et al., 2006] McBride, H. M., Neuspiel, M., and Wasiak, S. (2006). Mitochondria: more than just a powerhouse. *Current Biology*.
- [Métivier et al., 1998] Métivier, D., Dallaporta, B., Zamzami, N., Larochette, N., Susin, S. A., Marzo, I., and Kroemer, G. (1998). Cytofluorometric detection of mitochondrial alterations in early CD95/Fas/APO-1-triggered apoptosis of Jurkat T lymphoma cells. Comparison of seven mitochondrion-specific fluorochromes. *Immunology letters*, 61(2-3):157–163.
- [Michaelis et al., 2011] Michaelis, L., Menten, M. L., Johnson, K. A., and Goody, R. S. (2011). *The original Michaelis constant: translation of the 1913 Michaelis-Menten paper.*, volume 50. Department of Chemistry and Biochemistry, Institute for Cell and Molecular Biology, The University of Texas, Austin, Texas 78735, United States. ka-johnson@mail.utexas.edu.

- [Minamikawa et al., 1999] Minamikawa, T., Williams, D. A., Bowser, D. N., and Nagley, P. (1999). Mitochondrial permeability transition and swelling can occur reversibly without inducing cell death in intact human cells. *Experimental cell research*, 246(1):26–37.
- [Morris et al., 2011] Morris, M. K., Saez-Rodriguez, J., Clarke, D. C., Sorger, P. K., and Lauffenburger, D. A. (2011). Training Signaling Pathway Maps to Biochemical Data with Constrained Fuzzy Logic: Quantitative Analysis of Liver Cell Responses to Inflammatory Stimuli. *PLoS Computational Biology*, 7(3):e1001099.
- [Morris et al., 2010] Morris, M. K., Saez-Rodriguez, J., Sorger, P. K., and Lauffenburger, D. A. (2010). Logic-Based Models for the Analysis of Cell Signaling Networks. *Biochemistry*, 49(15):3216–3224.
- [Nechushtan et al., 2001] Nechushtan, A., Smith, C. L., Lamensdorf, I., Yoon, S. H., and Youle, R. J. (2001). Bax and Bak coalesce into novel mitochondria-associated clusters during apoptosis. *The Journal of Cell Biology*, 153(6):1265–1276.
- [Nelles, 2002] Nelles, O. (2002). Nonlinear System Identification. *Measurement Science and Technology*, 13(4):646–646.
- [Neuspiel et al., 2005] Neuspiel, M., Zunino, R., Gangaraju, S., Rippstein, P., and McBride, H. (2005). Activated mitofusin 2 signals mitochondrial fusion, interferes with Bax activation, and reduces susceptibility to radical induced depolarization. *The Journal of biological chemistry*, 280(26):25060–25070.
- [O’Shaughnessy et al., 2011] O’Shaughnessy, E. C., Palani, S., Collins, J. J., and Sarkar, C. A. (2011). Tunable Signal Processing in Synthetic MAP Kinase Cascades. *Cell*, 144(1):119–131.
- [Panka, 2006] Panka, D. J. (2006). The Raf Inhibitor BAY 43-9006 (Sorafenib) Induces Caspase-Independent Apoptosis in Melanoma Cells. *Cancer Research*, 66(3):1611–1619.
- [Park and Cho, 2006] Park, E.-M. and Cho, S. (2006). Enhanced ERK dependent CREB activation reduces apoptosis in staurosporine-treated human neuroblastoma SK-N-BE(2)C cells. *Neuroscience Letters*, 402(1-2):190–194.
- [Parra et al., 2007] Parra, V., Eisner, V., Chiong, M., Criollo, A., Moraga, F., Garcia, A., Hartel, S., Jaimovich, E., Zorzano, A., Hidalgo, C., and Lavandero, S. (2007). Changes in mitochondrial dynamics during ceramide-induced cardiomyocyte early apoptosis. *Cardiovascular Research*, 77(2):387–397.
- [Pastorino et al., 1998] Pastorino, J. G., Chen, S. T., Tafani, M., Snyder, J. W., and Farber, J. L. (1998). The overexpression of Bax produces cell death upon induction of the mitochondrial permeability transition. *The Journal of biological chemistry*, 273(13):7770–7775.
- [Paulsen et al., 2011] Paulsen, M., Legewie, S., Eils, R., Karaulanov, E., and Niehrs, C. (2011). Negative feedback in the bone morphogenetic protein 4 (BMP4) synexpression group governs its dynamic signaling range and canalizes development. *Proceedings of the National Academy of Sciences*, 108(25):10202–10207.



- [Pelkmans, 2012] Pelkmans, L. (2012). Cell Biology. Using cell-to-cell variability—a new era in molecular biology. *Science*, 336(6080):425–426.
- [Penefsky, 1985] Penefsky, H. S. (1985). Mechanism of inhibition of mitochondrial adenosine triphosphatase by dicyclohexylcarbodiimide and oligomycin: relationship to ATP synthesis. *Proceedings of the National Academy of Sciences of the United States of America*, 82(6):1589–1593.
- [Petit et al., 1998] Petit, P. X., Gubern, M., Diolez, P., Susin, S. A., Zamzami, N., and Kroemer, G. (1998). Disruption of the outer mitochondrial membrane as a result of large amplitude swelling: the impact of irreversible permeability transition. *FEBS letters*, 426(1):111–116.
- [Polzien et al., 2011] Polzien, L., Baljuls, A., Albrecht, M., Hekman, M., and Rapp, U. R. (2011). BAD Contributes to RAF-mediated Proliferation and Cooperates with B-RAF-V600E in Cancer Signaling. *Journal of Biological Chemistry*, 286(20):17934–17944.
- [Pontén et al., 2009] Pontén, F., Gry, M., Fagerberg, L., Lundberg, E., Asplund, A., Berglund, L., Oksvold, P., Björling, E., Hober, S., Kampf, C., Navani, S., Nilsson, P., Ottosson, J., Persson, A., Wernérus, H., Wester, K., and Uhlén, M. (2009). A global view of protein expression in human cells, tissues, and organs. *Molecular Systems Biology*, 5.
- [Puthalakath et al., 2007] Puthalakath, H., O’Reilly, L. A., Gunn, P., Lee, L., Kelly, P. N., Huntington, N. D., Hughes, P. D., Michalak, E. M., McKimm-Breschkin, J., Motoyama, N., Gotoh, T., Akira, S., Bouillet, P., and Strasser, A. (2007). ER stress triggers apoptosis by activating BH3-only protein Bim. *Cell*, 129(7):1337–1349.
- [Ramgolam et al., 2011] Ramgolam, K., Lauriol, J., Lalou, C., Lauden, L., Michel, L., de la Grange, P., Khatib, A.-M., Aoudjit, F., Charron, D., Alcaide-Loridan, C., and Al-Daccak, R. (2011). Melanoma Spheroids Grown Under Neural Crest Cell Conditions Are Highly Plastic Migratory/Invasive Tumor Cells Endowed with Immunomodulator Function. *PLoS ONE*, 6(4):e18784.
- [Reis et al., 2012] Reis, Y., Bernardo-Faura, M., Richter, D., Wolf, T., Brors, B., Hamacher-Brady, A., Eils, R., and Brady, N. R. (2012). Multi-Parametric Analysis and Modeling of Relationships between Mitochondrial Morphology and Apoptosis. *PLoS ONE*, 7(1):e28694.
- [Ringnér, 2008] Ringnér, M. (2008). What is principal component analysis? *Nature Biotechnology*, 26(3):303–304.
- [Rizzuto et al., 2009] Rizzuto, R., Marchi, S., Bonora, M., Aguiari, P., Bononi, A., De Stefani, D., Giorgi, C., Leo, S., Rimessi, A., and Siviero, R. (2009). Ca<sup>2+</sup> transfer from the ER to mitochondria: When, how and why. *Biochimica et Biophysica Acta (BBA) - Bioenergetics*, 1787(11):1342–1351.
- [Rizzuto et al., 1990] Rizzuto, R., Sandonà, D., Capaldi, R. A., and Bisson, R. (1990). Nucleotide sequence of the cDNA encoding subunit VIIe of cytochrome c oxidase from the slime mold *Dictyostelium discoideum*. *Nucleic acids research*, 18(22):6711.

- [Roberts and Der, 2007] Roberts, P. J. and Der, C. J. (2007). Targeting the Raf-MEK-ERK mitogen-activated protein kinase cascade for the treatment of cancer. *Oncogene*, 26(22):3291–3310.
- [Rocks et al., 2005] Rocks, O., Peyker, A., Kahms, M., Verveer, P. J., Koerner, C., Lumbierres, M., Kuhlmann, J., Waldmann, H., Wittinghofer, A., and Bastiaens, P. I. H. (2005). An acylation cycle regulates localization and activity of palmitoylated Ras isoforms. *Science*, 307(5716):1746–1752.
- [Saez-Rodriguez et al., 2009] Saez-Rodriguez, J., Alexopoulos, L. G., Epperlein, J., Samaga, R., Lauffenburger, D. A., Klamt, S., and Sorger, P. K. (2009). Discrete logic modelling as a means to link protein signalling networks with functional analysis of mammalian signal transduction. *Molecular Systems Biology*, 5:1–19.
- [Saez-Rodriguez et al., 2011] Saez-Rodriguez, J., Alexopoulos, L. G., and Stolovitzky, G. (2011). Setting the standards for signal transduction research. *Science Signaling*, 4(160):pe10.
- [Santos et al., 2007] Santos, S. D. M., Verveer, P. J., and Bastiaens, P. I. H. (2007). Growth factor-induced MAPK network topology shapes Erk response determining PC-12 cell fate. *Nature Cell Biology*, 9(3):324–330.
- [Saraste, 1999] Saraste, M. (1999). Oxidative phosphorylation at the fin de siècle. *Science*, 283(5407):1488–1493.
- [Sasagawa et al., 2005] Sasagawa, S., Ozaki, Y.-i., Fujita, K., and Kuroda, S. (2005). Prediction and validation of the distinct dynamics of transient and sustained ERK activation. *Nature Cell Biology*, 7(4):365–373.
- [Scarlett et al., 2000] Scarlett, J. L., Sheard, P. W., Hughes, G., Ledgerwood, E. C., Ku, H. H., and Murphy, M. P. (2000). Changes in mitochondrial membrane potential during staurosporine-induced apoptosis in Jurkat cells. *FEBS letters*, 475(3):267–272.
- [Sesaki and Jensen, 1999] Sesaki, H. and Jensen, R. E. (1999). Division versus fusion: Dnm1p and Fzo1p antagonistically regulate mitochondrial shape. *The Journal of Cell Biology*, 147(4):699–706.
- [Shaulian and Karin, 2001] Shaulian, E. and Karin, M. (2001). AP-1 in cell proliferation and survival. *Oncogene*, 20(19):2390–2400.
- [Shimizu and Pommier, 1997] Shimizu, T. and Pommier, Y. (1997). Camptothecin-induced apoptosis in p53-null human leukemia HL60 cells and their isolated nuclei: effects of the protease inhibitors Z-VAD-fmk and dichloroisocoumarin suggest an involvement of both caspases and serine proteases. *Leukemia : official journal of the Leukemia Society of America, Leukemia Research Fund, U.K.*, 11(8):1238–1244.
- [Sigal et al., 2006] Sigal, A., Milo, R., Cohen, A., Geva-Zatorsky, N., Klein, Y., Liron, Y., Rosenfeld, N., Danon, T., Perzov, N., and Alon, U. (2006). Variability and memory of protein levels in human cells. *Nature*, 444(7119):643–646.

- [Spencer et al., 2009] Spencer, S. L., Gaudet, S., Albeck, J. G., Burke, J. M., and Sorger, P. K. (2009). Non-genetic origins of cell-to-cell variability in TRAIL-induced apoptosis. *Nature*, 459(7245):428–432.
- [Spencer and Sorger, 2011] Spencer, S. L. and Sorger, P. K. (2011). Measuring and Modeling Apoptosis in Single Cells. *Cell*, 144(6):926–939.
- [Takagi and Sugeno, 1985] Takagi, T. and Sugeno, M. (1985). Fuzzy identification of systems and its applications to modeling and control. *IEEE Transactions on Systems, Man, and Cybernetics*, SMC-15(1):116–132.
- [Terfve and Saez-Rodriguez, 2012] Terfve, C. and Saez-Rodriguez, J. (2012). Modeling signaling networks using high-throughput phospho-proteomics. *Advances in experimental medicine and biology*, 736:19–57.
- [Thornton and Rincon, 2009] Thornton, T. M. and Rincon, M. (2009). Non-classical p38 map kinase functions: cell cycle checkpoints and survival. *International journal of biological sciences*, 5(1):44–51.
- [Toescu and Verkhatsky, 2000] Toescu, E. C. and Verkhatsky, A. (2000). Assessment of mitochondrial polarization status in living cells based on analysis of the spatial heterogeneity of rhodamine 123 fluorescence staining. *Pflügers Archiv : European journal of physiology*, 440(6):941–947.
- [Übeyli, 2009] Übeyli, E. D. (2009). Adaptive neuro-fuzzy inference system for classification of ECG signals using Lyapunov exponents. *Computer Methods and Programs in Biomedicine*, 93(3):313–321.
- [van den Berg et al., 2006] van den Berg, R. A., Hoefsloot, H. C. J., Westerhuis, J. A., Smilde, A. K., and van der Werf, M. J. (2006). Centering, scaling, and transformations: improving the biological information content of metabolomics data. *BMC Genomics*, 7:142.
- [Vander Heiden et al., 1997] Vander Heiden, M. G., Chandel, N. S., Williamson, E. K., Schumacker, P. T., and Thompson, C. B. (1997). Bcl-xL regulates the membrane potential and volume homeostasis of mitochondria. *Cell*, 91(5):627–637.
- [Villanueva et al., 2010] Villanueva, J., Vultur, A., Lee, J. T., Somasundaram, R., Fukunaga-Kalabis, M., Cipolla, A. K., Wubbenhorst, B., Xu, X., Gimotty, P. A., Kee, D., Santiago-Walker, A. E., Letrero, R., D’Andrea, K., Pushparajan, A., Hayden, J. E., Brown, K. D., Laquerre, S., McArthur, G. A., Sosman, J. A., Nathanson, K. L., and Herlyn, M. (2010). Acquired Resistance to BRAF Inhibitors Mediated by a RAF Kinase Switch in Melanoma Can Be Overcome by Cotargeting MEK and IGF-1R/PI3K. *Cancer Cell*, 18(6):683–695.
- [Vivanco et al., 2007] Vivanco, I., Palaskas, N., Tran, C., Finn, S. P., Getz, G., Kennedy, N. J., Jiao, J., Rose, J., Xie, W., Loda, M., Golub, T., Mellinghoff, I. K., Davis, R. J., Wu, H., and Sawyers, C. L. (2007). Identification of the JNK Signaling Pathway as a Functional Target of the Tumor Suppressor PTEN. *Cancer Cell*, 11(6):555–569.

- [Vivanco and Sawyers, 2002] Vivanco, I. and Sawyers, C. L. (2002). The phosphatidylinositol 3-Kinase AKT pathway in human cancer. *Nature Reviews Cancer*, 2(7):489–501.
- [von Kriegsheim et al., 2009] von Kriegsheim, A., Baiocchi, D., Birtwistle, M., Sumpton, D., Bienvenut, W., Morrice, N., Yamada, K., Lamond, A., Kalna, G., Orton, R., Gilbert, D., and Kolch, W. (2009). Cell fate decisions are specified by the dynamic ERK interactome. *Nature Cell Biology*, 11(12):1458–1464.
- [Wang and Palade, 2011] Wang, Z. and Palade, V. (2011). Building interpretable fuzzy models for high dimensional data analysis in cancer diagnosis. *BMC Genomics*, 12(Suppl 2):S5.
- [Ward et al., 2007] Ward, C. W., Lawrence, M. C., Streltsov, V. A., Adams, T. E., and McKern, N. M. (2007). The insulin and EGF receptor structures: new insights into ligand-induced receptor activation. *Trends in biochemical sciences*, 32(3):129–137.
- [Wasiak et al., 2007] Wasiak, S., Zunino, R., and McBride, H. M. (2007). Bax/Bak promote sumoylation of DRP1 and its stable association with mitochondria during apoptotic cell death. *The Journal of Cell Biology*, 177(3):439–450.
- [Waterhouse et al., 2001] Waterhouse, N. J., Goldstein, J. C., von Ahsen, O., Schuler, M., Newmeyer, D. D., and Green, D. R. (2001). Cytochrome c maintains mitochondrial transmembrane potential and ATP generation after outer mitochondrial membrane permeabilization during the apoptotic process. *The Journal of Cell Biology*, 153(2):319–328.
- [Whitmarsh and Davis, 1996] Whitmarsh, A. J. and Davis, R. J. (1996). Transcription factor AP-1 regulation by mitogen-activated protein kinase signal transduction pathways. *Journal of Molecular Medicine*, 74(10):589–607.
- [Wilhelm et al., 2004] Wilhelm, S. M., Carter, C., Tang, L., Wilkie, D., McNabola, A., Rong, H., Chen, C., Zhang, X., Vincent, P., McHugh, M., Cao, Y., Shujath, J., Gawlak, S., Eveleigh, D., Rowley, B., Liu, L., Adnane, L., Lynch, M., Auclair, D., Taylor, I., Gedrich, R., Voznesensky, A., Riedl, B., Post, L. E., Bollag, G., and Trail, P. A. (2004). BAY 43-9006 exhibits broad spectrum oral antitumor activity and targets the RAF/MEK/ERK pathway and receptor tyrosine kinases involved in tumor progression and angiogenesis. *Cancer Research*, 64(19):7099–7109.
- [Willis et al., 2007] Willis, S. N., Fletcher, J. I., Kaufmann, T., van Delft, M. F., Chen, L., Czabotar, P. E., Ierino, H., Lee, E. F., Fairlie, W. D., Bouillet, P., Strasser, A., Kluck, R. M., Adams, J. M., and Huang, D. C. S. (2007). Apoptosis initiated when BH3 ligands engage multiple Bcl-2 homologs, not Bax or Bak. *Science*, 315(5813):856–859.
- [Wolter et al., 1997] Wolter, K. G., Hsu, Y. T., Smith, C. L., Nechushtan, A., Xi, X. G., and Youle, R. J. (1997). Movement of Bax from the cytosol to mitochondria during apoptosis. *The Journal of Cell Biology*, 139(5):1281–1292.
- [Wynn et al., 2012] Wynn, M. L., Consul, N., Merajver, S. D., and Schnell, S. (2012). Logic-based models in systems biology: a predictive and parameter-free network analysis method. *Integrative Biology*, 4(11):1323.

- [Xia et al., 1995] Xia, Z., Dickens, M., Raingeaud, J., Davis, R. J., and Greenberg, M. E. (1995). Opposing effects of ERK and JNK-p38 MAP kinases on apoptosis. *Science*, 270(5240):1326–1331.
- [Yeh et al., 2007] Yeh, T. C., Marsh, V., Bernat, B. A., Ballard, J., Colwell, H., Evans, R. J., Parry, J., Smith, D., Brandhuber, B. J., Gross, S., Marlow, A., Hurley, B., Lyssikatos, J., Lee, P. A., Winkler, J. D., Koch, K., and Wallace, E. (2007). Biological Characterization of ARRY-142886 (AZD6244), a Potent, Highly Selective Mitogen-Activated Protein Kinase Kinase 1/2 Inhibitor. *Clinical Cancer Research*, 13(5):1576–1583.
- [Youle, 2007] Youle, R. J. (2007). Cell biology. Cellular demolition and the rules of engagement. *Science*, 315(5813):776–777.
- [Youle and Strasser, 2008] Youle, R. J. and Strasser, A. (2008). The BCL-2 protein family: opposing activities that mediate cell death. *Nature Reviews Molecular Cell Biology*, 9(1):47–59.
- [Zadeh, 1968] Zadeh, L. A. (1968). Probability measures of fuzzy events. *Journal of mathematical analysis and applications*, 23(2):421–427.
- [Zhang and Liu, 2002] Zhang, W. and Liu, H. T. (2002). MAPK signal pathways in the regulation of cell proliferation in mammalian cells. *Cell research*, 12(1):9–18.
- [Zi et al., 2005] Zi, Z., Cho, K.-H., Sung, M.-H., Xia, X., Zheng, J., and Sun, Z. (2005). In silico identification of the key components and steps in IFN-gamma induced JAK-STAT signaling pathway. *FEBS letters*, 579(5):1101–1108.



# List of Figures

1.1	Caspase-dependent and caspase-independent cell death pathways . . . . .	19
1.2	Mitochondrial control of programmed cell death . . . . .	20
1.3	BH3-only proteins regulate mitochondrial morphology changes . . . . .	23
1.4	Major MAPK signaling cascades in mammalian cells . . . . .	25
1.5	Numerous points of crosstalk are known in the MAPK signaling cascade . . .	28
1.6	Intracellular signaling networks regulate the operations of the cancer cell . . .	30
1.7	Schematic overview of modeling techniques suitable for study of signal transduction . . . . .	33
1.8	Steps in model implementation . . . . .	36
1.9	Accuracy comparison for different logic formalisms . . . . .	40
1.10	Representation of a dynamic linguistic fuzzy logic model . . . . .	41
1.11	Schematic overview of experimental techniques suitable for study of multivariate signal transduction . . . . .	45
4.1	Differential morphological states of mitochondria were imaged by high resolution fluorescence microscopy . . . . .	68
4.2	Apoptotic drugs for population analysis of mitochondrial morphology . . . . .	70
4.3	Population analysis of mitochondrial morphology . . . . .	71
4.4	Dataset acquired for $\Delta\psi_m$ loss . . . . .	72
4.5	Dataset acquired to capture Bax clustering under apoptotic stress . . . . .	74
4.6	Secondary dataset derived from acquired data . . . . .	75
4.7	Representative Single input-single output (SISO) model . . . . .	77
4.8	Hierarchy of apoptotic events suggested by exhaustive search . . . . .	79
4.9	Study of phosphorylation profiles to enable identification of signaling rearrangements . . . . .	82
4.10	Phosphorylation profiles suggests signaling plasticity . . . . .	83
4.11	Parameter reduction strategy and data-derived model implementation . . . . .	85
4.12	Data-derived sensitivity analysis validates accuracy and flexibility of approach . . . . .	89
4.13	Workflow for network definition, fitting and simulation. . . . .	93
4.14	Benchmarking our method shows high reproducibility, reduced bias and increased reusability at the cost of drastic increase of data requirements . . . . .	96
4.15	Own method error against benchmark method error . . . . .	97
4.16	Experimental data and model simulations for time-defined training subsets according to initial prior knowledge network . . . . .	98
4.17	Root-mean-squared error for time-defined model simulations according to initial prior knowledge network . . . . .	99

4.18	Model-suggested reimplementation of topology addresses emerging behavior .	100
4.19	Simulation after reimplementation of the initial prior knowledge network to account for emerging behavior . . . . .	101
4.20	Root-mean-squared error for simulation after reimplementation of the initial prior knowledge network . . . . .	102
4.21	Analysis of error evolution with upgraded topology reveals A-375-specific signaling rearrangement . . . . .	103
4.22	Model analysis provides rationale for hits identified . . . . .	104



# List of Tables

1.1	Components of the MAPK pathways in mammalian cells . . . . .	24
1.2	Certain signaling events can render reported interactions dysfunctional in own experiments . . . . .	48
4.1	Studies in literature supporting hierarchy of morphological and functional features of mitochondria suggested by the model. . . . .	80
4.2	Results of sensitivity analysis were reproduced upon inhibition conditions . .	92
4.3	References used to determine interactions used for model fitting . . . . .	95